Fast pyrolysis of cork for bio-oil production: Process modelling

Ali Umut Şen

Thesis to obtain the Master of Science Degree in

Chemical Engineering

Supervisors: Prof. Francisco Lemos
Dr. Axel Funke

Examination Comittee

Chairperson: Prof. Teresa Duarte
Supervisor: Prof. Francisco Lemos
Member of the Comittee: Prof. Carlos Henriques

November 2018

Es ist nicht genug, zu wissen, man muss auch anwenden; es ist nicht genug, zu wollen, man muss auch tun.

Johann Wolfgang von Goethe

Acknowledgements

It was an interesting challenge to study Chemical Engineering at IST. This project would not be possible without constant support and motivation of Professor Helena Pereira. Thank you Professora!

I would like to thank my advisor Professor Francisco Lemos, who was always available to discuss a wide range of topics that helped me during my study time and during thesis work.

I would like to thank Dr. Axel Funke, my advisor from KIT, for his kind help and suggestions both by online conversations and by personal conversations while I was in Germany. I'd like to thank also colleagues in the KIT lab and particularly Frederico and Daniel who helped me in Germany.

I would like to express my gratitude to Prof Amelia Lemos for her kind help both during the course of the thesis and in the reactor design step. Many thanks to Dr. Everton Santos for his help during bench scale pyrolysis experiments and Cristiana Alves for her help in Scanning Electron Microscopy observations.

I would like to extend my sincere thanks to Professors Carla Pinheiro, João Bordado, Licínio Ferreira, Teresa Reis, Helena Pinheiro and Vítor Geraldes.

Last but not least I'd like to thank my family and my friends. Thank you all!

Resumo Analítico

Resíduos de cortiça de carvalho da Turquia (*Quercus cerris*), bétula (*Betula pendula*) e pata de elefante (*Beaucarnea recurvata*) foram estudados para avaliar a possibilidade de serem valorizados através da pirólise. Os parâmetros cinéticos foram determinados através de análise termogravimétrica. Foram utilizados reatores de leito fixo de bancada e um reator de parafuso à escala piloto.

Os modelos utilizando seis pseudo-componentes ajustaram-se bem aos resultados. Utilizando um único conjunto de parâmetros cinéticos as amostras de cortiça e floema podem ser descritas por 5 pseudo-componentes: humidade, hemiceluloses, celulose, suberina e lignina. As energias de ativação destes pseudo-componentes da cortiça de *Q. cerris* variaram entre 31-38 kJ/mol, 228-259 kJ/mol, 141-168 kJ/mol, 247-325 kJ/mol e 130-307 kJ/mol. As composições relativas dos pseudo-componentes variaram 0,04-0,05, 0,21-0,24, 0,16-0,19, 0,16-0,25 e 0,08-0,12.

As experiências em escala laboratorial resultaram em baixos rendimentos de bioóleos, indicando a importância de maior rapidez de transferência de calor durante as reações de pirólise. O ensaio de pirólise rápida em escala piloto do floema de *Quercus cerris* resultou num rendimento de 52% em bioóleo, dos quais 85% correspondiam a uma fração orgânica. O rendimento em carvão vegetal foi de 15%. A análise por SEM revelou que a estrutura celular da cortiça se manteve após as experiências à escala de bancada a 500 °C dando origem a um bio carvão poroso. Os resultados indicam que cortiça de *Q. cerris* e outras espécies de cortiça, bem como o floema de *Q. cerris*, têm potencial para conversão em bioóleos e em carvão e podem ser valorizadas.

Palavras chave: Cortiça, modelação cinética, pirolise rápida, reator duplo parafuso

Abstract

Waste cork streams consisting of Turkey oak (*Quercus cerris*), Birch (*Betula pendula*) and Ponytail palm (*Beaucarnea recurvata*) corks were studied to assess the possibility of valorization through pyrolysis. Kinetic parameters were determined using thermogravimetric analysis and multicomponent parallel reaction modelling using six pseudo component approximation and global kinetic modelling. Fast pyrolysis experiments were carried in bench scale modified fixed bed reactor and pilot scale twin-screw reactor.

Six pseudo component model fitted well to experimental results. Global kinetic models show that cork and phloem samples can be described by 5 pseudo components, i.e. humidity, hemicelluloses, cellulose, suberin and lignin. The activation energies of these pseudo components of *Q. cerris* cork varied 31-38 kJ/mol, 228-259 kJ/mol, 141-168 kJ/mol, 247-325 kJ/mol, and 130-307 kJ/mol respectively. The relative compositions estimated for these pseudo components in the different samples varied 0.04-0.05, 0.21-0.24, 0.16-0.19, 0.16-0.25, and 0.08-0.12 respectively.

Bench scale pyrolysis experiment resulted in low bio-oil yields indicating the importance of higher heat transfer during pyrolysis reactions. Pilot scale fast pyrolysis experiment of *Quercus cerris* phloem resulted with 52 % bio-oil yield of which 85% was organic fraction. Bio char yield was approximately 15%. Scanning electron microscopy analysis revealed that cellular structure of cork was retained after 500 °C bench scale experiments giving rise to a porous bio char. Overall, the results indicate that *Q. cerris* and other cork species as well as *Q. cerris* phloem have potential for conversion of bio-oil and bio chars through fast pyrolysis. Thus cork-rich tree barks can be valorized.

Keywords: Cork, kinetic modelling, fast pyrolysis, twin-screw reactor

Nomenclature

β	Heating rate	°C min^{-1}
BFB	Bubbling fluid bed reactor	
CFB	Circulating fluid bed reactor	
CHP	Combined heat and power	
DSC	Differential scanning calorimetry	
DTG	Differential thermogravimetry	
Ea	Activation energy	kJ mol^{-1}
GC-FID	Gas chromatography with flame ionization detector	
H	Heat transfer coefficient	W $m^{-2}K^{-1}$
HHV	Higher heating value	MJ kg^{-1}
k0	Pre-exponential or frequency factor	s^{-1}
MWe	Megawatt electrical	
NMR	Nuclear magnetic resonance	
Py-GC/MS	Pyrolysis gas chromatography mass spectrometry	
PXRD	Powder x-ray diffraction	
R	Universal gas constant	J mol^{-1} K^{-1}
SEM	Scanning electron microscopy	
Std	Standard deviation	
TGA	Thermogravimetric analysis	
x	Biomass fraction	

Contents

Figures

Tables

1. Chapter 1 General Introduction

1.1. Research objectives

Fast pyrolysis is a thermal process where organic material is converted to organic vapors, pyrolysis gases and charcoal at temperatures between 450 °C to 600 °C in the absence of air. Fast pyrolysis has gained importance in valorization of biomass particularly in the last two decades because it allows a rapid conversion of biomass to bio-oils at relatively high yields (50 to 75 wt.%). The produced bio-oils have important advantages over solid fuels that they can be easily handled, stored and used with/without pretreatments in a variety of applications.

The overall aim of this dissertation is to understand kinetics of pyrolysis reactions and to apply fast pyrolysis for better valorization of cork wastes or unconventional corks. Since, cork wastes are usually burned in cork factories and unconventional corks are not economically exploited, fast pyrolysis of these materials will not only increase the efficiency of industrial cork processing but also it will present new valorization possibilities for unconventional corks such as *Quercus cerris* (Turkey oak) cork.

Having set the aim, the following specific objectives will be studied:

1. Review of fast pyrolysis of biomass and its applicability in cork industry;
2. Kinetic analysis and modelling of biomass pyrolysis;
3. Analysis of laboratory scale fixed bed fast pyrolysis experiments; analysis of pilot scale fast pyrolysis experiment;
4. Characterization of the three fast pyrolysis products i.e., bio char, organic vapors and pyrolysis gases by Scanning Electron Microscopy (SEM) observations, elemental compositions, higher heating value determinations, and GC-FID characterization.

1.2. Overview of biomass fast pyrolysis

Pyrolysis is a thermal conversion of biomass in the absence of oxygen where solid (bio char), liquid (bio-oil) and non-condensable gas products are obtained after complex heat and mass transfer process with thermochemical decomposition reaction.

The distribution of pyrolysis products depends on different factors such as final temperature, heating rate, vapor residence time, pressure, biomass composition, biomass particle size etc. In general, moderate temperatures and short vapor residence times favor liquid products (termed as bio-oil or bio crude) while low temperatures and higher vapor residence times favor charcoal production.

In the past pyrolysis was applied to produce solid fuel (charcoal) and tar as a secondary product. However, starting from the last two centuries and particularly in the last two decades, gas production (leading to liquid fuels production) has gained importance. Starting from 1970s, studies on fast pyrolysis of biomass has been focused on maximizing the bio-oil yield, reaction kinetics, reaction pathways and reactor development (Westerhof et al. 2010).

In fast or flash pyrolysis, biomass is heated rapidly and vapors are quenched rapidly to obtain liquid product termed as bio-oil. The usual applied conditions for fast pyrolysis of biomass are reaction temperature (300-600 ºC), heating rate (1000 ºC/s) and residence time of pyrolysis vapors (1-2 s) (Moens et al. 2009; Venderbosch and Prins, 2010; Patwardhan et al. 2011).

Bio-oils are dark brown and viscous liquids. They contain highly oxygenated compounds, microscopic agglomerates and solid particles (Ba et al., 2004b; Mohan et al. 2006). Physical composition of bio-oils differs depending on the raw material used.

The interest in producing bio-oils lies in those facts:

I. Bio-oil yield from biomass is high (approximately 75%) and transformation of biomass to bio-oil is very fast which implies that bio-oil production may offer a profitable process.
II. Bio-oils production reduce transport and storage cost of biomass. It is important especially in thermal transformation of low-density biomass. An example is cork wastes from cork stopper industry which have a density of 100 kg/m3. Bio-oil has a density around 1200 kg/m3 which would facilitate their transport for fuel usage. Also it is easier to store liquid bio-oils than solid biomass or gasified biomass.
III. Bio-oils are free from inorganics.
IV. Bio-oils are clean and renewable energy resources. Because biomass captures CO_2 from environment during its formation, its combustion does not increase net CO_2 levels in the environment (Zhang et al., 2007; Xiu and Shahbazi, 2012). Biomass-derived bio-oils contain low nitrogen and sulfur. Therefore, they practically don't contribute to SOx emissions to the atmosphere and NOx emissions are 50% lower than diesel oil (Xiu and Shahbazi, 2012).
V. Bio-oils burning allows a more efficient energy transformation of biomass in power production. Direct wood combustion in boiler has an efficiency of only 26% while bio-oil combustion in diesel engine has an efficiency of 45% in power generation (Czernik and Bridgwater, 2004; Gupta et al. 2010).
VI. Bio-oils production and processing can be integrated to existing petroleum refinery infrastructure
VII. Bio-oils production does not compete with food production

Bio-oils, therefore, offer an interesting alternative to petroleum derived oils. However, there are important challenges to overcome in bio-oils usage as fuel. These challenges can broadly be classified as:

I. Bio-oils have a chemical composition that is similar to biomass. This is the major difference between bio-oils and petroleum derived oils. Therefore, bio-oils contain an important amount of oxygenated compounds.
II. The acidic character of bio-oils (pH values between 2.5 and 3.5) makes its storage and processing difficult (Darmstadt et al. 2004).

III. Oxidative and thermal degradation may occur during storage causing increased viscosity

IV. Bio-oils contain important amount of water (around 15% and may reach to 25%). The presence of water in bio-oil lowers its heating value. If the biomass contains more than 10% of water, bio-oil may have phase separation problems during storage (Bridgwater, 1999). Water in bio-oil cannot be eliminated by simple distillation. Compounds in bio-oil polymerize upon heating.

V. Bio-oils do not mix with hydrocarbons. Therefore, their addition to common fuels requires pre-treatments.

VI. Aromatic compounds in bio-oils reduce their cetane index. Since aromatic compounds have higher boiling points than aliphatic compounds, they vaporize later than aliphatic compounds causing knocking in diesel engines.

VII. The solid particles and agglomerates in the bio oils increase oil viscosity, non-Newtonian flow behavior, poor combustion properties and frequency of plugging in the nozzles (Ba et al. 2004b).

Chemical treatments of bio-oils may become necessary prior to their use for fuel purposes. These treatments include hydro-treatment, catalytic cracking and steam reforming. Hydrotreatment converts oxygen in the bio-oil to water while catalytic cracking converts oxygen to carbon dioxide and water (Bridgwater, 2012a, 2012b). Steam reforming can convert bio-oil to hydrogen via syngas production (Wang et al. 1997; Vamvuka, 2011).

Treated or upgraded bio-oils are used in five important usage areas, namely, heat production, power production, combined heat and power production (CHP), transport fuel and chemicals production (Brammer et. al, 2006; Xiu and Shahbazi, 2012). (Figure 1). Chemicals production from bio-oils include a variety of products such as, acetic acid, levoglucosan, binders for asphalt, fertilizers, wood flavor, wood adhesives and wood preserving agents (Effendi et al. 2008; Venderbosch and Prins, 2010; Meng et al. 2012; Mohan et al. 2008) (Figure 2).

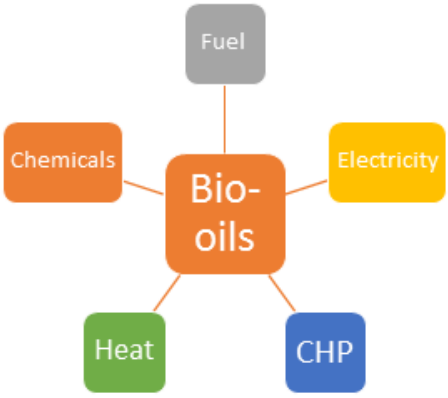

Figure 1 Main usage areas of bio-oils

Figure 2 Chemicals production from bio-oil

The production of bio-oils using flash pyrolysis is an economically promising fuel production method from biomass since biomass is converted to liquid fuel in a very short time (less than 2s) with high yields (75% yield in wood). Different biomass types can be used from whole tree biomass to furniture sawdust (Hassan et al. 2009; Heo et al. 2010).

The sustainability of the bio-oil production depends on its economic viability. The main costs of pyrolysis bio-oils production are biomass, electricity, staffing, finance, and other costs, respectively (Rogers and Brammer, 2012).

Dry biomass costs raange from 10-20 euros/tons to 160 euros/tons (average 70 euros/tons) across Europa (Bridgwater et al. 2012a). An overall cost of bio-oil is reported as 0.11-0.65 US dollars per liter (Wright et al. 2010). This value depends on the availability of a market. Since transportation fuels are the most expensive fuels, addition of bio-oils to diesel may decrease substantially the bio-oil cost. European Committee for Standardization or more specifically the working group CEN/TC 19/WG 41 prepared a standard for the quality standards and testing methods of fast pyrolysis bio oils in March 2017.

According to Bridgwater et al. (2002) a combination of fast pyrolysis and diesel engine systems may generate electricity at a profit in long term and at a lower cost than any other biomass to electricity systems at small scale (up to 5 MWe).

Economic competitiveness of bio-oil applications was analyzed in 14 European countries. A total of six countries (Italy, Netherlands, Denmark, Greece, Austria, and Spain) had at least one economically competitive bio-oil application. Heat-only applications were the most economically competitive, followed by CHP applications. Electricity-only applications were very rarely competitive (Brammer et al. 2006). According to Rogers and Brammer (2012) char sales could reduce production cost of bio-oil by 18% but this value is depended on the availability of a market. In Finland an industrial scale bio-oil production plant was constructed and connected to the Joensuu CHP plant.

1.3. Application of fast pyrolysis in valorization of cork waste

The cork is natural material extracted from the bark of certain tree species. The main tree species used to provide cork is cork oak (*Quercus suber*) although some other "unconventional" trees are shown to have potential for cork production by application of biorefineries concept. These cork-rich trees include *Quercus cerris*, *Betula pendula*, *Kiyelmeyera coriacea*, *Quercus variabilis*, *Phellodendron amurense* etc. The exact amount of these alternative feedstocks are unknown since these materials are usually regarded as waste streams. However, estimates can be made based on wood production such as the case of *Q. cerris* bark production which resulted approximately 2500 tons per year potential (Sen et al. 2016).

The main usage of cork is natural cork stoppers production. More than 15 thousand million stoppers are produced annually worldwide and sold to wine industry (Pereira, 2007). Approximately 70% of raw cork is converted to cork stoppers and cork products while 30% is converted to cork powder after grinding cutting and finishing operations (Gil, 1997; Pereira, 2007). The amount of cork powder generated is estimated to be 32000 to 37000 ton/year in Portugal (Gil, 1997).

Cork industry wastes are used to generate energy for steam treatment of reproduction cork. The leading cork stoppers company in the world is Amorim group based in Portugal. Amorim provides approximately 70% of its energy requirement from combustion of cork powders.

Cork products industry material flows are shown in Figure 3. Cork powders and unconventional corks can be used to produce bio-oils via fast pyrolysis rather than conventional combustion. The current knowledge on cork fast pyrolysis is scarce and new studies on kinetics and transport properties of fast pyrolysis reaction as well as different reactor experiments are necessary. Marques and Pereira (2014) studied bio-oils production from cork using analytical fast pyrolysis (Py-GC-MS) and concluded that bio-oil composition of cork and wood is similar but bio-oil yield from cork is about half of that from woods.

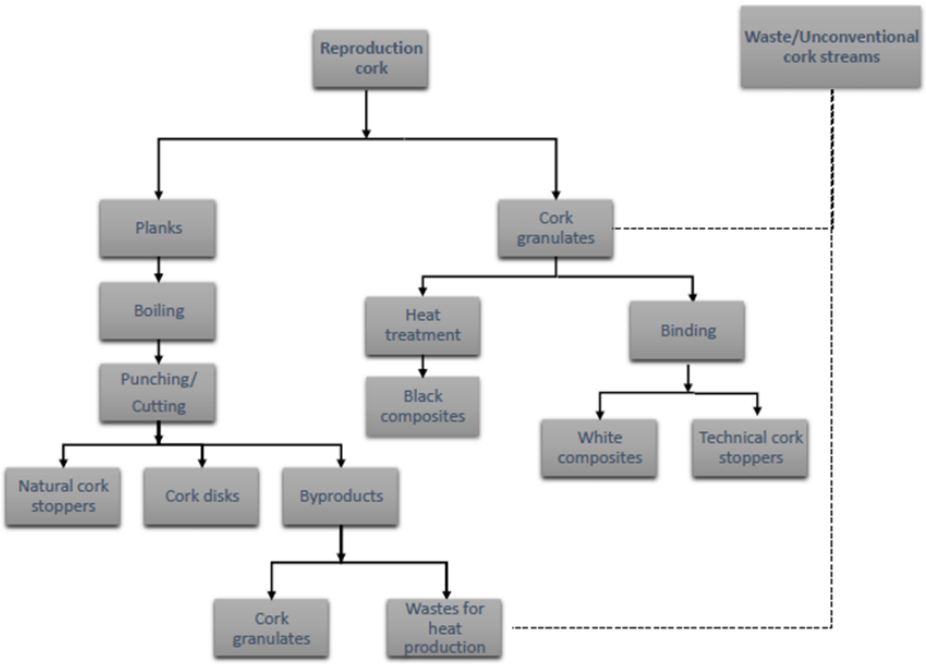

Figure 3 Cork products production lines (Adapted from Pereira, 2007)

1.4. Outline of the thesis

The thesis consists of six chapters.

In the first chapter, the aim and objectives of the dissertation was discussed, biomass fast pyrolysis was reviewed, and cork industry was analyzed considering application of fast pyrolysis for cork wastes.

In the second chapter, previous studies on biomass pyrolysis were reviewed and kinetics of pyrolysis was analyzed. Multicomponent first-order parallel reaction kinetic models were developed for pyrolysis reaction. In the third chapter thermogravimetric analyses including thermogravimetric analysis (TGA), differential scanning calorimetry (DSC), and differential thermogravimetry (DTG) were carried out using different cork species and the results of these analyses were compared.

In the fourth chapter, the experimental procedures and the results of bench scale and pilot scale reactor experiments that were carried in Portugal and Germany, were discussed. In the fifth chapter pyrolysis products were characterized including SEM, elemental composition and higher heating value analyses of bio char, GC-FID characterization of pyrolysis gases and characterization of bio-oils.

In the sixth chapter overall conclusions reached after the experiments were discussed in detail and future study possibilities were evaluated.

2. Chapter 2 State-of-the-Art

2.1. Literature review

Pyrolysis is the thermal decomposition of biomass in the absence of air. The reaction is carried to obtain three product classes i.e., bio char, condensable vapors (bio-oils) and incondensable gases. The conditions of the pyrolysis process determinates the distribution of pyrolysis product yields. In this section, the parameters that effect the fast pyrolysis reaction and product yields will be discussed.

The aim of fast pyrolysis is to produce liquid products (bio-oil). The reaction conditions (heating rate, final temperature, vapor residence time), reactor configurations (fixed bed, fluid bed, etc) and biomass properties (particle dimension, ash content, water content) affect bio-oil yield.

Maximum bio-oil yields are obtained with high heating rates (higher than 1000°C/min), at final reaction temperatures around 500°C and with short vapor residence times (1-2 s). (Bridgwater and Peacocke, 2000). These conditions minimize occurrence of the secondary reactions (Bridgwater, 1999). Thangalzhy-Gopakumar et al. (2011) found that phenols and toluene concentrations are increased with increased pyrolysis temperature in pine wood and switchgrass.

Pyrolysis temperature plays an important role in bio-oil yield and composition (Garcia-Perez et al. 2008). When pyrolysis temperature is increased, gas yield increases while char yield sharply decreases and becomes constant above 500º C. The decrease in char yield is possibly due to increased lignin conversion (Westerhof et al. 2009)

The lower temperature limit in flash pyrolysis of wood was considered as 430 ºC. That temperature gives at least 50% bio-oil; while maximum temperature limit is considered as 520 ºC (Bridgwater, 1999).

Vapor residence times vary between 30 and 1500 ms (Bridgwater, 1999). Shorter residence times favor incomplete depolymerisation of lignin, while longer residence times cause secondary cracking of the primary bio-oil products, reducing bio-oil yield and adversely affecting bio-oil properties (Bridgwater, 1999).

Fast pyrolysis reactors should provide three conditions: high heating and heat transfer rates (i); moderate and carefully controlled temperatures (ii); and rapid cooling or quenching of the pyrolysis vapors (iii) (Bridgwater and Peacocke, 2000). The main fast pyrolysis reactors are listed in

Table 1. Each reactor configuration has advantages and disadvantages and none of them can be considered as the best.

Fluid beds are the most common fast pyrolysis reactors (Figure 4). Because they provide good mixing and temperature uniformity. Bubbling fluid beds (BFB) and circulating fluid beds (CFB) are commercial reactors while other reactor types are either laboratory scale, pilot scale or demonstration scale. Ablative and Vacuum reactors are tolerant to larger biomass size but they need high quality gas and their scale up is not easy. Vacuum pyrolysis results with little char formation which is beneficial for bio-oil yield and quality.

Table 1 Fast pyrolysis reactor types (Wang and Brown, 2017)

Reactor type	Bio-oil yield %	Feed size	Inert gas requirements	Specific reactor Size
BFB	75	< 2 mm	medium	medium
CFB	75	up to 6 mm	medium	medium
Entrained	60	< 2 mm	high	medium
Rotating cone	70	< 200 µm	low	low
Ablative	75	large	low	low
Auger (Screw)	60	medium	low	low
Vacuum	60	large	low	high

Fast pyrolysis can also be carried differently such as using microwave power or by modification of current reactor systems conditions, for example by the combination of a catalyst (catalytic pyrolysis), using hydrogen (hydro pyrolysis), oxygen (auto thermal pyrolysis) or a polymer such as poly lactic acid and polyhydroxybutyrate (co-pyrolysis). Using these methods bio-oil yield change significantly. (Cornelissen et al. 2009).

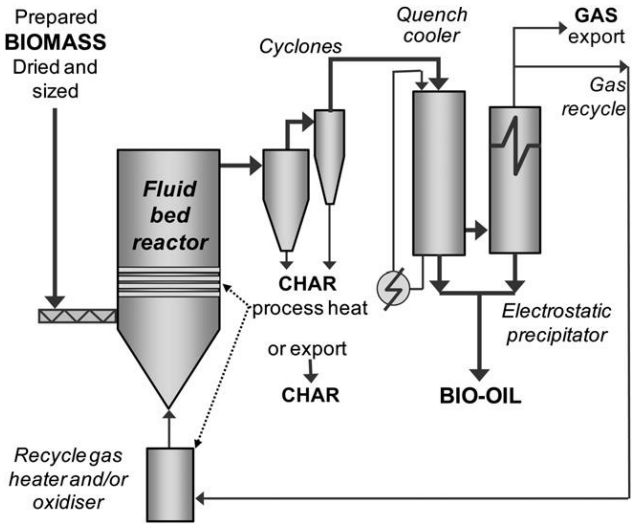

Figure 4 Bubbling fluid bed reactor (Taken from Bridgwater, 2012)

Biomass humidity is an important factor in fast pyrolysis process. It is usually below 10% to minimize water content in bio-oil (Bridgwater, 2012).

Biomass inorganic fraction consist mainly of alkali metals. This fraction is converted mostly to char product and does not present a problem in fast pyrolysis. However, high ash containing biomass species may cause erosion and corrosion in fast pyrolysis system (Brigdwater, 2012).

Biomass particle size affects the bio-oil composition. In most fast pyrolysis applications biomass particle sizes smaller than 2 mm are used. The reactor design is the determining factor of particle size. Ablative and vacuum pyrolysis reactors are more tolerant to particle size while fluid bed reactors require finely ground biomass. Different biomass dimensions were reported by different authors such as down to 10 µm (Hornung, 2014), less than 2-3 mm in BFB (bubbling fluized bed) and 1-2 mm in CFB (circulating fluized bed) (Bridgwater, 2010; Kanterelis et al. 2013).

As the particle size increase, thermal conversion of biomass to bio-oil will be incomplete. Garcia-Perez et al. (2008) found that water content of the bio-oil will increase as particle size increase. Ren et al (2013) found that as the particle size decrease phenol content of bio-oil was increased

Bio-oils are composed of water soluble (polysaccharide-derived) and water insoluble (lignin-derived) phases (Figure 5). Water-insoluble fraction of fast pyrolysis bio-oil constitutes 20-30% mass of whole bio-oil. This fraction is called as pyrolytic lignin as it is composed of lignin degradation oligomers (Czernik and Bridgwater, 2004). The number of compounds in bio-oil depends on raw material and cited as more than 400 (Huber et al. 2006).

Bio-oil compounds are mainly classified into 5 categories: hydroxyaldehydes, hydroxyketones, sugars and dehydro sugars, carboxylic acids and phenolic compounds (Mohan et al. 2006). Garcia-Perez et al. (2007) provided a more detailed description of bio-oil composition as mixture of water, monolignols, polar compounds with moderate volatility, sugars, extractive-derived compounds, heavy polar and non-polar compounds, methanol–toluene insoluble compounds and volatile organic compounds. The effect of chemical components of bio-oil on bio-oil quality are summarized in Table 2.

Bio-oils from forest wastes (including tree barks) are two phase colloidal systems at room temperature while bio-oils obtained from wood feedstock is one-phase system (Oasmaa et al. 2003; Ba et al. 2004a). According to Oasmaa et al. 2003, the phase-separation occurs because of significant polarity, solubility, and density difference of extractives and the highly hydrophilic pyrolysis liquid compounds. Garcia-Perez et al. (2006) explain the occurrence of multiphase systems in biomass pyrolysis oils as the presence of waxy materials, char particles, aqueous and non-aqueous droplets and micelles formed of heavy compounds in a matrix of polysaccharide-derived compounds and water.

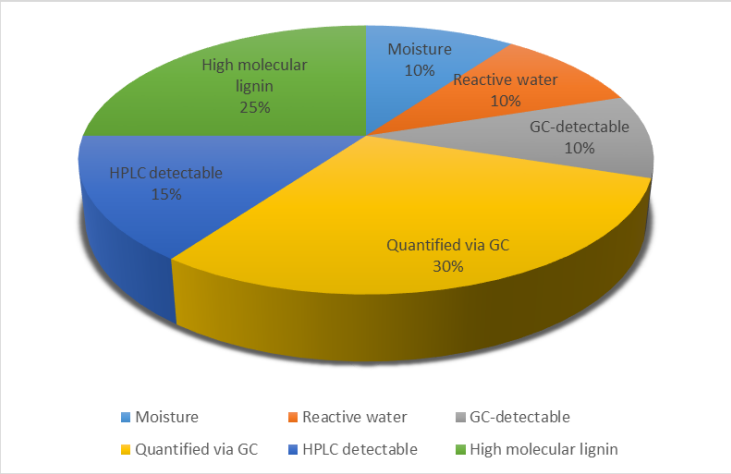

Figure 5 Chemical composition of bio-oil (Mohan et al. 2006))

Table 2 Bio-oil components and chemical groups and bio-oil quality

Bio-oil components		Effects on bio-oil quality
Oxygenated compounds		decrease oil stability, pH, volatility and heating value increase viscosity
Water		decrease heating value, viscosity, increase pumping efficiency and atomization
Inorganics		presence higher than 3% decrease bio-oil stability
Chemicals according to chemical group		
	Phenolics	decrease cetane index
	Ketons	make bio-oils hydrophilic
	Steroids	
	Oxygenates (Ethers or alcohols)	
	Acids	decrease pH
	Sugars	decrease cetane index
	Hydrocarbons	
	Aldehydes	Increase hydrophilicity
	Alcohols	
	Esters	

Chemical composition of bio-oils is different than diesel and fuel oil (Table 3). Chemical composition affects fuel performance and storage properties. The acidity of fast pyrolysis bio-oils is mainly derived (60-70%) from volatile acids. Other groups of compounds in fast pyrolysis bio-oils that influence acidity include phenolics, fatty and resin acids, and hydroxy acids (Oasmaa et al. 2010).

In addition to high oxygen and water content as well as high acidity, the important parameters defining oil quality are cetane number, viscosity, density and higher heating value (Ramirez-Verduzco et al., 2012).

Fuel production from bio-oils by upgrading bio-oils has gained importance in the recent years. Pyrolysis-derived bio-oils have been tested for use in Diesel engines since 1995 (Calabria et al. 2007). Because of the chemical composition of unmodified bio-oils (high viscosity, high acidity, water and oxygen contents) diesel engines have to be modified to use bio-oil/diesel/methanol mixtures and this increased cost of the engine (Chiaramonti et al. 2003a, 2003b).

Table 3 Comparative properties of bio-oil, diesel and heavy fuel oil (Bridgwater et al. 2002; Pant and Mohanty, 2014)

Propertiy	Bio-oil	Diesel	Heavy fuel oil
Density (kg/m^3)	900-1200	820-845	
pH	2.5-3.5		
Oxygen content (%)	37.0		
Water content (%)	15-25	0.1	0.1
Kinematic viscosity at 40 ºC (Stokes)	0.25-10	0.025	3.51
Cetane number	48-65		
Sulfur content	0	0.15	2.5
Iodine number	90-125		
Volumetric energy content (GJ/m^3)	10.6	39.1	

Preparation of bio-oil/diesel emulsions to allow bio-oil use in unmodified diesel engines was also suggested (Chiaramonti et al. 2003a, 2003b; Ikura et al., 2003, Calabria et al. 2007). Problems such as filter and nozzle plugging, jamming and sticking of the injection system after stopping the operation and agglomeration of materials in bio-fuel recirculation system are encountered in engine combustion tests (Ba et al. 2004a).

Bio oils must be deoxygenated in order for them to be used as transport fuels such as gasoline, diesel, kerosene, methane or LPG, bio-oils. Partial upgrade methods are also applied to improve fuel quality (Bridgwater 2012a).

Several methods are applied to stabilize bio-oils including filtration, solvent addition, emulsification, hydrotreatment, catalytic cracking or steam reforming. Because of the chemical composition of bio-oil (high oxygenated compounds, reactive components such as acids and aldehydes) its components tend to polymerize upon heating. This is the reason why distillation is not suitable for upgrading bio-oils. Upon heating viscosity increases. Aging effect was found to be more pronounced at the bottom layer than the upper layer (Chaala et al. 2004). Therefore, alternative methods must be used to fractionate the bio oil such as molecular distillation, supercritical CO_2 extraction or solvent extraction.

Chars contain inorganic metals that catalyze secondary reactions in bio-oil. Filtration of the solids from bio-fuel was found to be the key factor improving stability of bio-oils (Elliot et al. 2012).

Solvent addition such as methanol, ethanol or furfural to bio-oil is a simple and useful method for improving bio-oil properties. These solvents bind with acids and aldehydes forming esters and acetals. As a result of reduced bio-oil acidity and viscosity (maximum kinematic viscosity should be 17 cP) as well as better miscibility with diesel, usage of bio-oil in diesel engines becomes possible and higher heating value is attained (Moens et al., 2009; Boucher et al. 2000a; Bridgwater, 2012b, Xiu and Shahbazi, 2012).

Diebold and Czernik (1997a) showed that a 10% wt methanol addition to bio-oil improved its stability and reduced viscosity. The effect of methanol addiction was attributed to reduction in the concentration of reactive aldehydes through the conversion to hemiacetals and acetals, transacetalizing large hemiacetals and acetals to lower molecular weight acetals, conversion of reactive organic acids to esters, and transesterification of large esters to lower molecular weight esters. (Diebold and Czernik, 1997; Hilten and Das, 2010). Esterification is not only the neutralization and stabilization of the acids in bio-oil with alcohols, but also the stabilization of reactive aldehydes, furans and sugars in bio-oil via various acid-catalysed reactions (Hu et al. 2012). Boucher et al. (2000b) obtained a higher bio-oil stability after methanol addiction. Oasmaa et al. (2004) tested methanol, ethanol and isopropanol and found that methanol was the most effective alcohol to decrease viscosity while increasing stability and heating value. They also found that alcohol additions retarded bio-oil aging from a few months up to a year. Hilten et al. (2009) esterified bio-oil vapor with ethanol and obtained bio-oil with lower water content and lower viscosity and higher pH

Preparation of bio-oil diesel emulsions using surfactants is another method of improving bio-oil burning properties. Chiaramonti et al. (2003a, 2003b) showed increased burning efficiency of emulsified bio-oils in diesel engines. However, emulsions are likely to accelerate corrosion in the engine (Chiaramonti et al. 2007). Also cetane and heating values were not found sufficient after emulsification (Junming et al. 2008).

Atmospheric distillation is not suitable for fractionating or purification of bio-oil as compounds tend to polymerize upon heating. Wang et al. (2009) used molecular distillation to separate bio-oil into three fractions without coking or polymerization. Guo et al. (20010) successfully separated water and acid compounds by vacuum distillation. Mahfud et al (2007) used reactive distillation with n-butanol to decrease water content of pyrolysis oil. Junming et al. (2008) stabilized bio-oil by reactive rectification. Wei et al. (2014) extracted bio-oil with hexane, petroleum ether and chloroform to separate bio-oil into different chemical groups and improve their stability properties. They found optimum extraction conditions with chloroform. Solvent extraction, molecular distillation, aqueous sodium hydroxide extraction, supercritical CO_2 extractions, Ca^{2+} complex method were studied to extract phenolic compounds from bio-oil (Wang et al. 2014). Gooty et al. (2014) reduced water content of bio-oil less than 1% using three condenser fractionation of pyrolysis vapors. Zhao et al. (2009) proposed alkanes production from bio-oil by hydrogenation, hydrolysis and dehydration of phenolic bio-oil. Ben et al. (2013) studied two stage hydrogenation of water-insoluble bio-oil fraction using pine wood ethanol organosolv lignin. They accomplished to convert bio-oil to aliphatic alcohols and other aliphatic components that could be used as a renewable gasoline. Nowakowski et al (2010) studied fast pyrolysis of lignin. They found that concentrated lignin (50% lignin and 50% cellulose) behaves like biomass with only a smaller reduction in bio-oil yield while purified lignin is difficult to process in pyrolysis reactors and the bio-oil yield is much lower.

Scholze and Meier (2001) and Hilten and Das (2010) suggested a quick evaluation method of bio-oil stability by studying carbonyl adsorption bands at 1701, 1652, and 1600 $cm^{-1}$with FTIR. Since changing of oxygen content affects mainly carbonyl bond. Lievens et al. (2011) studied bio-oils with FTIR and

found that carbonyl concentrations were different in bio-oils obtained from bark, wood and leaves because of the chemical composition differences of these materials

Two main deoxygenation methods have been studied to increase heating value of bio-oil. These methods are catalytic vapor cracking and hydrodexoxgenation (Junming et al. 2008; Bridgwater, 2012a). Catalytic cracking is bio-oil cracking over solid acid catalysts (HZSM-5) at atmospheric pressure (Fisk et al. 2009, Mortensen et al. 2011). Hydrodeoxygenation is hydrogenation of unsaturated groups at high pressures in combination with conventional Co–MoS_2/Al_2O_3 or Pd/C catalysts (Fisk et al. 2009, Mortensen et al. 2011). According to Bridgwater (2012) hydrodeoxygenation and catalytic cracking reactions are shown as:

$C_1H_{1.33}O_{0.43} + 0.77\ H_2 \rightarrow CH_2\ + 0.43\ H_2O$ (hydrodeoxygenation)

$C_1H_{1.33}O_{0.43}\ + 0.26\ O_2\ \rightarrow 0.65\ CH_{1.2} + 0.34\ CO_2\ + 0.27\ H_2O$ (catalytic cracking)

Hydrodeoxygenation results with a high grade oil while zeolite cracking results with a low grade-oil (heating value approximately 25% lower than crude oil) (Mortensen et al. 2011). However, hydrodeoxygenation has catalyst life time limit and dependence of hydrogen gas reduces economic viability of the process (Mahfud et al. 2007; Mortensen et al. 2011). Catalytic cracking is cheaper than hydrodeoxygenation but high coking (8-25 % wt) and poor quality of fuels are obtained (Zhang et al. 2007; Deng et al. 2008, French and Czernik, 2010). Different catalysts are tried, best bio-oil qualities with catalytic cracking are obtained with HZSM-5 or ZSM-5 catalyst (Fisk et al. 2009; Lu et al. 2010a, 2010b; Bridgwater, 2012a). Nokkosmäki et al. (2000) showed that ZnO does not reduce bio-oil yield but it affects the composition of bio-oil by decomposing water-soluble fraction. Steam reforming is a catalytic conversion of bio-oil to hydrogen in high temperatures (800-900 ºC). Steam reforming and water-gas shift reactions during steam reforming produces hydrogen gas (Wang et al. 1997; Xiu and Shahbazi, 2012). The most important parameters for steam reforming of the bio-oil were found to be temperature, the molar ratio of steam to carbon fed (S/C), and the reforming catalyst types (Wang et al. 2007).

2.2. Kinetic modelling

Fast pyrolysis reactions occur in a very short time, usually in a few seconds. In these reactions heat and mass transfer as well as reaction kinetics are the most important factors that determine the product yields and selectivity. Thus these factors are used in designing new reactors or process conditions. In this section, kinetic analysis and modelling of pyrolysis reactions will be discussed.

The kinetic analysis of biomass pyrolysis is carried either by thermogravimetric analysis (TGA), differential scanning calorimetry (DSC), powder x-ray diffraction (PXRD), nuclear magnetic resonance analysis (NMR) or reactor experiments. The objective is to calculate the kinetic parameters such as activation energy and pre-exponential (frequency) factor. In order to obtain kinetic parameters modelling (curve-fitting) or model-free (isoconversional) methods are commonly used.

The modelling method uses a theoretical description and a mathematical approximation to explain the experimental results. In modelling of a pyrolysis reaction, solid state reaction models are applied (Khawam and Flanagan, 2006).

A Solid-state reaction rate can be described by Eq.1

$$\frac{d\alpha}{dt} = k\, f(\alpha) \quad (1)$$

where α is the conversion, k is reaction rate constant and f(α) is the reaction model. The reaction rate constant is dependent on temperature and explained by Arrhenius equation (Eq. 2).

$$k = k0\ x\ e\text{^}(-\frac{Ea}{RT}) \quad (2)$$

ko is the frequency factor, *Ea* is the activation energy, R is the universal gas constant (8.314 J/ K mol) and T is the temperature (K)

This model can be used to study isothermal pyrolysis kinetics. In studying nonisothermal reaction rate, however, the equation 1 is modified using heating rate (β) to obtain equations 3 and 4.

$$\frac{d(\alpha)}{dT} = \frac{d(\alpha)}{dt} x \frac{dt}{dT} \quad (3)$$

$$\frac{d(\alpha)}{dT} = \frac{k0}{\beta}\ x\ \mathrm{e}\ \text{^}\left(-\frac{\mathrm{Ea}}{\mathrm{RT}}\right) \mathrm{x}\ \mathrm{f}(\alpha) \quad (4)$$

The integral form of these equations g(α) is obtained after separation of variables and solution of the equations 1 and 4 to obtain equations 5 and 6.

$$g(\alpha) = k0\ e^{-Ea/RT}\ t \quad (5)$$

$$g(\alpha) = k0/\beta\ e^{-Ea/RT}\ dT \quad (6)$$

In applying these equations to model pyrolysis reactions, the most important step is choosing appropriate models. In solid reactions kinetics several models are suggested. These models apply different mechanistic assumptions such as nucleation, geometrical contraction, diffusion and order. Kwaham and Flaganan (2006) resumes these models and their differential forms (Table 4).

In pyrolysis kinetics studies, one of the issue is the reaction order models; particularly first order reaction model is frequently used because of its simplicity and its similarity to homogeneous reaction kinetics. However, other models such as Nuclei growth and Avrami-Erofeev models are also applied to explain pyrolysis kinetics.

Kinetic studies on biomass pyrolysis started as early as 1960's. The first studies concentrated on cellulose pyrolysis since cellulose is the main component of biomass and its extraction is relatively simple than that of lignin. Following cellulose pyrolysis, hemicellulose and lignin pyrolysis studies were carried. Therefore, the first modelling attempts of biomass pyrolysis kinetics are based on cellulose degradation (Antal et al. 1980). Pyrolytic degradation of lignin is complex and involves a high number of free-radical reactions. A lumped kinetic scheme was developed for lignin pyrolysis consisting of about 100 molecular and radical species and 500 elementary reactions (Faravelli et al. 2010).

Some important works on biomass pyrolysis were carried by Broido and Nelson (1975) who suggested a one-step, first order, two competitive parallel reactions for cellulose pyrolysis (Figure 6). In the first reaction cellulose undergoes dehydration to form anhydrocellulose which later decomposes to yield char and gases. In the second reaction, cellulose decomposes at high temperatures to levoglucosan which decomposes in further secondary reactions to yield char, tar and gases (Antal et al. 1980).

Table 4 Solid-state reaction-models (Kwaham and Flanagan, 2006)

Reaction Models $\frac{d\alpha}{dt} = k\, f(\alpha)$		Differential form $f(\alpha)$
Nucleation models	Power law	$2\alpha^{1/2}$
	Power law	$3\alpha^{2/3}$
	Power law	$4\alpha^{3/4}$
	Avarami Erofeev	$2(1-\alpha)[-\ln(1-\alpha)]^{1/2}$
	Avarami Erofeev	$3(1-\alpha)[-\ln(1-\alpha)]^{2/3}$
	Avarami Erofeev	$4(1-\alpha)[-\ln(1-\alpha)]^{3/4}$
Contraction models	Area	$2(1-\alpha)^{1/2}$
	Volume	$3(1-\alpha)^{3/4}$
Diffusion models	1-D	$1/2\alpha$
	2-D	$[-\ln(1-\alpha)]^{-1}$
	3-D	$(3(1-\alpha)^{2/3})/(2(1-(1-\alpha)^{1/3}))$
	Gintsling-Brounhstein	$3/2((1-\alpha)^{-1/3})-1)$
Order models	Zero order	1
	First order	$(1-\alpha)$
	Second-order	$(1-\alpha)^2$
	Third-order	$(1-\alpha)^3$

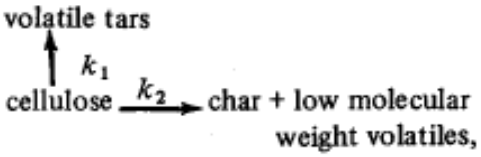

Figure 6 Broido-Nelson pyrolysis model

Broido suggested one year later a multi-step competitive reactions using an intermediate (active cellulose, B in the Figure) formation (Broido, 1976) **(**Figure 7**).**

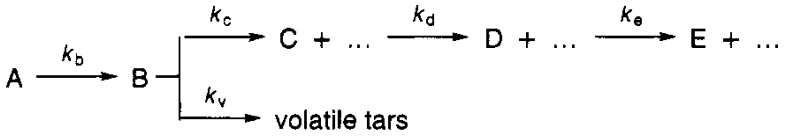

Figure 7 Broido pyrolysis model

In these reaction models, Broido and his co-workers used large biomass samples and the reactivity of volatile fraction was not considered. Shafizadeh and Chin (1977) and later Bradbury, Sakai and Shafizadeh (1979) improved models of Broido et al. by considering reactivity of volatile fraction (Figure 8).

According to Shafizadeh and Chin (1977) wood is decomposed by three competing parallel, first order reactions to form gas, volatile liquid (tar) and solid (char) product in primary reactions. The volatile fraction undergoes secondary reactions to form gas and char (4, and 5 respectively).

Bradburry et al (1979) suggested a multi-step reaction scheme for cellulose pyrolysis using formation of an active cellulose. In this model, after active cellulose is formed, two competitive parallel reactions take place to form volatiles and char and gases.

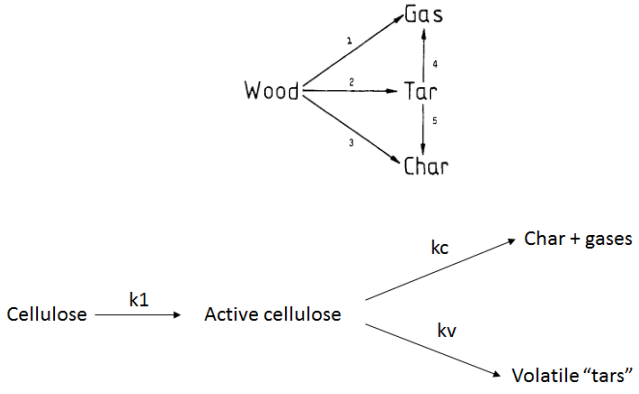

Figure 8 Shafizadeh-Chin and Bradbury-Sakai-Shafizadeh pyrolysis models

These two models are all irreversible, first-order models and are commonly applied in biomass kinetic studies. These models assume lower activation energies for char production and higher activation energies for volatile formation.

Piskorz et al. (1986, 1989) showed (Figure 9). that at low temperatures a competitive reaction occurs to form char and active cellulose with lower degree of polymerization. At higher temperatures a further two competition paths take place at higher temperatures and with catalysis of cations and at lower temperatures, leading to formation of glycolaldehyde (hydroxyacetaldehyde) by ring fragmentation and formation of levoglucosan by transglycosylation, respectively (DiBlasi, 2008).

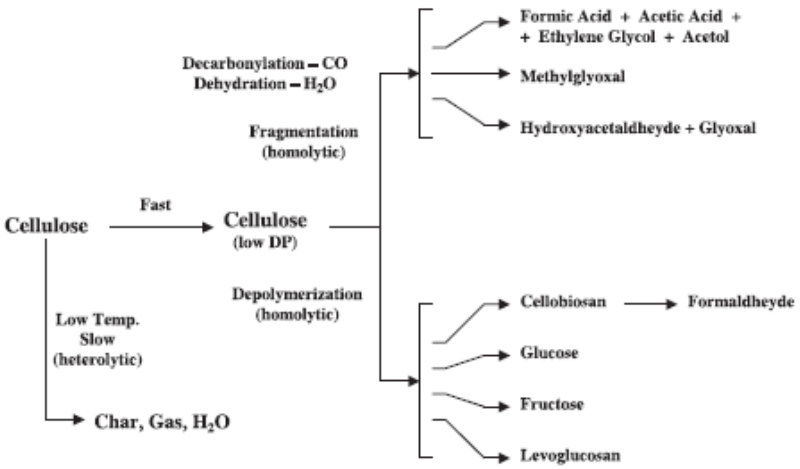

Figure 9 Piskorz et al.(1989) pyrolysis model

Ranzi et al. (2008) developed multi-step lumped decomposition models for three biomass components, cellulose, hemicelluloses and lignin (Figure 10). This model is particularly useful in fast pyrolysis because it allows predictions of gas, bio-oil and char yields.

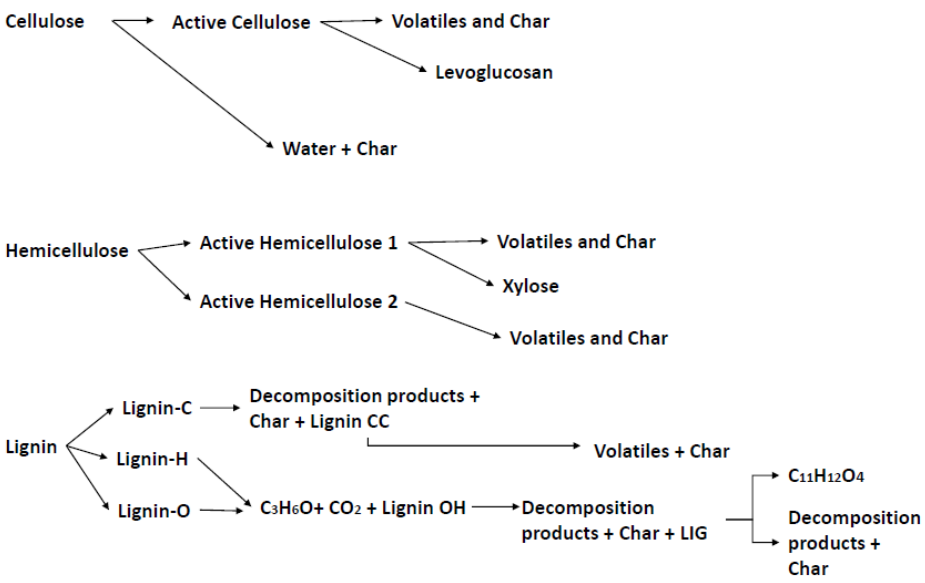

Figure 10 Ranzi et al. (2008) pyrolysis model

A second general mathematical method to obtain kinetic data is isoconversional or model-free method. Isoconversional methods used to calculate activation energy as a function of conversion. The basic assumption is that reaction rate at a constant extent of conversion depends only on temperature and the reaction mechanism model is not depended on heating rate (Cai and Bi, 2009). Isoconversional methods require using different heating rates and same conversion (α) values at these heating rates are used to calculate activation energy. Friedman, Kissenger, Kissenger-Akahira-Sunose (KAS), Flynn-Wall-Ozawa (FWO) and Coats-Redfern (CR) methods are important isoconversional methods.

Friedman method calculates activation energy by plotting ln(βdα/dT) against 1/T for a constant conversion value (Equations 7-8).

$$\beta x \frac{d(\alpha)}{dT} = \frac{d(\alpha)}{dt} = k0\ e\text{^}\left(-\frac{Ea}{RT}\right) xf(\alpha) \quad (7)$$

$$\ln\left(\beta x \frac{d(\alpha)}{dT}\right) = \ln k0 - \left(\frac{Ea}{R}\right) x1/T \ (8)$$

The Kissenger method calculates activation energy by derivation of Arrhenius equation with temperature data of the reaction rate (Tm) at each heating rate (Eq.9).

$$\ln(\frac{\Delta T}{\Delta t} / Tm^2) = \ln(\frac{k0Ea}{R}) - \frac{Ea}{R} xTm \quad (9)$$

Kissenger-Akahira-Sunose (KAS) method is used to calculate activation energy at fixed certain conversions assuming k0, f(α) and Ea is dependent of T while k0 and Ea is independent of α (Eq. 10)

$$\ln g(\alpha) = \ln(\frac{k0Ea}{R}) - \ln\beta + \ln p(\frac{Ea}{RT}) \ (10)$$

Flynn-Wall-Ozawa (FWO) method use Doyle's approximation for the integral and activation energy is calculated as Equation 11.

$$\ln \beta = \ln(\frac{k0Ea}{Rg(\alpha)} - 5.331 - \frac{1.052xEa}{RT} \quad (11)$$

Coats-Redfern method (CR) is also an integral method and the activation energy is calculated as Equation 12.

$$\ln\left(\frac{g(\alpha)}{T^2}\right) = \ln\left(\frac{k0R}{\beta E}\right) - \frac{Ea}{RT} \quad (12)$$

Both modelling approach and isoconversional approach assume constant activation energies. Different values reported for activation energies using modelling methods and using of isoconversional methods for heterogeneous biomass raise concerns on the reliability of the results. Anca-Couce et al. (2014) showed that considering first order reaction models for all biomass components may lead incorrect results in estimation of activation energy of lignin. Kwaham and Flanagan (2006) suggested first using of isoconversional methods to select reaction model and later applying of model-fitting methods. The kinetic models are explained in combination with differential thermogravimetry (DTG) and differential scanning calorimetry (DSC). Biomass pyrolysis results typically present with one, two or three distinct DTG peaks. These peaks are attributed to hemicelluloses and cellulose decompositions at temperatures 225 to 325 °C and 325 to 400 °C respectively. No distinct peak is observed for lignin pyrolysis indicating a large decomposition range for lignin (200 to 600 °C) (Antal and Varhegyi, 1995). Mok and Antal (1983a, 1983b) showed using DSC that longer residence times between solid and vapor phase promotes exothermic reactions while shorter residence times results with endothermic reactions. They also conclude that higher pressures favor char and CO_2 formation. Chaiwat et al. (2009) analyzed cross-linking during cellulose pyrolysis by FTIR and XRD patterns and concluded that dehydration reaction occurs simultaneously with glycosidic cleavage reaction which produces char. At lower temperature pyrolysis dehydration and cross-linking dominates while at higher temperatures glycosidic cleavage occurs (Figure 11)

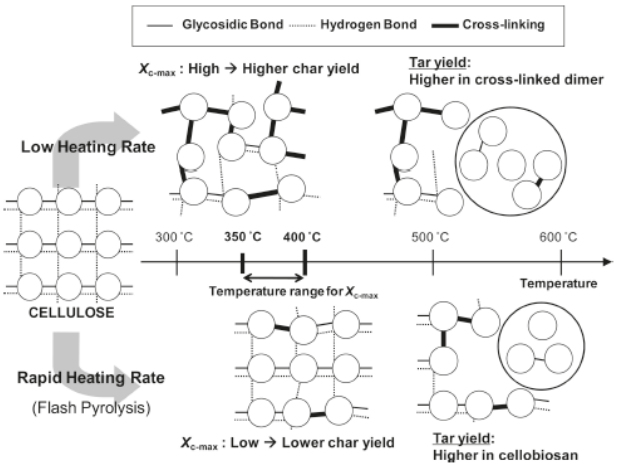

Figure 11 Cross-linking mechanism (Chaiwat et al. 2009)

These results indicate that apart from biomass properties which determine final product composition and pyrolysis efficiency (heat and mass transfer limitations), pyrolysis kinetics depends on pyrolysis

conditions (heating rate, final temperature and pressure). The complex nature of biomass pyrolysis reactions complicates the calculation of kinetic parameters and simulation of pyrolysis reactions. However, computational fluid dynamics was already used to simulate fast pyrolysis reaction of biomass in bubbling fluid bed reactors (Papadikis et al. 2008, 2009). Recently an open-code program “Biotc” was developed for use in OpenFOAM (Xiong et al. 2014).

2.2.1. First-order parallel competitive reaction models

Biomass samples contain more than one chemical components. The lignocellulosic biomass components can be classified as water, extractive components, hemicelluloses, cellulose, lignin and suberin (in barks).

The model of first-order independent parallel reactions is useful in nonisothermal kinetic analysis of mixtures (Varhegyi et al., 1989) (Eq.13).

In this model mass loss is defined as

$$-\frac{dm}{dt} = \sum_{k=1}^{n} ci\ d\alpha/dt \quad (13)$$

n is number of biomass components, ci is relative amount of component I multiplied by the amount of volatiles formed from a unit mass of that component (Varhegyi et al., 1989).

A separate conversion for each component is defined as (Eq. 14)

$$\frac{d\alpha}{dt} = k0\ e^{-\frac{Ea}{RT}}(1 - \alpha)\text{^}n\text{i} \quad (14)$$

Because of the overlaps observed in biomass mass loss, the term “pseudo component” is used instead of biomass components in evaluating parallel reaction mechanisms, i.e., biomass mass is assumed to be sum of its main pseudo components (DiBlasi, 2008).

These pseudo components are usually considered being closely identified as cellulose, hemicellulose and lignin. In this approximation, however, the proportions of each pseudo-component are not the same as real components because of the interactions between the components and influence of water (Anca-Couce et al. 2014).

The activation energies of the pseudo-components in parallel reaction mechanism are usually similar to activation energies of the original or real components. The reported activation energies of biomass components vary significantly which increased the concerns on the reliability of the experiments and analyzed data (Anca-Couce et al. 2014).

According to Anca-Couce et al. (2014) the difference observed in activation energies of different biomass pseudo components may be caused mainly by the combination of three factors:

1. Heat and mass transport limitations
2. Secondary reactions in experiments
3. Analysis of the data

In analyzing the pyrolysis reaction first a model is postulated which is usually first-order parallel reactions approximation and reaction rate is defined as (Eq. 15)

$$\frac{d\alpha}{dt} = k0\, e^{-\frac{Ea}{RT}}(1 - \alpha) \quad (15)$$

Where α is conversion, k0 is pre-exponential factor, Ea is activation energy, R is gas constant, T (K) is temperature.

After the model selection, the model parameters are fitted using least squares method. In the present work, the Arrhenius equation is approximated by Euler's method and least squares method is performed to minimize the sum of square differences between experimental values of biomass conversion and model conversion.

The fit qualities were calculated using the following equation (Eq. 16).

$$Fit\ quality = \left(1 - \sqrt{\frac{OF}{N}}\right) * 100 \quad (17)$$

OF is the objective function after least squares fitting and N is number of data points.

An interesting utility of first-order parallel reaction model of biomass is that using this model relative composition of biomass can be obtained in addition to activation energy information (Orfão et al.1999). This is a faster method than wet chemical methods in obtaining biomass composition).

2.2.2. Distributed Activation Energy Model (DAEM)

This model assumes that a large number of competing parallel reactions take place during pyrolysis. The distribution of activation energies of these infinite reactions is represented by distribution function of the activation energy f(Ea). The overall reaction kinetics is dependent on distribution function of activation energy and reaction order (Jain et al. 2006). The biomass pyrolysis reaction using DAEM is shown in the Figure 12 (Cai et al. 2013, 2014).

$$\frac{d\alpha}{dT} = \begin{cases} \int_0^\infty \frac{A}{\beta} \exp\left(-\frac{E}{RT}\right)\left[1-(1-n)\int_{T_0}^{T}\frac{A}{\beta}\exp\left(-\frac{E}{RT}\right)dT\right]^{n/(1-n)} f(E)dE & n \neq 1 \\ \int_0^\infty \frac{A}{\beta} \exp\left[-\frac{E}{RT} - \int_{T_0}^{T}\frac{A}{\beta}\exp\left(-\frac{E}{RT}\right)dT\right] f(E)dE & n = 1 \end{cases}$$

Figure 12 Distributed activation energy model

The distribution function used in DAEM is usually taken as Gaussian distribution. The exact analytical solution of DAEM is usually difficult, therefore numerical methods are applied with appropriate mathematical software.

Different biomass pyrolysis reactions were already modelled using DAEM and activation energies and biomass compositions were obtained for biomass components (Cai et. Al. 2013).

2.2.3. Monte Carlo Model

Biomass is a heterogeneous material. Conventional models used for biomass degradation can involve solutions of a high number of differential-algebraic equations. In the kinetic Monte Carlo model, it is assumed all possible reaction pathways to predict the products evolution. The macroscopic reaction

rate and products evolution are estimated using a chemical master equation that determines the probabilistic population of a chemical species at a given future time (Gillespie, 1977, 2007).

Pyrolysis kinetics of different materials such as poly(styrene peroxide) and phenethyl phenyl ether (a lignin model compound) were modelled with Monte Carlo model (Beste and Buchanan, 2012, Vinu et al., 2012, Wang et al., 2017). The model formulations are shown below which include probability distributions of reaction rates and time step (Figure 13).

$$p_r = \frac{R_r}{\sum_{i=1}^{N} R_i}$$

$$\sum_{i=1}^{\mu-1} p_i < x_1 < \sum_{i=1}^{\mu} p_i$$

$$\tau = \frac{1}{\sum_{r=1}^{N} R_i} \ln\left(\frac{1}{x_2}\right)$$

Figure 13 Monte Carlo kinetic model

3. Chapter 3 Thermogravimetric Analyses

3.1. TGA-DSC Experimental Procedure

A Perkin Elmer STA 6000 was used to carry thermogravimetric analysis (TGA) of biomass samples (Figure 14). In pyrolysis experiments a stepwise heating program was used. In the first step biomass samples were kept isothermally at 30 °C for 10 min., this step was followed by a heating step till 800 °C with heating rates varied between 5 to 200 °C/min. In the third step biomass samples are kept isothermal for 10 min. at 800 °C. In the fourth step biomass samples were cooled with a programmed cooling rate of 50 °C/min. In all pyrolysis experiments nitrogen flow rate was set to 20 ml/min and alumina pans are used. Biomass weights were registered 500 times per minute.

Analyzed biomass types include Turkey oak (*Quercus cerris*) corks of 20-40, 40-60, and 60-80 mesh particle sizes, *Q. cerris* phloem of 40-60 mesh particle size, Ponytail palm (*Beaucarnea recurvata*) cork of 40-60 mesh particle size and birch (*Betula pendula*) cork of 40-60 mesh particle size.

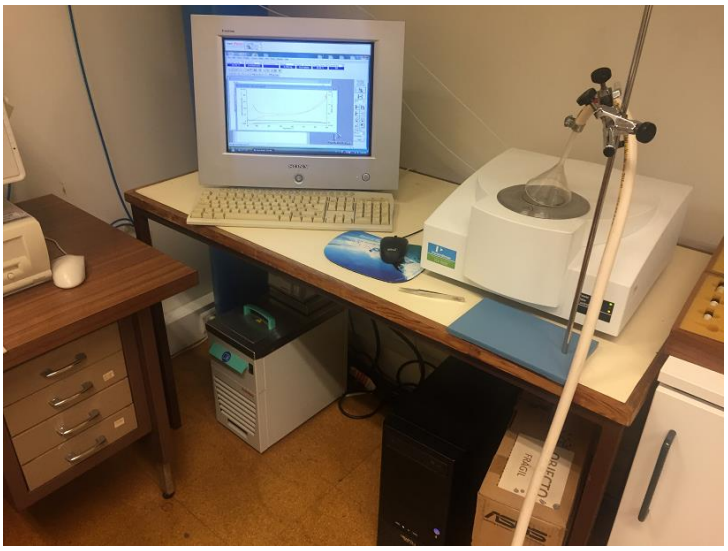

Figure 14 Thermogravimetric Analyzer

3.2. Overview of pyrolysis experiments and kinetic modelling

In all pyrolysis experiments cork samples started decomposing approximately at 200 °C and a fast mass loss pattern is observed until 470 °C followed by a slow decomposition step (Figure 15). It is interesting to note that at lower temperatures and fast decomposition step biomass thermograms almost superimposed while at high temperatures and slow decomposition steps vary in reproducibility tests (Figure 15). This variation can be due to the natural variability of the biomass in terms of its detailed composition, which is translated into differences in the perceived pseudo components.

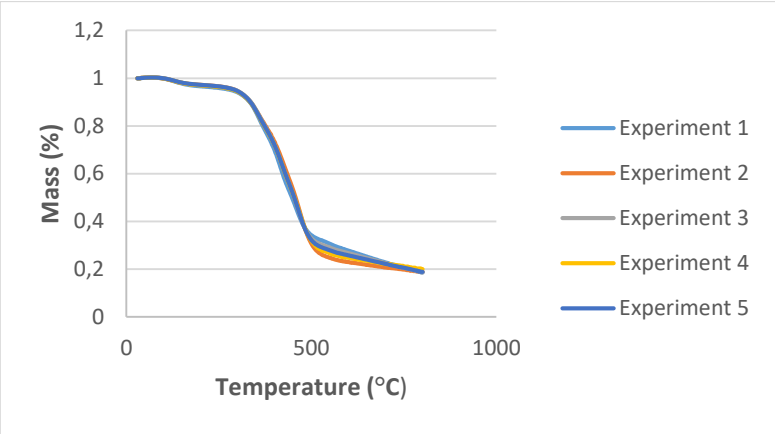

*Figure 15 Comparison of reproducibility experiments (*Q. cerris *cork, 40-60 mesh, 50 °C/min heating rate)*

In general, all six biomass types start decomposition at approximately 200 °C and 10-25% unconverted product or char was obtained. Mass loss curves shifted to the right with increasing heating rates (Figure 16, Figure 17, Figure 18). The higher mass loss values obtained with higher heating rates of 150 °C/min and 200 °C/min must be related with the variation of biomass chemical composition.

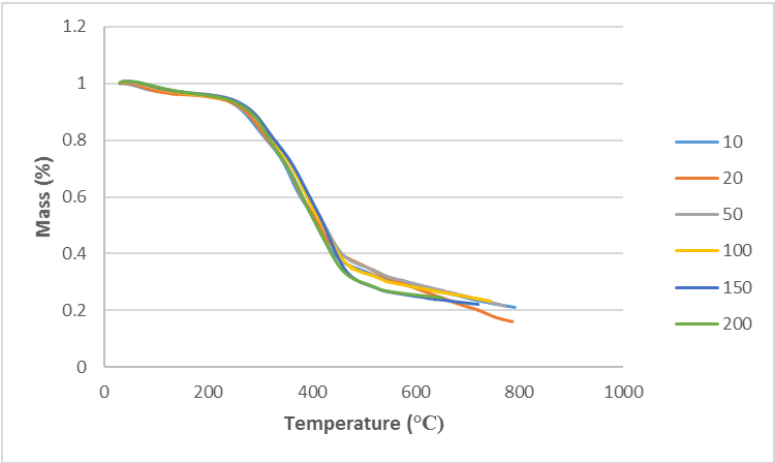

Figure 16 Comparison of cork pyrolysis (20-40 mesh) at different heating rates (°C/min)

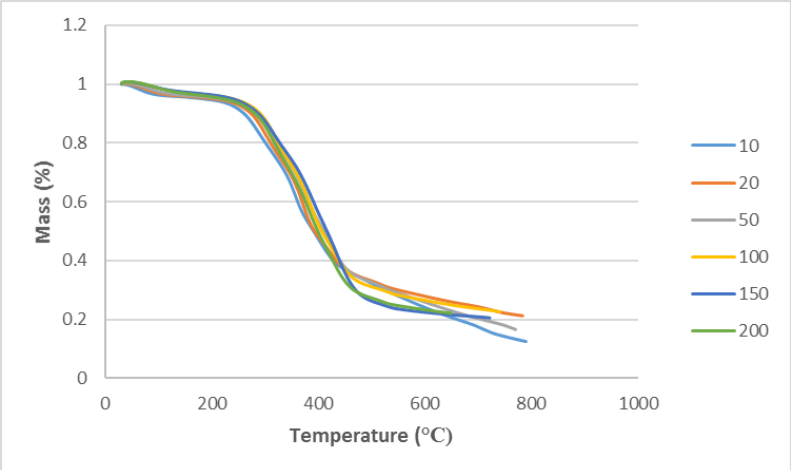

Figure 17 Comparison of cork pyrolysis (40-60 mesh) at different heating rates (°C/min)

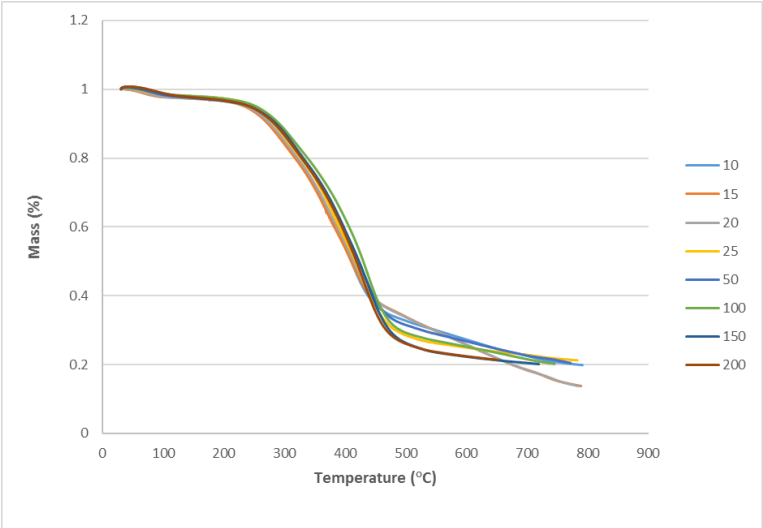

Figure 18 Comparison of cork pyrolysis (60-80 mesh) at different heating rates (°C/min)

First-order parallel reaction modelling allowed good fits to the experimental data. The detailed results of these experiments are shown in Appendix I-VI.

In the beginning of the modelling experiments four, five, and six pseudo component plus char models were developed as explained in the kinetic modelling section. These models were tested using 40-60 mesh (0.25-0.42 mm) and 60-80 mesh (0.18-0.25 mm) *Q. cerris* cork particles at different heating rates for their subsequent application in all biomass types. The results show that four and five pseudo component models fitted best with 40-60 mesh particles, while six pseudo component models fitted best with 60-80 mesh particles (Figure 19). Since fast pyrolysis of biomass require fine biomass particles, six pseudo component modelling was applied in the following experiments. The modelling results of 6 biomass types are summarized in Appendix VII-VIII.

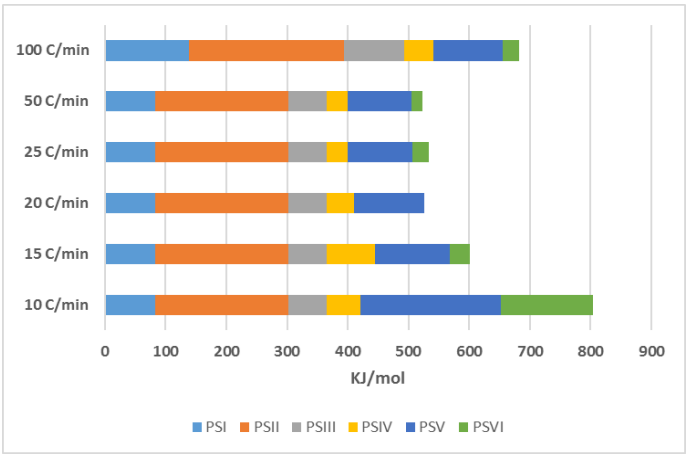

Figure 19 Comparison of activation energies obtained after modelling of pyrolysis for six pseudo components (Program temperature is used for comparison, 60-80 mesh Q. cerris cork was used)

The individual fitting qualities are generally good. In the next step, using six pseudo component models, global and flexible modellings were developed to combine all modellings into one global model. The global model simultaneously takes into account of changes in model parameters (frequency factor, activation energy and biomass composition) at different heating rates. Activation energies for each pseudo components as well as biomass compositions were calculated by this way. In Table 5 and Table 6 the results of global models were shown.

Table 5 Global Model Quercus cerris corks

Pseudo components	*Q. cerris* cork 20-40 mesh		*Q. cerris* cork 40-60 mesh		*Q. cerris* cork 60-80 mesh	
	Ea (kJ/mol)	x	Ea (kJ/mol)	x	Ea (kJ/mol)	x
Ps 1	32.0	0.05	30.7	0.05	37.7	0.04
Ps 2	241.5	0.22	228.1	0.19	259.4	0.21
Ps 3	141.5	0.17	136.3	0.24	167.7	0.16
Ps 4	36.7	0	81.2	0.18	222.4	0.08
Ps 5	247.3	0.21	311.9	0.16	325.2	0.25
Ps 6	130.4	0.12	220.5	0.09	307.3	0.08
Char		0.23		0.09		0.18

Table 6 Global Model Quercus cerris phloem, Ponytail palm cork, Birch cork

Pseudo components	*Q. cerris* phloem 40-60 mesh		Ponytail palm cork 40-60 mesh		Birch cork 40-60 mesh	
	Ea (kJ/mol)	x	Ea (kJ/mol)	x	Ea (kJ/mol)	x
Ps 1	75.4	0.06	96.2	0.09	87.6	0.08
Ps 2	252.6	0.10	214.2	0.22	222.3	0.11
Ps 3	123.9	0.46	237.3	0.28	553.7	0.24
Ps 4	120.1	0.06	111.4	0.16	283.8	0.19
Ps 5	543.8	0.04	376.1	0.14	164.7	0.12
Ps 6	113.8	0.04	39.3	0	62.7	0.09
Char		0.24		0.11		0.17

From the activation energies and compositions indicated in Table 5 and Table 6 it is possible to assign components to each pseudo component. Therefore, the first pseudo component is clearly assigned to moisture. Its content is much lower in *Q. cerris* corks than other biomass types. Second and third pseudo components were assigned to hemicelluloses and cellulose. The higher activation energy pseudo component possibly corresponds to cellulose degradation. Their similar biomass ratio (close to 1) in corks supports this assumption. The fourth pseudo component is unclear. It may belong to overlapping decompositions of biomass components or extractives. The fifth pseudo component is assigned to suberin. Its relative composition is relatively higher in *Q. cerris* cork; it is present as a residual suberin in phloem and its content is lower in ponytail palm and birch corks. The last pseudo component is assigned to lignin. This is also supported by the amount of char since lignin contributes mainly to char formation (DiBlasi, 2008).

Flexible modelling is similar to global kinetic modelling but instead of adjusting all three model parameters i.e., activation energy (Ea), frequency factor (k0), and biomass composition (x) into a rigid model, it allows for variation of biomass composition. This was included since, as it was observed in the reproducibility tests, the apparent fraction corresponding to each mass loss varies for the same sample under the same condition, probably due to the differences in the detailed composition of each individual sample. The results of flexible modelling are shown in Table 7 and in Table 8.

Table 7 Flexible Model Quercus cerris corks

Pseudo components	*Q. cerris* cork 20-40 mesh		*Q. cerris* cork 40-60 mesh		*Q. cerris* cork 60-80 mesh*	
	Ea (kJ/mol)	x range	Ea (kJ/mol)	x range	Ea (kJ/mol)	x range
Ps 1	82.5	0.03-0.08	82.5	0.01-0.06	42.5	0.02-0.03
Ps 2	219.8	0.02	275.0	0-0.02	438.4	0.01-0.09
Ps 3	62.5	0.29-0.65	87.3	0.28-0.61	62.5	0.28-0.58
Ps 4	35.3	0-0.27	6.1	0.28-0.29	55.8	0.10-0.28
Ps 5	125.7	0-0.29	105.9	0-0.23	231.2	0-0.11
Ps 6	49.2	0-0.12	26.7	0-0.69	151.2	0-0.24
Char range		0.08-0.18		0.15-0.20		0.06-0.19

*15 °C/min and 25 °C/min heating rates were used instead of 150°C/min and 200 °C/min

Table 8 Flexible Model Quercus cerris phloem, Ponytail palm cork, Birch cork

Pseudo components	*Q. cerris* phloem 40-60 mesh		Ponytail palm cork 40-60 mesh		Birch cork 40-60 mesh	
	Ea (kJ/mol)	x range	Ea (kJ/mol)	x range	Ea (kJ/mol)	x range
Ps 1	49.6	0.01	64.0	0.03-0.08	71.3	0.05-0.06
Ps 2	234.5	0.08	139.6	0-0.07	134.2	0-0.07
Ps 3	116.2	0.12-0.31	94.1	0.49-0.67	118.6	0.17-0.36
Ps 4	6.1	0	190.7	0	98.6	0.16-0.22
Ps 5	8.8	0.66-0.72	40.3	0.11-0.31	315.7	0.11-0.25
Ps 6	47.3	0-0.39	18.8	0.05-0.06	28.9	0
Char range		-		0.05-0.11		-

The flexible modelling results show that by allowing this sort of variability indicates that the six pseudo component model is not entirely satisfactory to explain the experimental data and that the number of pseudo components can actually be reduced. Therefore, the number of pseudo components were reduced to five and the modelling was repeated. The resulting model provided a better fit (Table 9).

Table 9 Modeling of Birch cork pyrolysis kinetics with five pseudo components model

Pseudo components	Flexible model		Global model	
	Ea (kJ/mol)	x range	Ea (kJ/mol)	x
Ps 1	43.5	0.06-0.07	38.6	0.07
Ps 2	143.8	0.07-0.26	380.7	0.18
Ps 3	561.8	0-0.15	234.4	0.06
Ps 4	141.3	0.19-0.26	369.7	0.26
Ps 5	46.9	0.13-0.40	232.2	0.24
Char range		0.19-0.25		0.19

As it can be seen from the Table 9, although five pseudo component flexible and global models give similar biomass compositions, they differ in the estimated activation energy values.

Bootstrap method was used to evaluate uncertainty and % errors of the kinetic models. The evaluation includes variability in six pseudo component values with respect to three kinetic parameters (Ea, k0 and xi). A total of 15 repetitions were carried, one third of the model data (3698 data points in each model) were randomly replaced and new simulations were carried.

The results showed that % Error in activation energies (95% confidence level) varied between 0.1% an 8.9%; while in compositions the variation was between 0.1% and 1.2%.

3.3. DSC Analysis

Heat flow (the amount of energy absorbed or released by the sample) during pyrolysis reactions is an important parameter to understand pyrolysis reactions. The heat flow in this work was measured with the same TGA/DSC equipment simultaneously with the mass evolution.

The results of DSC analysis are somewhat surprising (Figure 20**,** Figure 21**,** Figure 22**,** Figure 23**,** Figure 24**,** Figure 25). At lower heating rates pyrolysis reaction is essentially endothermic, while at higher heating rates it becomes exothermic. This is exactly opposite of what was expected, i.e., at lower heating rates the dehydration reaction is expected to predominate leading to formation of new bonds and heat release and at higher heating rates decomposition reaction is expected preferentially (Chaiwat et al. 2009). In order to check that the heat flow correctly assigned, a drop of water was added to 60-80 mesh *Q. cerris* cork before heating it at 200 °C/min program. Blank heat flow experiments were carried to subtract blank heat flow from the actual heat flows.

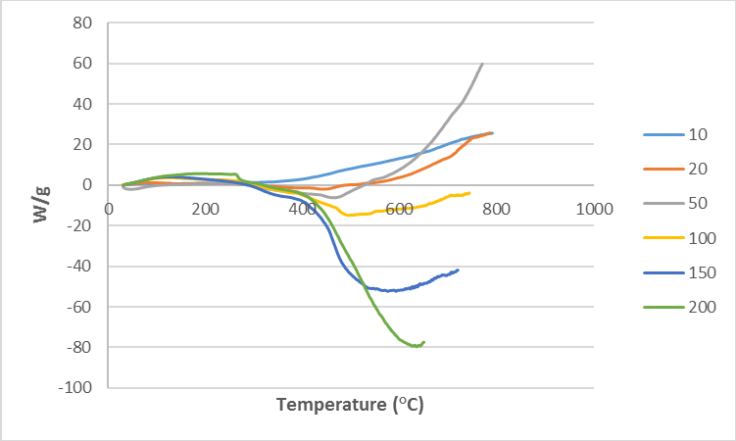

Figure 20 Heat flow Q. cerris cork 20-40 mesh

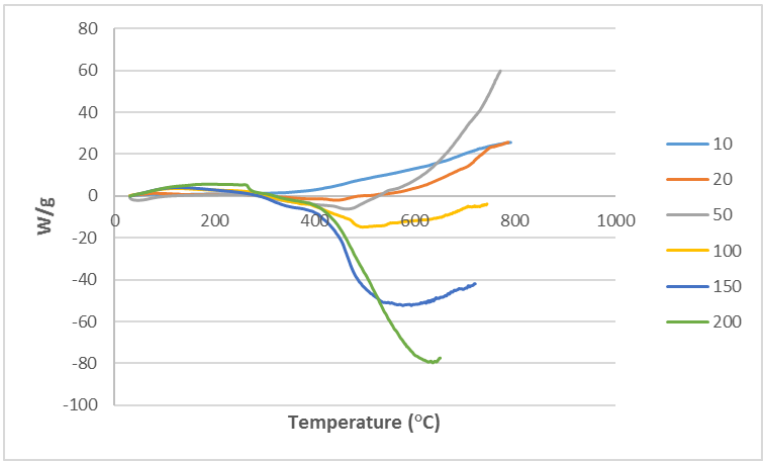

Figure 21 Heat flow Q. cerris cork 40-60 mesh

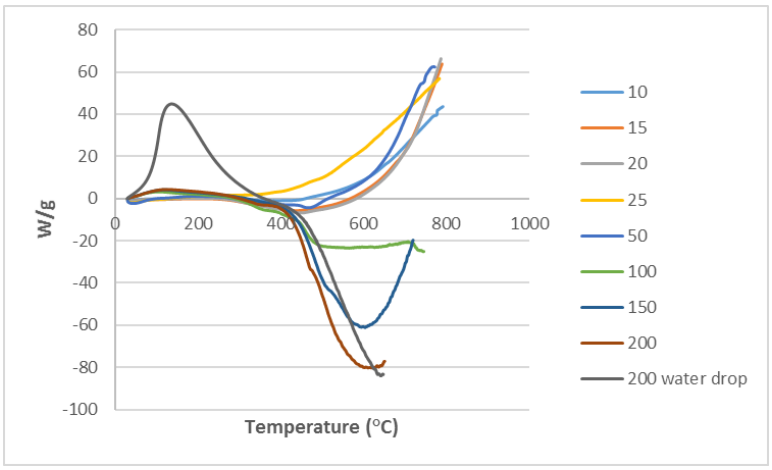

Figure 22 Heat flow Q. cerris cork 60-80 mesh

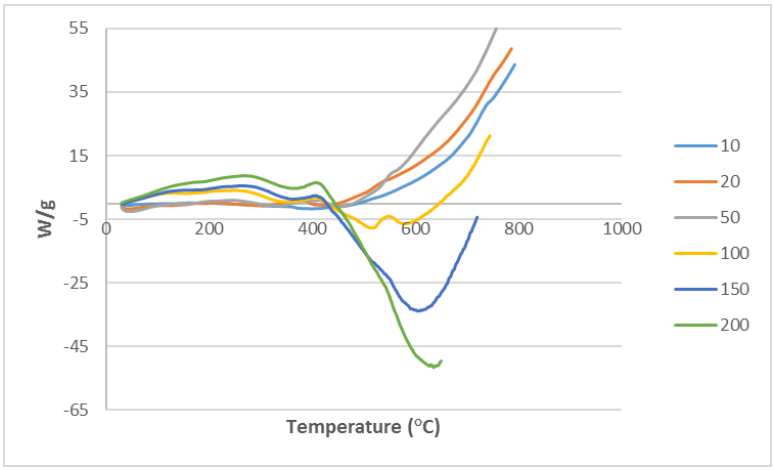

Figure 23 Heat flow Q. cerris phloem

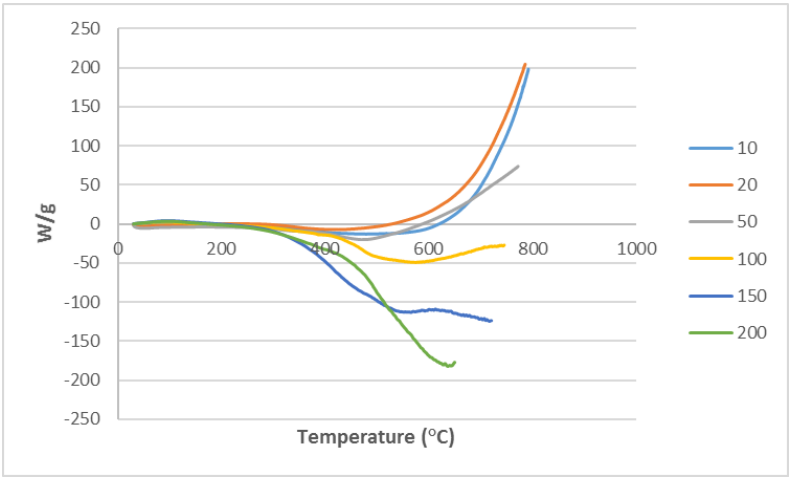

Figure 24 Heat flow B. recurvata cork

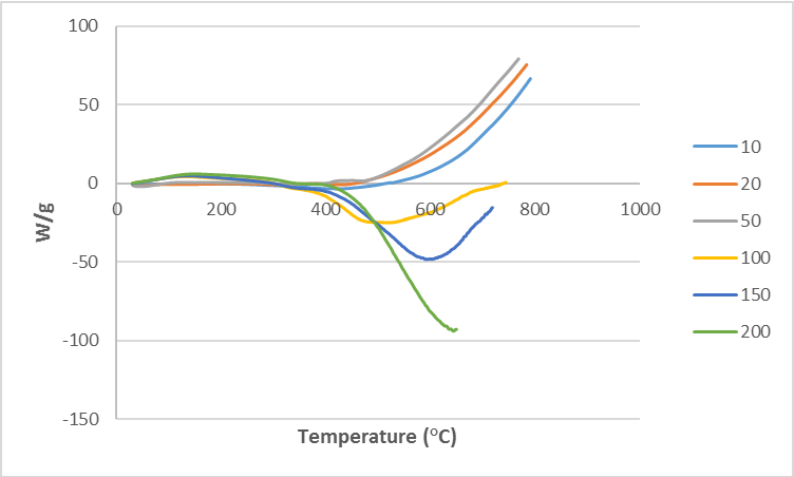

Figure 25 Heat flow B. pendula cork

3.4. DTG Analysis

Differential thermogravimetry (DTG) is another tool to study the pyrolysis reaction. By applying DTG analysis it is possible to identify the number of different decompositions during pyrolysis reaction. These decompositions can be assigned to different pseudo components of biomass. The DTG curves of *Q. cerris* cork shows distinct peaks at temperatures approximately 100 °C, 325 °C, 380 °C, 435 °C and 700 °C (Figure 26). The pyrolysis reaction of 60-80 mesh *Q. cerris* cork seems to be more homogeneous than 40-60 and 20-40 mesh particle sizes, indicating a possible difference in chemical composition or a heat transfer limitation in bigger particles. Lédé and Villermaux (1993), Lédé (1994) and Narayan and Antal (1996) showed that large thermal gradients occur in pyrolysis when large biomass samples are used or when high heat fluxes are used.

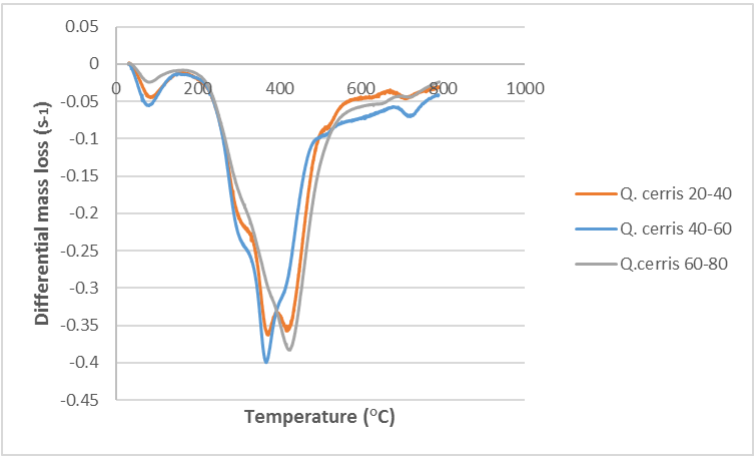

Figure 26 Q. cerris DTG peaks (heating rate: 10 °C/min)

At higher heating rates these peaks become more evident and new peaks such as the peak at 530 °C is observed (Figure 27).

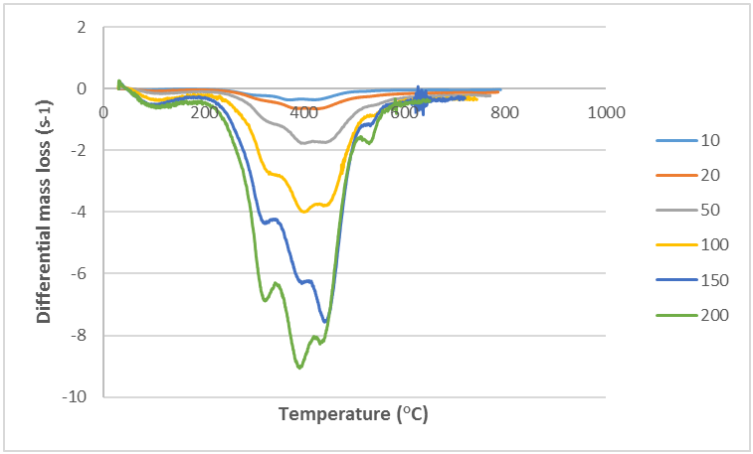

Figure 27 Q. cerris *20-40 mesh DTG curves at different heating rates (°C/min)*

The other corks and phloem shows similar DTG pattern. Between these biomass types ponytail palm cork undergoes a relatively homogeneous degradation (Figure 28).

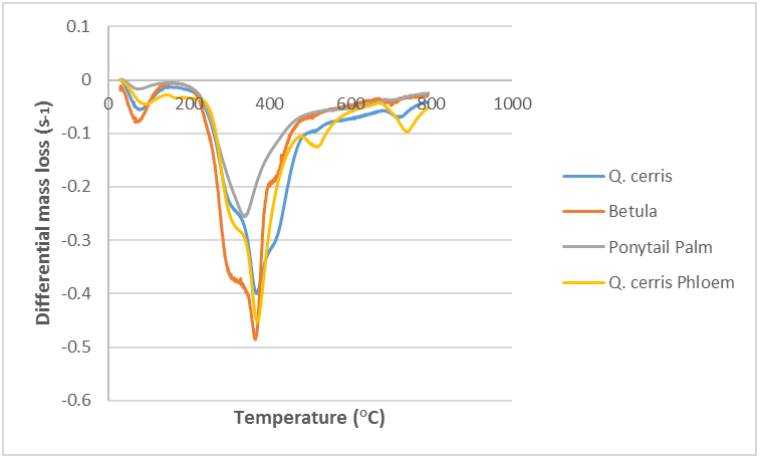

Figure 28 DTG curves comparision of different corks

It is possible to model the DTG curves by multi-peak fitting using Qtiplot software. The DTG curve of 20-40 mesh *Q. cerris* cork is modelled using 5 component Gaussian function or 6 component Lorentz function (Figure 29, Figure 30). In these models, the highest peak at higher temperature is assigned to suberin decomposition. The smaller peaks at lower temperatures are assigned to hemicelluloses and cellulose degradation. The first peaks is assigned to humidity and the last curve is assigned to lignin degradation which occurs a broad range of temperatures.

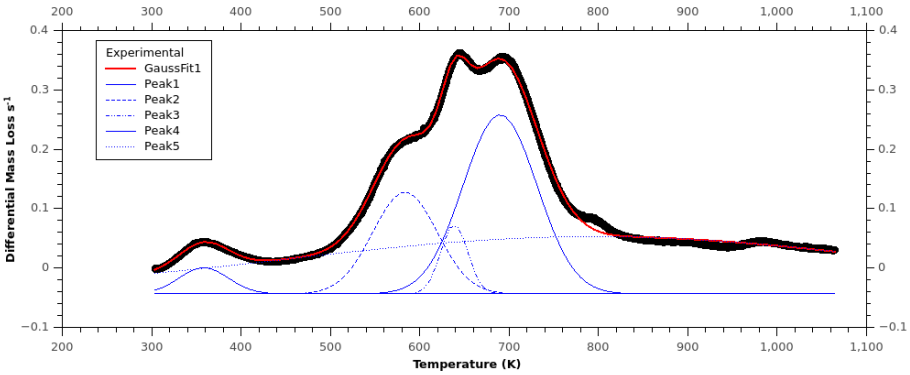

Figure 29 Gaussian fitting DTG curve of Q. cerris cork (20-40 mesh)

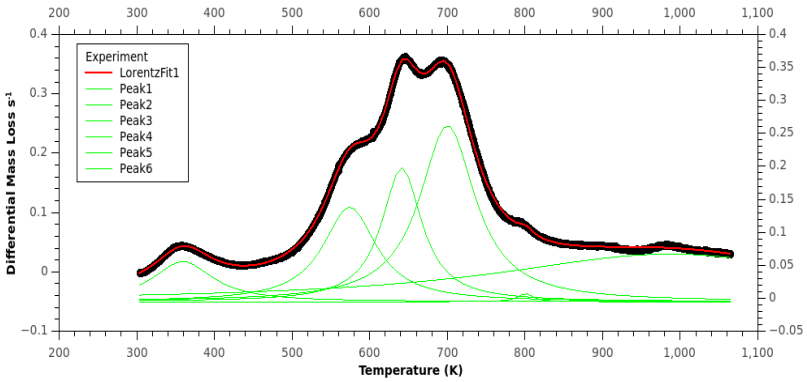

Figure 30 Lorentz fitting Q. cerris cork (20-40 mesh)

4. Chapter 4 Fast Pyrolysis Experiments

In fast pyrolysis fluid bed reactors are most widely used reactors. Because they offer high heat transfer rates and good temperature control (Papadikis et al. 2008). According to Van Velden et al. (2010) the heat transfer coefficient (h) vary between 10 to several hundred W $m^{-2}K^{-1}$ from static beds to fluid bed reactors. However, fluid bed reactors have disadvantage of char entrainment in vapor phase resulting secondary cracking in the vapor phase and reduced bio-oil stability (Park et al. 2009).

In this chapter, the results of the fast pyrolysis experiments carried in bench-scale in Portugal and in pilot-scale at Karlsruhe Institute of Technology in Germany are discussed. For bench scale fast pyrolysis analysis, two glass fixed-bed reactors were designed and tested under high nitrogen gas velocities. For pilot scale experiments a screw-type reactor was used.

4.1. Bench scale modified fixed bed reactor

In the first experiment approximately 60-80 mesh *Q. cerris* cork was pyrolyzed at 500 °C using the designed temperature-controlled Schlenk-type reactor (Figure 31, Figure 32).

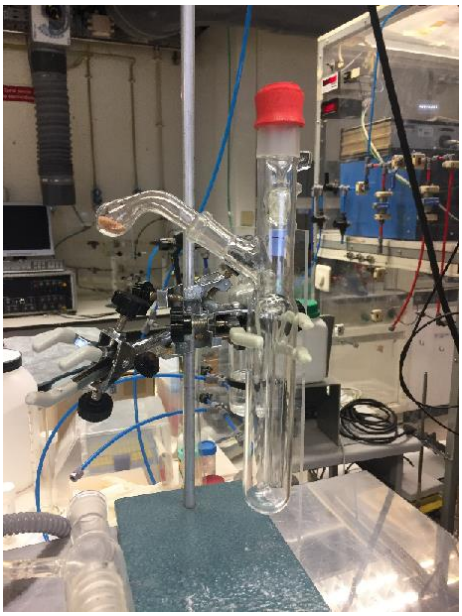

Figure 31 Bench scale test reactor

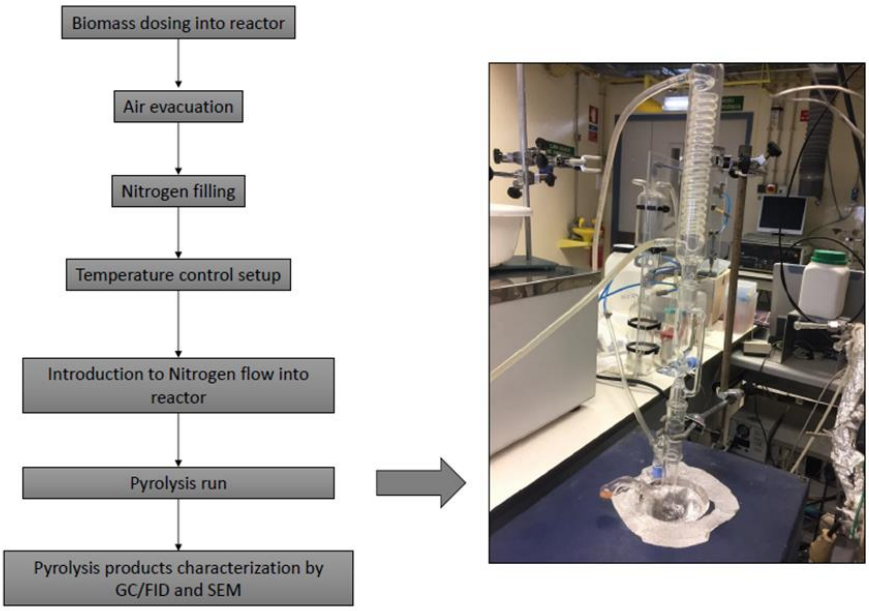

Figure 32 Bench scale pyrolysis experiment

The reaction was carried considering short vapor residence time. The solid residence time was set to 1h. After the reaction was completed the product yields were calculated. The pyrolysis reaction resulted with approximately 6% liquid yield and 60% solid yield. The gas yield was calculated by difference. The low liquid yield is related to insufficient heat transfer.

In the second experiment, a bigger reactor with the same design was used to allow higher amount of mass conversion. The reactor was immediately shut down after the cork was introduced leading to a decreasing temperature gradient for solid product (char). The product yields of this experiment were not different from first experiment. These results show that short vapor residence time alone is not sufficient to obtain high bio-oil yields. Higher heating rates using a heat carrier and sweeping gas must be introduced in the bottom of the reactor in fluid bed or spout bed type.

4.2. Pilot scale twin-screw reactor experiments

The fast pyrolysis unit of Karlsruhe Institute of Technology (KIT) is a part of Bioliq® project in which agricultural wastes are converted to high quality fuels by fast pyrolysis followed by gasification.

The purpose of twin-screw mixing reactor is to mix biomass samples with pre-heated heat carrier. Thus high heat transfer rates are obtained. The heat carrier used is steel balls which is recirculated with a bucket elevator, re-heated with electrical heater and re-used in the reactor. The input capacity of the process is 10 kg h^{-1} biomass (Figure 33) (Funke et al. 2016).

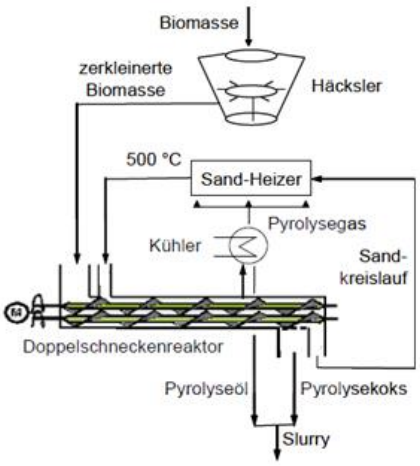

Figure 33 Twin-screw fast pyrolysis reactor (Kaltschmitt et al. 2009)

The fast pyrolysis process results with three products: aqueous condensate, organic condensate or bio-oil and solid char. The process flow diagram of the fast pyrolysis process clarifies the procedure (8-char storage, 10-organic condensate storage and 14-aqueous condensate storage) (Funke et al. 2016) (Figure 34).

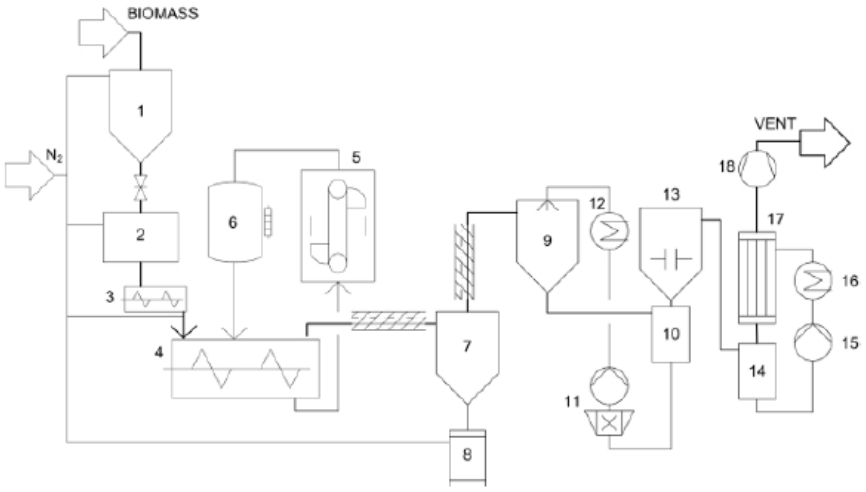

Figure 34 Process flow diagram of fast pyrolysis process (Funke et al. 2016)

The process is particularly suitable to convert high ash containing biomass such as wheat straw. Although high ash content in biomass increases gas and char yields (thus reduces organic yield), it also causes two-phase bio-oils which is easier to separate. Also ash-rich biosyncrude (bio-oil and char mixture) can be used for gasification process in slagging-type reactors for producing fuels and chemicals (Dahmen et al. 2012).

In the present study, low-grade cork and phloem samples from ground *Q. cerris* bark were tested in the pilot plant to calculate product yields and to obtain product compositions (Table 12). A twin-screw reactor was used to pyrolyze ground *Q. cerris* cork and phloem fractions at 500 °C (Std: 1.4 °C).

The operational procedure was following:

Reactor length is 1.5 m, screw diameter is 4 cm. Biomass feed rate was 10 kg h^{-1}. Vapor residence time was less than 2 s. The mass ratio of biomass to heat carrier (steel balls) was between 1:100. After the experiment two condensate (organic-rich, and water-rich, respectively) fractions were obtained at temperatures approximately 86 °C and 12 °C respectively (Std: 3.8 °C and 0.5 °C, respectively) in addition to bio char fraction (Kaltschmitt et al. 2009, Dahmen et al. 2012, Funke et al. 2016). First cork and phloem test samples were weighted and introduced to dosing system, after this step the biomass was fed to reactor with computer controlled system. After the pyrolysis experiments char and liquid product fractions were obtained (Figure 35**,** Figure 36**,** Figure 37**,** Figure 38).

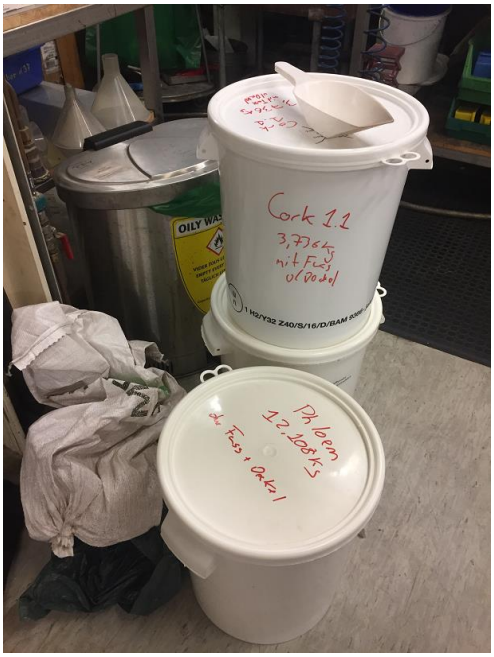

Figure 35 Preparation of biomass for fast pyrolysis experiments

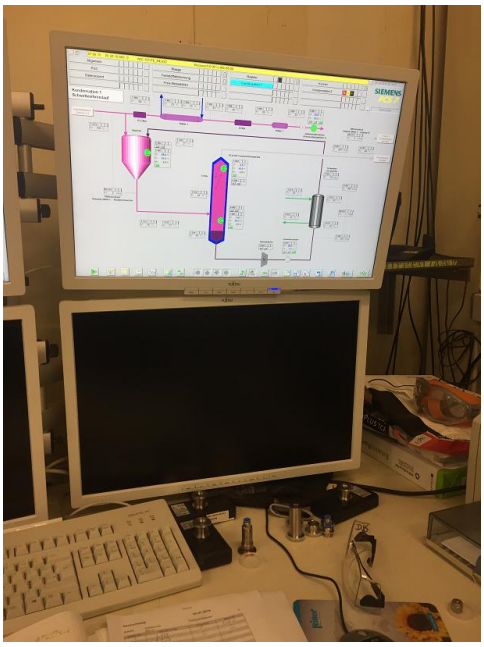

Figure 36 Process control during fast pyrolysis

Figure 37 Char storage after fast pyrolysis

Figure 38 Bio-oil fractions

Unfortunately, it was not possible to pyrolyze the cork fraction due to problems encountered in the feeding system when using that fraction due to the plasticity of the material. The phloem fraction, however was well pyrolyzed. The results of the fast pyrolysis of phloem show that 48-56% bio-oil yield is possible in an as received basis (Table 10). As dry basis the bio-oil yield reduces to approximately 37% (Table 11). It can be concluded that the organic yield is comparably high given the high amount of ash contained in the feedstock. For comparison, typical organic yield for wheat straw in the twin-screw reactor is also 30 % although the ash content is much lower (typically 6-8 % on a dry weight basis) (Funke et al. 2016).

Table 10 Results of the phloem fast pyrolysis yields as received basis

	Organic condensate (%)	Aqueous condensate (%)	Char (%)	Gas (%)	Deficit (%)
Experiment 1	41	7	14	21	17
Experiment 2	48	8	17	20	7

Table 11 Results of the phloem fast pyrolysis yields as dry basis

	Organic condensate (%)	Aqueous condensate (%)	Char (%)	Gas (%)	Deficit (%)
Experiment 1	29	4	16	23	28
Experiment 2	37	3	20	22	18

5. Chapter 5 Biomass and Pyrolysis Products Characterization

Pyrolysis reaction results with solid (char), liquid (bio-oil) and gas products. Characterizations of the pyrolysis products are important in determining their potential applications. Proximate analysis allows a screening of biomass based on their fuel properties. Therefore, in this chapter the characterizations of these products are discussed.

5.1. Proximate Analysis and HHV Modelling

Proximate analysis is the determination of moisture, volatile (volatile matter), fixed carbon and ash (inorganic) contents of biomass. It is used mainly characterizations and classification of coals (Speight, 2015). In the present study, the proximate analysis was carried with thermogravimetric analyzer by application of pyrolysis and combustion heat treatments. The moisture content and volatile matter data was obtained from pyrolysis experiments. The ash content was obtained from combustion experiments. The fixed carbon content was calculated by mass difference.

The results of the proximate analysis show that in general cork species contain 2.7 % moisture, 81.5 % volatiles, 13.2 % fixed carbon and 2.8 % ash (Table 12). Highest standard deviation was observed in ash contents (2.7 %) while in fixed carbon, volatile and moisture contents the standard deviation values were 2.0 %, 1.5% and 0.7%, respectively. *Q. cerris* phloem and *B. recurvata* corks contained highest and lowest amount of ash contents, respectively.

Table 12 Proximate analysis of cork species

Parameter (%)	*Q. cerris* cork 20-40 mesh	*Q. cerris* cork 40-60 mesh	*Q. cerris cork* 60-80 mesh	*Q. cerris* phloem 40-60 mesh	*B. recurvata cork* 40-60 mesh	*B. pendula cork* 40-60 mesh
Moisture	2.5	3.0	2.0	2.7	1.7	4.0
Volatile Mat.	81.6	82.2	81.8	79.7	84	79.5
Fixed Carbon	12.4	12.7	14.6	9.4	14.2	15.4
Ash	3.6	2.1	1.6	8.2	0.1	1.1

Proximate analysis can be used to predict higher heating values (HHV's). Different mathematical models were developed based on proximate analysis to estimate higher heating values (Demirbas, 1997, Cordero et al. 2001, Nhuchhen and Salam 2012, Vargas-Moreno et al. 2012).

The model suggested by Demirbas (1997) only takes fixed carbon content and estimates HHV as

HHV (MJ/kg) = 0.196 X Fixed Carbon (%) + 14.199;

The two models by Cordero et al. (2011) also consider volatile matter and ash contents.

The estimates of HHV is

HHV (MJ/kg) = 0.3543 x Fixed carbon (%) + 0.1708 x Volatile matter (%), (1)

HHV (Mj/kg) = 35.43- 0.1835 x Volatile matter (%). 0.35.43 x Ash (%); (2)

The estimate of Nhuchhen and Salam (2012) calculates HHV as

HHV (MJ/kg) = 19.288-0.2135 x Volatile matter (%)/Fixed carbon (%) + 0.0234 x Fixed carbon (%)/ Ash (%)- 1.9584 x Ash (%)/volatile matter (%)

The estimates of higher heating values by using the above-mentioned models are given in Table 13.

Table 13 Modelling of higher heating values of biomass based on proximate analysis

Estimates of HHV (MJ/kg)	*Q. cerris* cork 20-40 mesh	*Q. cerris* cork 40-60 mesh	*Q. cerris cork* 60-80 mesh	*Q. cerris* phloem 40-60 mesh	*B. recurvata cork* 40-60 mesh	*B. pendula cork* 40-60 mesh
Demirbas (1997)	16.6	16.7	17.1	16.0	17.0	17.2
Cordero et al. 2001 (1)	19.0	19.3	19.9	17.6	20.1	19.7
Cordero et al. 2001 (2)	19.2	19.6	19.9	17.6	20.1	19.7
Nhuchen and Salam (2012)	17.9	18.0	18.3	17.3	21.3	18.5

It was found in the current study that the estimate of Cordero et al. (2001) (1) can be used to model cork HHV.

5.2. Charcoal

Charcoal or biochar is the solid fraction produced in all pyrolysis process. The char yields vary up to 80 % in torrefaction to 12 % in fast pyrolysis (Bridgwater, 2012). The char fraction obtained after pyrolysis of biomass is free from sulfur, it may have very small amount of nitrogen, and it has lower ash content than coal (Antal and Gronli, 2003). Charcoals can be used for energy production or it can be used in various applications including soil-amendment and carbon sequestration (Laird, 2008; Ronsse et al. 2013).

In order to characterize the charcoal samples scanning electron microscopy (SEM) analyses were carried at Instituto Superior de Agronomia, using Hitachi TM3030Plus electron microscope (Figure 39). The instrument was operated at 15 kV acceleration potential and a working distance of 1 mm.

Figure 39 Scanning Electron Microscope

The analyzed samples were char samples obtained after bench-scale experiments (identified as temperature gradient and isothermal samples). Also cork samples that were subject to three different final temperatures (400 °C, 450 °C, and 500 °C respectively) in TGA/DSC equipment with 100 °C/min heating rate program were also analyzed.

The results of the SEM analyzes show that the degradation of cellular structure of *Q. cerris* cork increases with pyrolysis temperature and pyrolysis time (Figure 40). Char samples retain their cellular structure after 400 °C final treatment (Figure 41). Cell collapses and degradations were observed at 450 °C final treatment (Figure 42). Even after 500 °C final treatment cork cell structure were conserved but cell wall thicknesses were significantly reduced with high amount of cell collapses (Figure 43**).** Calcium oxalate crystals becomes visible after 500 °C final treatment **(**Figure 44).

Second bench scale pyrolysis experiment resulted more porous chars than the first experiment where the treatment was considered as isothermal since the thermal degradation occurs essentially in the first hour of heat treatment (Figure 45, Figure 46).

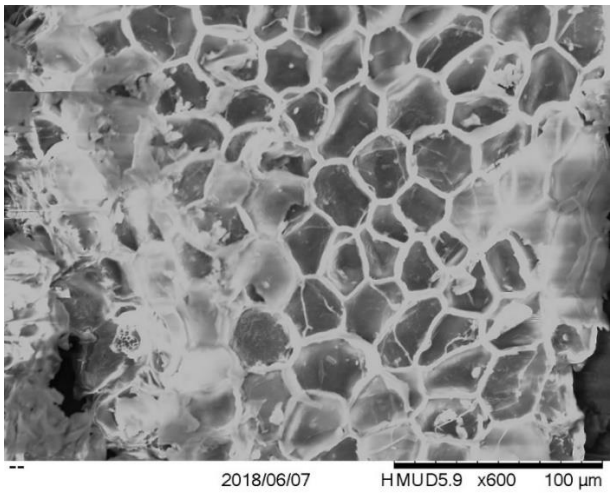

Figure 40 Untreated cork particle

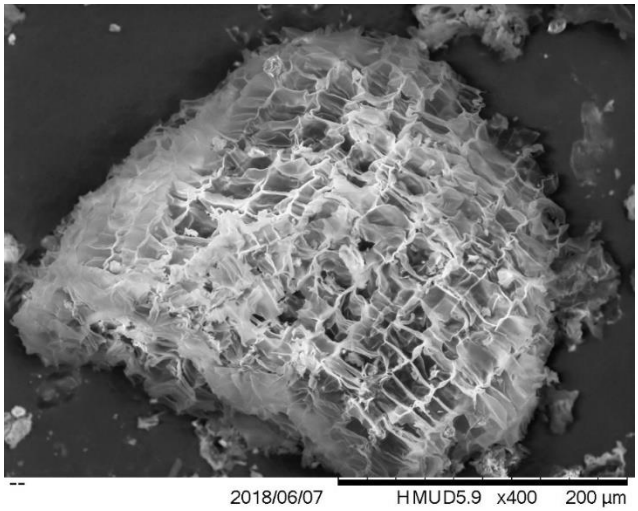

Figure 41 Cork particle pyrolyzed at 400 °C

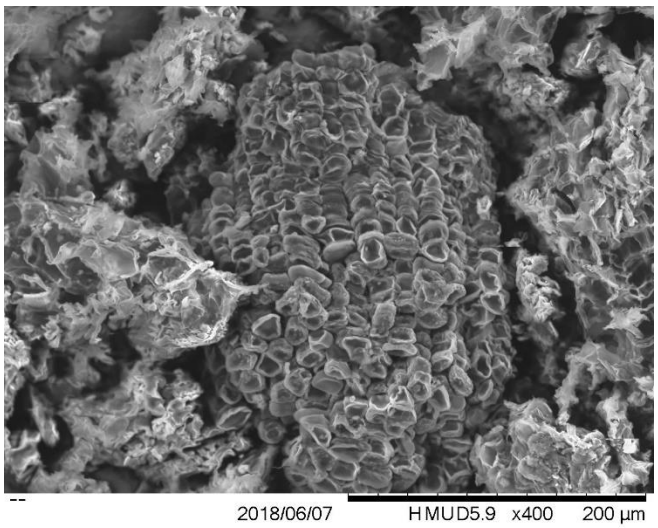

Figure 42 Cork particle pyrolyzed at 450 °C

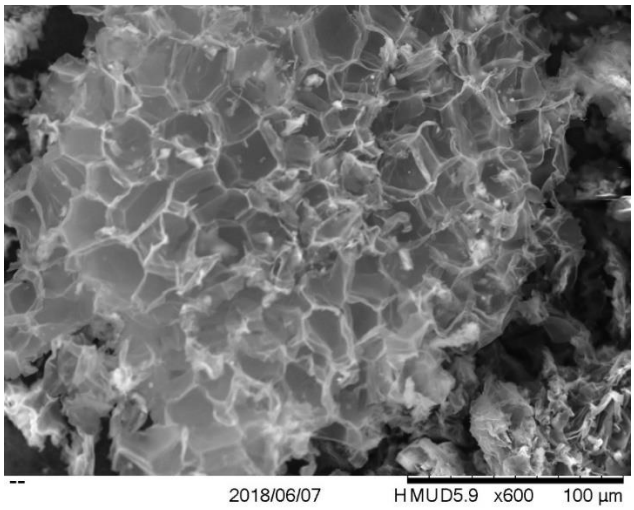

Figure 43 Cork particle pyrolyzed at 500 °C

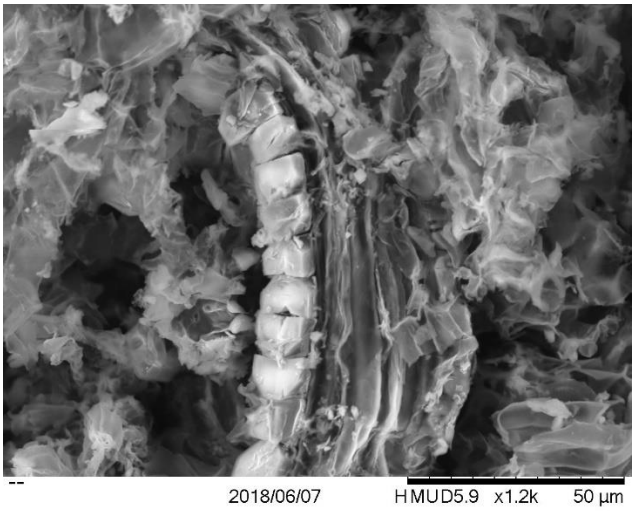

Figure 44 Calcium oxalate crystals in cork particle pyrolyzed at 500 °C

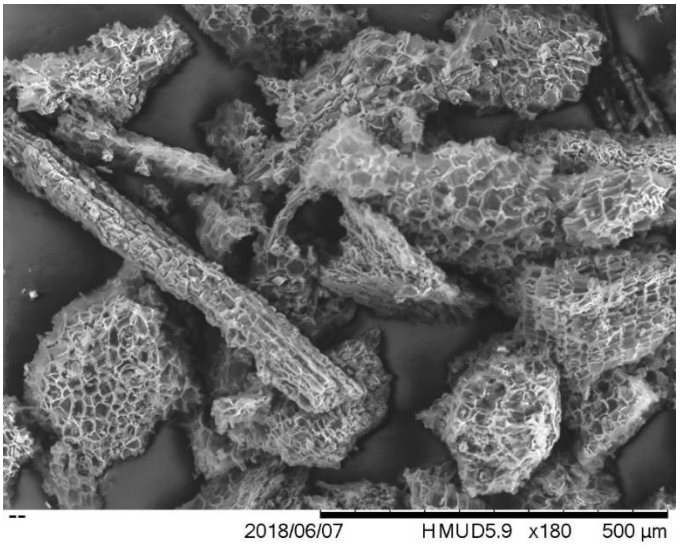

Figure 45 Cork particles obtained after bench scale temperature gradient pyrolysis

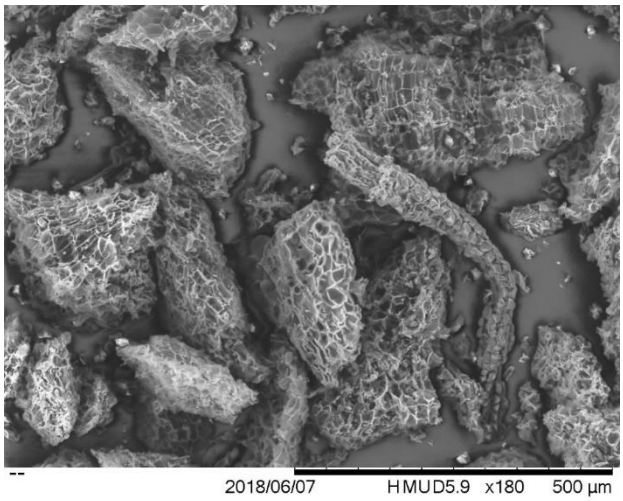

Figure 46 Cork particles obtained after isothermal pyrolysis

The overall results indicate that biochars obtained from *Q. cerris* corks have a promising potential to be used as soil amendment agents. Because they retain their cellular structure, they have low density and they have liming potential as indicated by the presence of calcium oxalate crystals. However, for best adsorption performance, heat treatment final temperature should be lower than 500 °C and in reactor experiments gradient type heating should be used.

5.3. Bio-oil

In order to characterize the second pyrolysis product bio-oil, a Perkin-Elmer Clarus 680 gas chromatograph (Figure 47) was used. The chromatograph is equipped with a flame ionization detector (FID) and an SGE BP1 capillary column 30m long x 0.25mm width (Table 14). The injector and detector were kept at 340 ºC during the experiment, and nitrogen was used as carrier gas. The flow rates used in the detector were 45 $cm^3\ min^{-1}$ of hydrogen and 450 $cm^3\ min^{-1}$ of air, measured at atmospheric pressure and room temperature.

Figure 47 Perkin-Elmer Clarus 680 gas chromatograph

The temperature program used for the column is shown in Figure 48**.**

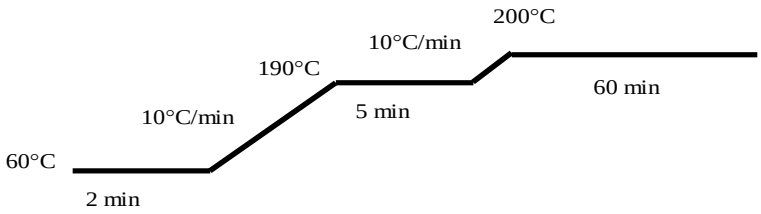

Figure 48 Temperature profile used on the Shimadzu GC-9A and Perkin-Elmer Clarus 680

Table 14 Gas Chromatograph Properties

	Gas chromatography (GC) Perkin-Elmer
Column	BP1
Column Length	30m x 250 µm
Carrier Gas	N_2 and He
Flow rate/ Pressure	0.5 mL/min
Split	50 mL/min
Injection Temp.	250 ºC
Detector Temp	250 ºC
Injection volume	0.1 µl

Before injection in the GC-FID the bio-oil samples were diluted in acetone and toluene. The results show that the acetone fraction mainly consists of compounds that have less than 5 carbon atoms, while toluene fraction is composed of compounds that have 5 to 12 carbon atoms where compounds with 8 carbon atoms were the most abundant fraction (Figure 49**,** Figure 50).

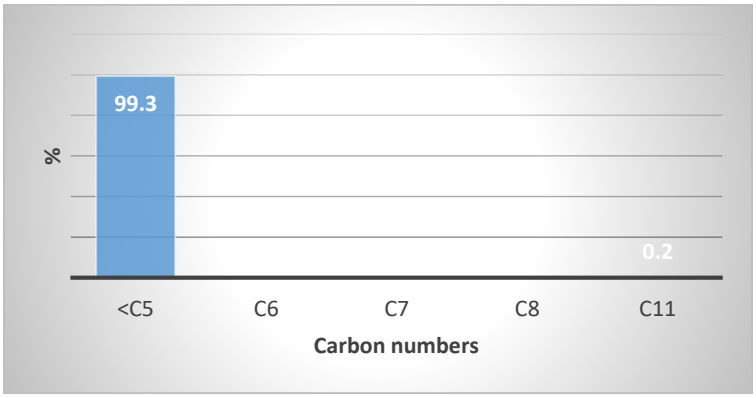

Figure 49 Bio-oil composition (acetone dilution)

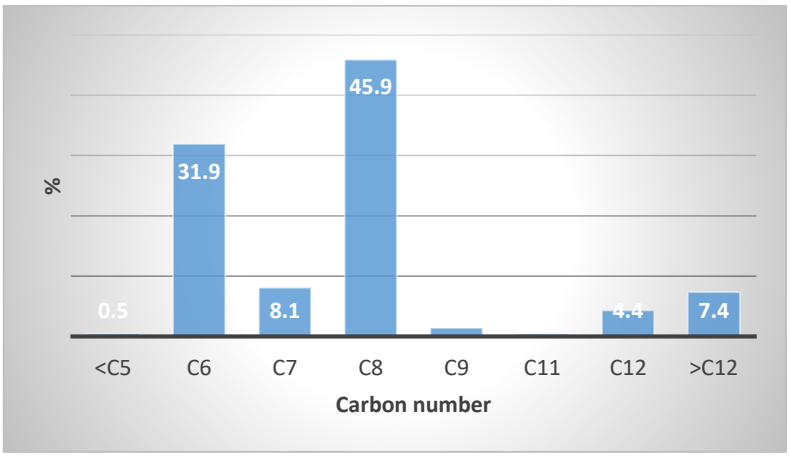

Figure 50 Bio-oil composition (toluene dilution)

The bio-oil samples obtained after the second bench scale experiment were diluted only in toluene. It was possible to trap and collect 4 distinct fractions, namely, top (over the condenser), condenser, liquid collector and reactor. The top fraction consists of essentially compounds with 7 carbon compounds. The less volatile condenser and collector bio-oils were composed of 5 to 12 carbon compounds. The most abundant fraction in condenser were 8 carbon atom compounds while in collector the most abundant fraction was 12 carbon atom compounds followed by 8 and 11 carbon atom compounds. In the reactor again the most abundant fraction was 8 carbon compounds (Figure 51**,** Figure 52**,** Figure 53**,** Figure 54) These results indicate that hydrocarbon fraction of cork bio-oil is composed of mainly 8 carbon compounds and its compounds range 6 to 12 carbon compounds.

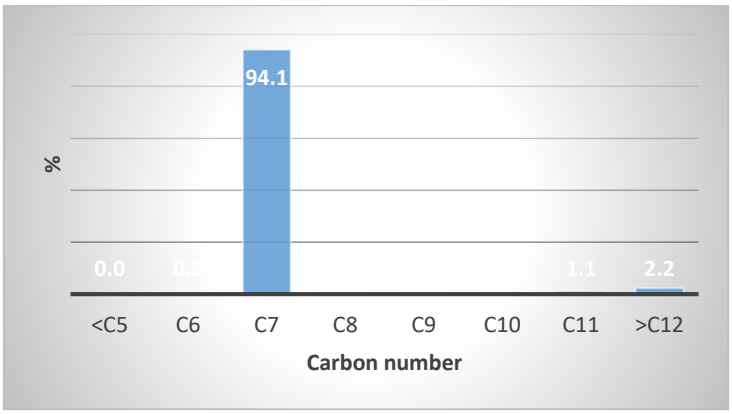

Figure 51 Bio-oil composition (top fraction)

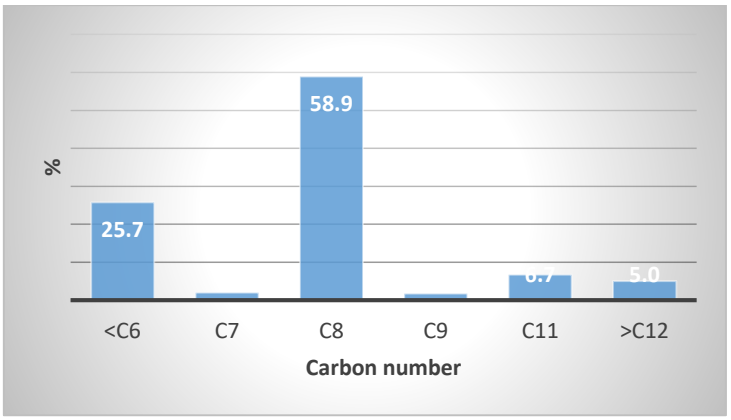

Figure 52 Bio-oil composition (condenser fraction)

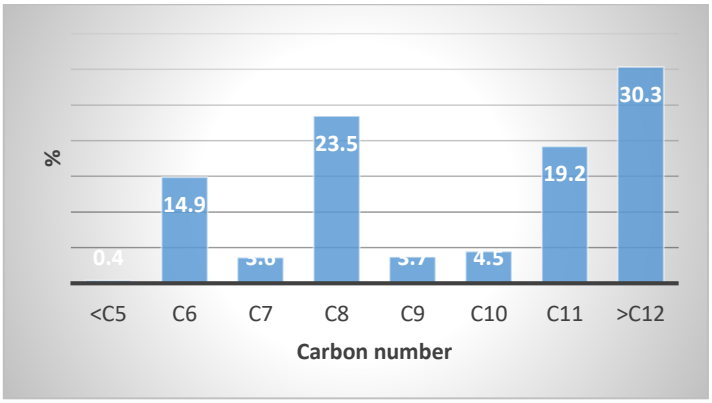

Figure 53 Bio-oil composition (collector fraction)

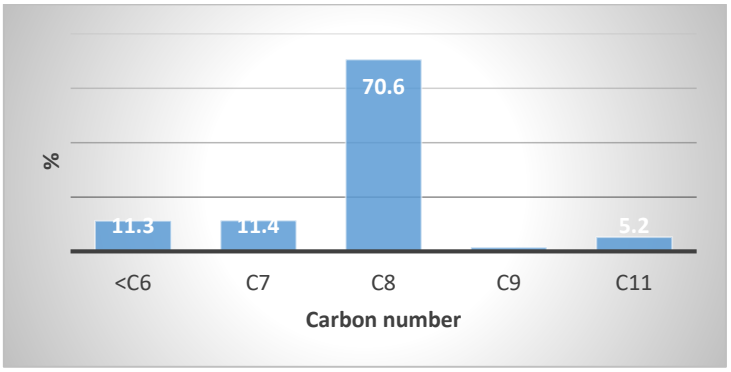

Figure 54 Bio-oil composition (reactor fraction)

5.4. Pyrolysis gases

The gas composition was analyzed only after the first bench scale experiment using the same procedure and equipment explained in bio-oil characterization. The result indicate that the main fraction detected consists of less than 5 carbon atom compounds. C6-C8 compounds were also detected in a lesser extent (Figure 55).

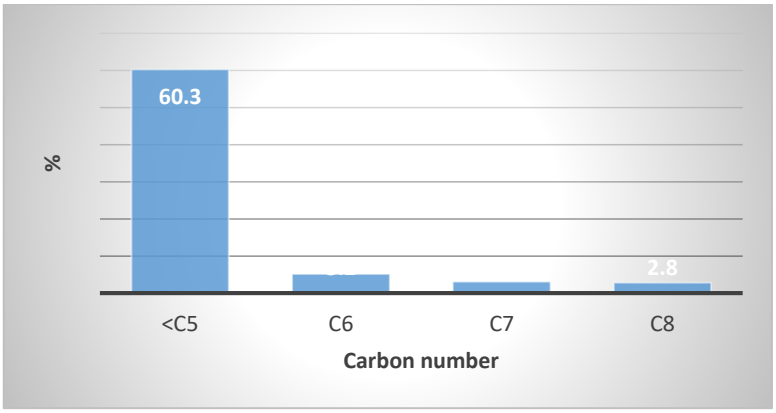

Figure 55 Pyrolysis gas composition

6. Chapter 6 Conclusions and Future Work

In this chapter the results obtained after pyrolysis experiments carried in thermogravimetric analyzer, bench scale fixed bed reactor and twin-screw fast pyrolysis reactor will be analyzed, kinetic modelling approaches will be discussed and characterizations of pyrolysis products will be analyzed. After having examined the results, the future works based on these results will be determined.

6.1 Summary and conclusions

Unconventional corks are obtained from tree barks that contain high amount of corks. These tree barks are often underutilized and considered as waste streams. Thermal conversion methods such as fast pyrolysis present an interesting approach for valorization of these barks by converting them into bio-oils in a very short time and with high yields.

The current knowledge on fast pyrolysis of cork is scarce although many works were already carried on fast pyrolysis of wood. Many unknowns exist for successful fast pyrolysis operation of cork. These unknowns include knowledge on kinetic parameters, fast pyrolysis yields and product compositions on different operating conditions. The current study aims to solve these problems. A total of six biomass types were studied where five of them are corks and the last one is phloem, a by-product of cork separation. Also the effect of particle size was tested on three different *Q. cerris* corks.

The experimental studies started with thermogravimetric analyses in order to determine kinetic parameters, particularly activation energy. Also biomass compositions were calculated using the kinetic modelling. First-order parallel reaction model was used to explain the experimental data. Six different heating rates were used and a total of 108 individual fittings were carried in all biomass types. Based on the individual fits global and flexible models were developed and activation energies and biomass compositions were calculated. Differential scanning calorimetry (DSC) and differential thermogravimetry (DTG) analyses were also carried in parallel with kinetic modelling.

In the second part of the experimental work, two glass reactors were designed, built and tested to obtain bio-oils and biochar from the *Q. cerris* cork in bench scale. After the bench scale experiments, in the third part of the experimental work a twin-screw fast pyrolysis reactor was used to pyrolyze *Q. cerris* cork and *Q. cerris* phloem in pilot scale. These experimental studies were followed by pyrolysis products characterizations. Scanning electron microscopy (SEM) was applied to characterize chars obtained after bench scale pyrolysis experiments and thermogravimetric analyses with three different final temperatures. Bio-oils samples and gas product obtained after bench scale pyrolysis experiments were characterized by gas chromatography (GC-FID).

The thermogravimetric analysis results showed that cork and phloem samples start to degrade at temperatures over 200 °C. A fast mass loss occurs between 280 °C and 450 °C and mass loss continues until 800 °C. The DTG analysis results revealed different mass loss processes that occurred during pyrolysis experiments. A total of 5 peaks temperatures were detected at temperatures 100 °C, 325 °C, 380 °C, 435 °C and 700 °C respectively indicating relatively more heterogeneous composition of cork than wood. The DSC analysis results showed that pyrolysis of cork and phloem is endothermic at lower heating rates and it becomes exothermic at higher heating rates, contrary to expected indicating

at lower heating rates the dominant reaction is decomposition while at higher heating rates dehydration reaction predominate.

The first-order parallel reaction model successfully predicted activation energies and cork chemical composition. By applying six component parallel reaction model and six heating rates global and flexible reaction models were developed with the former models, fitting were good (fit qualities were over 99%). The activation energies and biomass compositions were calculated for five pseudo components and char product. The results indicate that cork and phloem samples can be described as consisting of 5 pseudo components, i.e. humidity, hemicelluloses, cellulose, suberin and lignin. The activation energies of the pseudo components of *Q. cerris* cork varied 31-38 kJ/mol, 228-259 kJ/mol, 141-168 kJ/mol, 247-325 kJ/mol, and 130-307 kJ/mol respectively. The relative compositions of the pseudo components varied 0.04-0.05, 0.21-0.24, 0.16-0.19, 0.16-0.25, and 0.08-0.12 respectively. The char content varied between 9% and 23%. The results of bench scale pyrolysis experiments showed that keeping vapor residence time alone was not sufficient to obtain high bio-oil yields. Higher heat transfer rates are necessary and fluid or spout bed reactor systems should be developed for higher bio-oil yieldsThe biochars obtained after 400 °C final pyrolysis temperature and temperature gradient fixed bed experiments were shown to retain their cellular structure indicating to be good alternatives for soil amendment treatments. The bio-oil composition showed compounds having six to twelve carbons which imply its utilization as gasoline alternative.

Technical problems were encountered in feeding cork samples into the twin-screw fast pyrolysis reactor. However, fast pyrolysis experiments of phloem samples resulted with approximately 52% bio-oil yields as received basis where organic fraction made up approximately 45%. Overall, the results show that *Q. cerris* and other cork species as well as *Q. cerris* phloem have potential for conversion of bio-oil and biochars through fast pyrolysis. Thus cork-rich tree barks which are considered as waste streams, can be valorized.

6.2. Future work

After having completed the current study, which studies would be carried becomes clear. First, new fluid bed or spouted bed bench scale reactor will be designed considering higher heat transfer rate. In parallel, technical problems will be solved in transporting cork into twin-screw fast pyrolysis reactor and the experiments will be finalized and compared with those of bench scale experiments.

Finally, fast pyrolysis of cork will be simulated with OpenFoam using the kinetic parameters obtained and modellings applied in this work as well as results obtained from bench scale and pilot scale fast pyrolysis experiments. A techno-economic analysis will be carried to evaluate the overall results for valorization of unconventional corks and phloem.

References

Anca-Couce, A., Mehrabian, R., Scharler, R., Obernberger, I. (2014). Kinetic scheme of biomass pyrolysis considering secondary charring reactions. Energy conversion and management, 87, 687-696.

Antal Jr, M. J., Friedman, H. L., Rogers, F. E. (1980). Kinetics of cellulose pyrolysis in nitrogen and steam. Combustion science and technology, 21(3-4), 141-152.

Antal, M. J. J., Varhegyi, G. (1995). Cellulose pyrolysis kinetics: the current state of knowledge. Industrial & Engineering Chemistry Research, 34(3), 703-717.

Antal, M. J., Grønli, M. (2003). The art, science, and technology of charcoal production. Industrial & Engineering Chemistry Research, 42(8), 1619-1640.

Ba, T., Chaala, A., Garcia-Perez, M., Rodrigue, D., Roy, C. (2004). Colloidal properties of bio-oils obtained by vacuum pyrolysis of softwood bark. Characterization of water-soluble and water-insoluble fractions. Energy & Fuels, 18(3), 704-712.

Ba, T., Chaala, A., Garcia-Perez, M., Roy, C. (2004). Colloidal properties of bio-oils obtained by vacuum pyrolysis of softwood bark. Storage stability. Energy & fuels, 18(1), 188-201.

Ben, H., Mu, W., Deng, Y., Ragauskas, A. J. (2013). Production of renewable gasoline from aqueous phase hydrogenation of lignin pyrolysis oil. Fuel, 103, 1148-1153.

Beste, A., Buchanan III, A. C. (2012). Kinetic simulation of the thermal degradation of phenethyl phenyl ether, a model compound for the β-O-4 linkage in lignin. Chemical Physics Letters, 550, 19-24.

Boucher, M. E., Chaala, A., Roy, C. (2000). Bio-oils obtained by vacuum pyrolysis of softwood bark as a liquid fuel for gas turbines. Part I: Properties of bio-oil and its blends with methanol and a pyrolytic aqueous phase. Biomass and Bioenergy, 19(5), 337-350.

Boucher, M. E., Chaala, A., Pakdel, H., Roy, C. (2000). Bio-oils obtained by vacuum pyrolysis of softwood bark as a liquid fuel for gas turbines. Part II: Stability and ageing of bio-oil and its blends with methanol and a pyrolytic aqueous phase. Biomass and Bioenergy, 19(5), 351-361.

Bradbury, A. G., Sakai, Y., Shafizadeh, F. (1979). A kinetic model for pyrolysis of cellulose. Journal of applied polymer science, 23(11), 3271-3280.

Brammer, J. G., Lauer, M., Bridgwater, A. V. (2006). Opportunities for biomass-derived “bio-oil” in European heat and power markets. Energy policy, 34(17), 2871-2880.

Bridgwater, A. V., Meier, D., Radlein, D. (1999). An overview of fast pyrolysis of biomass. *Organic geochemistry*, *30*(12), 1479-1493.

Bridgwater, A. V., Peacocke, G. V. C. (2000). Fast pyrolysis processes for biomass. Renewable and sustainable energy reviews, 4(1), 1-73.

Bridgwater, A. V., Toft, A. J., Brammer, J. G. (2002). A techno-economic comparison of power production by biomass fast pyrolysis with gasification and combustion. Renewable and Sustainable Energy Reviews, 6(3), 181-246.

Bridgwater, A. V. (2010). Fast pyrolysis of biomass for energy and fuels. In Thermochemical conversion of biomass to liquid fuels and chemicals (pp. 146-191). RSC Publishing Cambridge, England, UK.

Bridgwater, A. V. (2012). Review of fast pyrolysis of biomass and product upgrading. Biomass and bioenergy, 38, 68-94.

Bridgwater, A. V. (2012). Upgrading biomass fast pyrolysis liquids. Environmental Progress & Sustainable Energy, 31(2), 261-268.

Broido, A., Nelson, M. A. (1975). Char yield on pyrolysis of cellulose. Combustion and Flame, 24, 263-268.

Broido, A. (1976). Kinetics of solid-phase cellulose pyrolysis. In Symposium on Thermal Uses and Properties of Carbohydrates and Lignins, San Francisco, Calif.(USA), 1976. Academic Press.

Cai, J. M., Bi, L. S. (2009). Kinetic analysis of wheat straw pyrolysis using isoconversional methods. Journal of Thermal Analysis and Calorimetry, 98(1), 325-330.

Cai, J., Wu, W., Liu, R., Huber, G. W. (2013). A distributed activation energy model for the pyrolysis of lignocellulosic biomass. Green Chemistry, 15(5), 1331-1340.

Cai, J., Wu, W., Liu, R. (2014). An overview of distributed activation energy model and its application in the pyrolysis of lignocellulosic biomass. Renewable and Sustainable Energy Reviews, 36, 236-246.

Calabria, R., Chiariello, F., Massoli, P. (2007). Combustion fundamentals of pyrolysis oil based fuels. Experimental Thermal and Fluid Science, 31(5), 413-420.

Chaala, A., Ba, T., Garcia-Perez, M., Roy, C. (2004). Colloidal properties of bio-oils obtained by vacuum pyrolysis of softwood bark: aging and thermal stability. Energy & fuels, 18(5), 1535-1542.

Chaiwat, W., Hasegawa, I., Tani, T., Sunagawa, K., Mae, K. (2009). Analysis of cross-linking behavior during pyrolysis of cellulose for elucidating reaction pathway. Energy & Fuels, 23(12), 5765-5772.

Chiaramonti, D., Bonini, M., Fratini, E., Tondi, G., Gartner, K., Bridgwater, A. V., Grimm, H.P., Soldaini, I., Webster, A., Baglioni, P. (2003). Development of emulsions from biomass pyrolysis liquid and diesel and their use in engines—Part 1: emulsion production. Biomass and bioenergy, 25(1), 85-99.

Chiaramonti, D., Bonini, M., Fratini, E., Tondi, G., Gartner, K., Bridgwater, A. V., Grimm, H.P., Soldaini, I., Webster, A., Baglioni, P. (2003). Development of emulsions from biomass pyrolysis liquid and diesel and their use in engines—Part 2: tests in diesel engines. Biomass and Bioenergy, 25(1), 101-111.

Chiaramonti, D., Oasmaa, A., Solantausta, Y. (2007). Power generation using fast pyrolysis liquids from biomass. Renewable and sustainable energy reviews, 11(6), 1056-1086.

Cordero, T., Marquez, F., Rodriguez-Mirasol, J., Rodriguez, J. J. (2001). Predicting heating values of lignocellulosics and carbonaceous materials from proximate analysis. Fuel, 80(11), 1567-1571.

Cornelissen, T., Jans, M., Stals, M., Kuppens, T., Thewys, T., Janssens, G. K., Pastijn, H., Yperman, J., Reggers, G., Carleer, R. (2009). Flash co-pyrolysis of biomass: The influence of biopolymers. Journal of Analytical and Applied Pyrolysis, 85(1-2), 87-97.

Czernik, S., Bridgwater, A. V. (2004). Overview of applications of biomass fast pyrolysis oil. Energy & fuels, 18(2), 590-598.

Dahmen, N., Dinjus, E., Kolb, T., Arnold, U., Leibold, H., Stahl, R. (2012). State of the art of the bioliq® process for synthetic biofuels production. Environmental progress & sustainable energy, 31(2), 176-181.

Darmstadt, H., Garcia-Perez, M., Adnot, A., Chaala, A., Kretschmer, D., Roy, C. (2004). Corrosion of metals by bio-oil obtained by vacuum pyrolysis of softwood bark residues. An X-ray photoelectron spectroscopy and auger electron spectroscopy study. Energy & fuels, 18(5), 1291-1301.

Deng, L., Fu, Y., Guo, Q. X. (2008). Upgraded acidic components of bio-oil through catalytic ketonic condensation. Energy & Fuels, 23(1), 564-568.

Demirbaş, A. (1997). Calculation of higher heating values of biomass fuels. Fuel, 76(5), 431-434.

Di Blasi, C. (2008). Modeling chemical and physical processes of wood and biomass pyrolysis. *Progress in energy and combustion science*, *34*(1), 47-90.

Diebold, J. P., Czernik, S. (1997). Additives to lower and stabilize the viscosity of pyrolysis oils during storage. Energy & Fuels, 11(5), 1081-1091.

Diebold, J. P., Milne, T. A., Czernik, S., Oasmaa, A., Bridgwater, A. V., Cuevas, A., Gust., S., Huffman, D., Piskorz, J. (1997). Proposed specifications for various grades of pyrolysis oils. In Developments in thermochemical biomass conversion (pp. 433-447). Springer, Dordrecht.

Effendi, A., Gerhauser, H., Bridgwater, A. V. (2008). Production of renewable phenolic resins by thermochemical conversion of biomass: a review. Renewable and Sustainable Energy Reviews, 12(8), 2092-2116.

Faravelli, T., Frassoldati, A., Migliavacca, G., Ranzi, E. L. I. S. E. O. (2010). Detailed kinetic modeling of the thermal degradation of lignins. Biomass and Bioenergy, 34(3), 290-301.

Fisk, C. A., Morgan, T., Ji, Y., Crocker, M., Crofcheck, C., Lewis, S. A. (2009). Bio-oil upgrading over platinum catalysts using in situ generated hydrogen. Applied Catalysis A: General, 358(2), 150-156.

French, R., Czernik, S. (2010). Catalytic pyrolysis of biomass for biofuels production. Fuel Processing Technology, 91(1), 25-32.

Funke, A., Richter, D., Niebel, A., Dahmen, N., Sauer, J. (2016). Fast pyrolysis of biomass residues in a twin-screw mixing reactor. Journal of visualized experiments: JoVE, (115).

Garcia-Perez, M., Chaala, A., Pakdel, H., Kretschmer, D., Rodrigue, D., Roy, C. (2006). Evaluation of the influence of stainless steel and copper on the aging process of bio-oil. Energy & fuels, 20(2), 786-795.

Garcia-Perez, M., Chaala, A., Pakdel, H., Kretschmer, D., Roy, C. (2007). Vacuum pyrolysis of softwood and hardwood biomass: comparison between product yields and bio-oil properties. Journal of Analytical and Applied Pyrolysis, 78(1), 104-116.

Garcia-Perez, M., Wang, X. S., Shen, J., Rhodes, M. J., Tian, F., Lee, W. J., Wu, H., Li, C. Z. (2008). Fast pyrolysis of oil mallee woody biomass: effect of temperature on the yield and quality of pyrolysis products. Industrial & engineering chemistry research, 47(6), 1846-1854.

Gil, L. (1997). Cork powder waste: an overview. Biomass and Bioenergy, 13(1-2), 59-61.

Gillespie, D. T. (1977). Exact stochastic simulation of coupled chemical reactions. The journal of physical chemistry, 81(25), 2340-2361.

Gillespie, D. T. (2007). Stochastic simulation of chemical kinetics. Annu. Rev. Phys. Chem., 58, 35-55.

Gooty, A. T., Li, D., Briens, C., Berruti, F. (2014). Fractional condensation of bio-oil vapors produced from birch bark pyrolysis. Separation and Purification Technology, 124, 81-88.

Guo, X., Wang, S., Guo, Z., Liu, Q., Luo, Z., Cen, K. (2010). Pyrolysis characteristics of bio-oil fractions separated by molecular distillation. Applied Energy, 87(9), 2892-2898.

Gupta, K. K., Rehman, A., Sarviya, R. M. (2010). Bio-fuels for the gas turbine: A review. Renewable and Sustainable Energy Reviews, 14(9), 2946-2955.

Hassan, E. M., Yu, F., Ingram, L., Steele, P. (2009). The potential use of whole-tree biomass for bio-oil fuels. Energy Sources, Part A: Recovery, Utilization, and Environmental Effects, 31(20), 1829-1839.

Heo, H. S., Park, H. J., Park, Y. K., Ryu, C., Suh, D. J., Suh, Y. W., Yim, J.H., Kim, S. S. (2010). Bio-oil production from fast pyrolysis of waste furniture sawdust in a fluidized bed. Bioresource technology, 101(1), S91-S96.

Hilten, R. N., Bibens, B. P., Kastner, J. R., Das, K. C. (2009). In-line esterification of pyrolysis vapor with ethanol improves bio-oil quality. Energy & Fuels, 24(1), 673-682.

Hilten, R. N., Das, K. C. (2010). Comparison of three accelerated aging procedures to assess bio-oil stability. Fuel, 89(10), 2741-2749.

Hornung, A. (2014). Transformation of biomass: theory to practice. John Wiley & Sons.

Hu, X., Gunawan, R., Mourant, D., Lievens, C., Li, X., Zhang, S., Chaiwat, W., Li, C. Z. (2012). Acid-catalysed reactions between methanol and the bio-oil from the fast pyrolysis of mallee bark. Fuel, 97, 512-522.

Huber, G. W., Iborra, S., Corma, A. (2006). Synthesis of transportation fuels from biomass: chemistry, catalysts, and engineering. Chemical reviews, 106(9), 4044-4098.

Ikura, M., Stanciulescu, M., Hogan, E. (2003). Emulsification of pyrolysis derived bio-oil in diesel fuel. Biomass and bioenergy, 24(3), 221-232.

Jain, A. A., Mehra, A., Ranade, V. V. (2016). Processing of TGA data: Analysis of isoconversional and model fitting methods. Fuel, 165, 490-498.

Junming, X., Jianchun, J., Yunjuan, S., Yanju, L. (2008). Bio-oil upgrading by means of ethyl ester production in reactive distillation to remove water and to improve storage and fuel characteristics. Biomass and bioenergy, 32(11), 1056-1061.

Kaltschmitt, M., Hartmann, H., Hofbauer, H. Energie aus Biomasse-Grundlagen, Techniken und Verfahren. 2009.

Kantarelis, E., Yang, W., Blasiak, W. (2013). Production of liquid feedstock from biomass via steam pyrolysis in a fluidized bed reactor. Energy & Fuels, 27(8), 4748-4759.

Khawam, A., Flanagan, D. R. (2006). Solid-state kinetic models: basics and mathematical fundamentals. The journal of physical chemistry B, 110(35), 17315-17328.

Laird, D. A. (2008). The charcoal vision: a win–win–win scenario for simultaneously producing bioenergy, permanently sequestering carbon, while improving soil and water quality. Agronomy journal, 100(1), 178-181.

Lédé, J. (1994). Reaction temperature of solid particles undergoing an endothermal volatilization. Application to the fast pyrolysis of biomass. Biomass and Bioenergy, 7(1-6), 49-60.

Lédé, J., Villermavx, J. (1993). Comportement thermique et chimique de particules solides subissant une réaction de décomposition endothermique sous l'action d'un flux de chaleur externe. The Canadian Journal of Chemical Engineering, 71(2), 209-217.

Lievens, C., Mourant, D., He, M., Gunawan, R., Li, X., Li, C. Z. (2011). An FT-IR spectroscopic study of carbonyl functionalities in bio-oils. Fuel, 90(11), 3417-3423.

Lu, Q., Zhang, Z. F., Dong, C. Q., Zhu, X. F. (2010). Catalytic upgrading of biomass fast pyrolysis vapors with nano metal oxides: an analytical Py-GC/MS study. Energies, 3(11), 1805-1820.

Lu, Q., Zhang, Y., Tang, Z., Li, W. Z., Zhu, X. F. (2010). Catalytic upgrading of biomass fast pyrolysis vapors with titania and zirconia/titania based catalysts. Fuel, 89(8), 2096-2103.

Mahfud, F. H., Melian-Cabrera, I., Manurung, R., Heeres, H. J. (2007). Biomass to fuels: upgrading of flash pyrolysis oil by reactive distillation using a high boiling alcohol and acid catalysts. Process Safety and Environmental Protection, 85(5), 466-472.

Marques, A. V., Pereira, H. (2014). Aliphatic bio-oils from corks: A Py–GC/MS study. Journal of Analytical and Applied Pyrolysis, 109, 29-40.

Meng, J., Park, J., Tilotta, D., Park, S. (2012). The effect of torrefaction on the chemistry of fast-pyrolysis bio-oil. Bioresource technology, 111, 439-446.

Moens, L., Black, S. K., Myers, M. D., Czernik, S. (2009). Study of the neutralization and stabilization of a mixed hardwood bio-oil. Energy & Fuels, 23(5), 2695-2699.

Mohan, D., Pittman, C. U., Steele, P. H. (2006). Pyrolysis of wood/biomass for bio-oil: a critical review. Energy & fuels, 20(3), 848-889.

Mohan, D., Shi, J., Nicholas, D. D., Pittman Jr, C. U., Steele, P. H., Cooper, J. E. (2008). Fungicidal values of bio-oils and their lignin-rich fractions obtained from wood/bark fast pyrolysis. Chemosphere, 71(3), 456-465.

Mok, W. S. L., Antal Jr, M. J. (1983). Effects of pressure on biomass pyrolysis. I. Cellulose pyrolysis products. Thermochimica acta, 68(2-3), 155-164.

Mok, W. S. L., Antal Jr, M. J. (1983). Effects of pressure on biomass pyrolysis. II. Heats of reaction of cellulose pyrolysis. Thermochimica Acta, 68(2-3), 165-186.

Mortensen, P. M., Grunwaldt, J. D., Jensen, P. A., Knudsen, K. G., Jensen, A. D. (2011). A review of catalytic upgrading of bio-oil to engine fuels. Applied Catalysis A: General, 407(1-2), 1-19.

Narayan, R., Antal, M. J. (1996). Thermal lag, fusion, and the compensation effect during biomass pyrolysis. Industrial & engineering chemistry research, 35(5), 1711-1721.

Nhuchhen, D. R., Salam, P. A. (2012). Estimation of higher heating value of biomass from proximate analysis: A new approach. Fuel, 99, 55-63.

Nokkosmäki, M. I., Kuoppala, E. T., Leppämäki, E. A., Krause, A. O. I. (2000). Catalytic conversion of biomass pyrolysis vapours with zinc oxide. Journal of Analytical and Applied Pyrolysis, 55(1), 119-131.

Nowakowski, D. J., Bridgwater, A. V., Elliott, D. C., Meier, D., de Wild, P. (2010). Lignin fast pyrolysis: results from an international collaboration. Journal of Analytical and Applied Pyrolysis, 88(1), 53-72.

Oasmaa, A., Kuoppala, E., Solantausta, Y. (2003). Fast pyrolysis of forestry residue. 2. Physicochemical composition of product liquid. Energy & fuels, 17(2), 433-443.

Oasmaa, A., Kuoppala, E., Selin, J. F., Gust, S., Solantausta, Y. (2004). Fast pyrolysis of forestry residue and pine. 4. Improvement of the product quality by solvent addition. Energy & Fuels, 18(5), 1578-1583.

Oasmaa, A., Elliott, D. C., Korhonen, J. (2010). Acidity of biomass fast pyrolysis bio-oils. Energy & Fuels, 24(12), 6548-6554.

Orfao, J. J. M., Antunes, F. J. A., Figueiredo, J. L. (1999). Pyrolysis kinetics of lignocellulosic materials—three independent reactions model. Fuel, 78(3), 349-358.

Pant, K., Mohanty, P. (2014). Biomass, conversion routes and products–an overview. Europe, 2214(1005), 45.

Papadikis, K., Bridgwater, A. V., Gu, S. (2008). CFD modelling of the fast pyrolysis of biomass in fluidised bed reactors, Part A: Eulerian computation of momentum transport in bubbling fluidised beds. Chemical Engineering Science, 63(16), 4218-4227.

Papadikis, K., Gu, S., Bridgwater, A. V. (2009). CFD modelling of the fast pyrolysis of biomass in fluidised bed reactors. Part B: Heat, momentum and mass transport in bubbling fluidised beds. Chemical Engineering Science, 64(5), 1036-1045.

Park, H. J., Park, Y. K., Dong, J. I., Kim, J. S., Jeon, J. K., Kim, S. S., Kim, J., Song, B., Park, J., Lee, K. J. (2009). Pyrolysis characteristics of Oriental white oak: kinetic study and fast pyrolysis in a fluidized bed with an improved reaction system. Fuel Processing Technology, 90(2), 186-195.

Patwardhan, P. R., Brown, R. C., Shanks, B. H. (2011). Product distribution from the fast pyrolysis of hemicellulose. ChemSusChem, 4(5), 636-643.

Pereira, H. (2007). Cork: Biology. Production and Uses.

Piskorz, J., Radlein, D., Scott, D. S. (1986). On the mechanism of the rapid pyrolysis of cellulose. Journal of Analytical and Applied pyrolysis, 9(2), 121-137.

Piskorz, J., Radlein, D. S. A., Scott, D. S., Czernik, S. (1989). Pretreatment of wood and cellulose for production of sugars by fast pyrolysis. Journal of Analytical and Applied Pyrolysis, 16(2), 127-142.

Ramírez-Verduzco, L. F., Rodríguez-Rodríguez, J. E., del Rayo Jaramillo-Jacob, A. (2012). Predicting cetane number, kinematic viscosity, density and higher heating value of biodiesel from its fatty acid methyl ester composition. Fuel, 91(1), 102-111.

Ranzi, E., Cuoci, A., Faravelli, T., Frassoldati, A., Migliavacca, G., Pierucci, S., Sommariva, S. (2008). Chemical kinetics of biomass pyrolysis. Energy & Fuels, 22(6), 4292-4300.

Ren, X., Gou, J., Wang, W., Li, Q., Chang, J., Li, B. (2013). Optimization of bark fast pyrolysis for the production of phenol-rich bio-oil. BioResources, 8(4), 6481-6492.

Rogers, J. G., Brammer, J. G. (2012). Estimation of the production cost of fast pyrolysis bio-oil. biomass and bioenergy, 36, 208-217.

Ronsse, F., Van Hecke, S., Dickinson, D., Prins, W. (2013). Production and characterization of slow pyrolysis biochar: influence of feedstock type and pyrolysis conditions. Gcb Bioenergy, 5(2), 104-115.

Şen, A., Leite, C., Lima, L., Lopes, P., Pereira, H. (2016). Industrial valorization of Quercus cerris bark: Pilot scale fractionation. Industrial Crops and Products, 92, 42-49.

Scholze, B., Meier, D. (2001). Characterization of the water-insoluble fraction from pyrolysis oil (pyrolytic lignin). Part I. PY–GC/MS, FTIR, and functional groups. Journal of Analytical and Applied Pyrolysis, 60(1), 41-54.

Shafizadeh, F., Chin, P. P. (1977). Thermal deterioration of wood. In ACS Symposium Series American Chemical Society.

Speight, J. G. (2015). Handbook of coal analysis. John Wiley & Sons.

Thangalazhy-Gopakumar, S., Adhikari, S., Gupta, R. B., Fernando, S. D. (2011). Influence of pyrolysis operating conditions on bio-oil components: a microscale study in a pyroprobe. Energy & Fuels, 25(3), 1191-1199.

Vamvuka, D. (2011). Bio- oil, solid and gaseous biofuels from biomass pyrolysis processes—an overview. International Journal of Energy Research, 35(10), 835-862.

Van de Velden, M., Baeyens, J., Brems, A., Janssens, B., Dewil, R. (2010). Fundamentals, kinetics and endothermicity of the biomass pyrolysis reaction. Renewable energy, 35(1), 232-242.

Vargas-Moreno, J. M., Callejón-Ferre, A. J., Pérez-Alonso, J., Velázquez-Martí, B. (2012). A review of the mathematical models for predicting the heating value of biomass materials. Renewable and sustainable energy reviews, 16(5), 3065-3083.

Varhegyi, G., Antal Jr, M. J., Szekely, T., Szabo, P. (1989). Kinetics of the thermal decomposition of cellulose, hemicellulose, and sugarcane bagasse. Energy & Fuels, 3(3), 329-335.

Venderbosch, R. H., Prins, W. (2010). Fast pyrolysis technology development. Biofuels, bioproducts and biorefining, 4(2), 178-208.

Vinu, R., Levine, S. E., Wang, L., Broadbelt, L. J. (2012). Detailed mechanistic modeling of poly (styrene peroxide) pyrolysis using kinetic Monte Carlo simulation. Chemical engineering science, 69(1), 456-471.

Wang, D., Czernik, S., Montane, D., Mann, M., Chornet, E. (1997). Biomass to hydrogen via fast pyrolysis and catalytic steam reforming of the pyrolysis oil or its fractions. Industrial & Engineering Chemistry Research, 36(5), 1507-1518.

Wang, Z., Pan, Y., Dong, T., Zhu, X., Kan, T., Yuan, L., Torimoto, Y., Sadakata, M., Li, Q. (2007). Production of hydrogen from catalytic steam reforming of bio-oil using C12A7-O−-based catalysts. Applied Catalysis A: General, 320, 24-34.

Wang, K., Brown, R. C. (2017). Prospects for Fast Pyrolysis of Biomass. In Fast Pyrolysis of Biomass (pp. 1-11).

Wang, S., Gu, Y., Liu, Q., Yao, Y., Guo, Z., Luo, Z., Cen, K. (2009). Separation of bio-oil by molecular distillation. Fuel Processing Technology, 90(5), 738-745.

Wang, S., Wang, Y., Cai, Q., Wang, X., Jin, H., Luo, Z. (2014). Multi-step separation of monophenols and pyrolytic lignins from the water-insoluble phase of bio-oil. Separation and Purification Technology, 122, 248-255.

Wang, S., Dai, G., Yang, H., Luo, Z. (2017). Lignocellulosic biomass pyrolysis mechanism: a state-of-the-art review. Progress in Energy and Combustion Science, 62, 33-86.

Wei, Y., Lei, H., Wang, L., Zhu, L., Zhang, X., Liu, Y., Chen, S., Ahring, B. (2014). Liquid–liquid extraction of biomass pyrolysis bio-oil. Energy & Fuels, 28(2), 1207-1212.

Westerhof, R. J., Brilman, D. W., van Swaaij, W. P., Kersten, S. R. (2009). Effect of temperature in fluidized bed fast pyrolysis of biomass: oil quality assessment in test units. Industrial & Engineering Chemistry Research, 49(3), 1160-1168.

Westerhof, R. J. M., Oudenhoven, S., Brilman, D. W. F., van Swaaij, W. P. M., Kersten, S. R., Spitzer, J., Dallemand, J.F., Baxter, D., Ossenbrink, H. (2010). Effect of particle size on the fast pyrolysis of biomass.

Wright, M. M., Daugaard, D. E., Satrio, J. A., Brown, R. C. (2010). Techno-economic analysis of biomass fast pyrolysis to transportation fuels. Fuel, 89, S2-S10.

Xiong, Q., Aramideh, S., Passalacqua, A., Kong, S. C. (2014). BIOTC: an open-source CFD code for simulating biomass fast pyrolysis. Computer Physics Communications, 185(6), 1739-1746.

Xiu, S., Shahbazi, A. (2012). Bio-oil production and upgrading research: A review. Renewable and Sustainable Energy Reviews, 16(7), 4406-4414.

Zhang, Q., Chang, J., Wang, T., Xu, Y. (2007). Review of biomass pyrolysis oil properties and upgrading research. Energy conversion and management, 48(1), 87-92.

Zhao, C., Kou, Y., Lemonidou, A. A., Li, X., Lercher, J. A. (2009). Highly selective catalytic conversion of phenolic bio- oil to alkanes. Angewandte Chemie International Edition, 48(22), 3987-3990.

Appendix I *Q. cerris* cork (20-40 mesh) kinetic modelling

10 °C /min heating rate

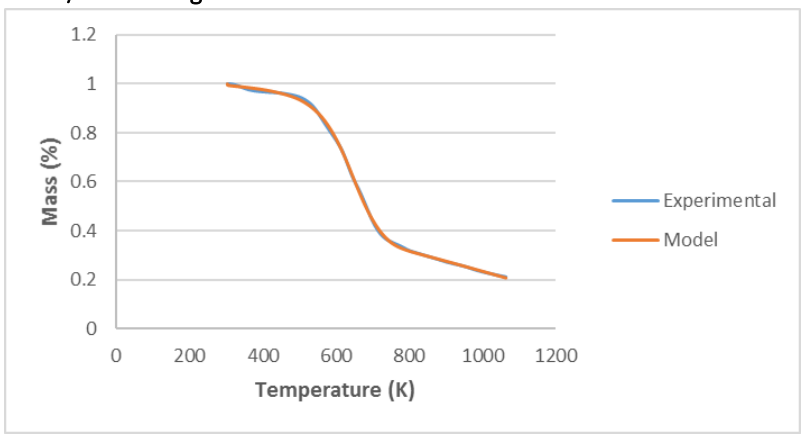

Figure 56 Four-pseudo component model

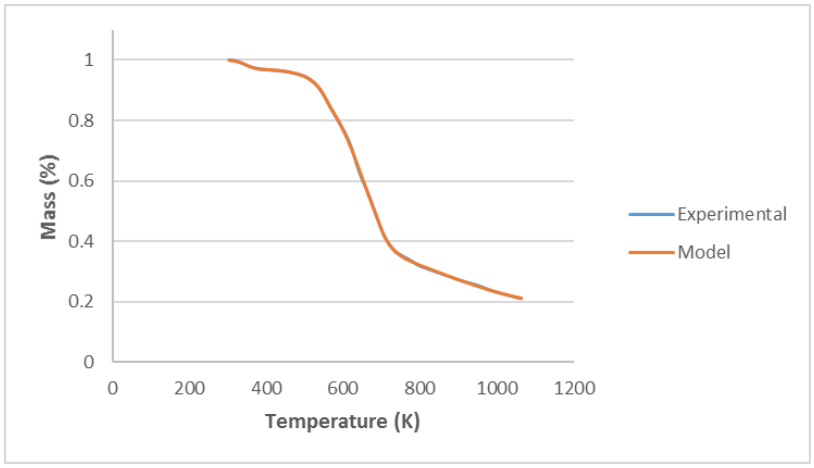

Figure 57 Five pseudo component model

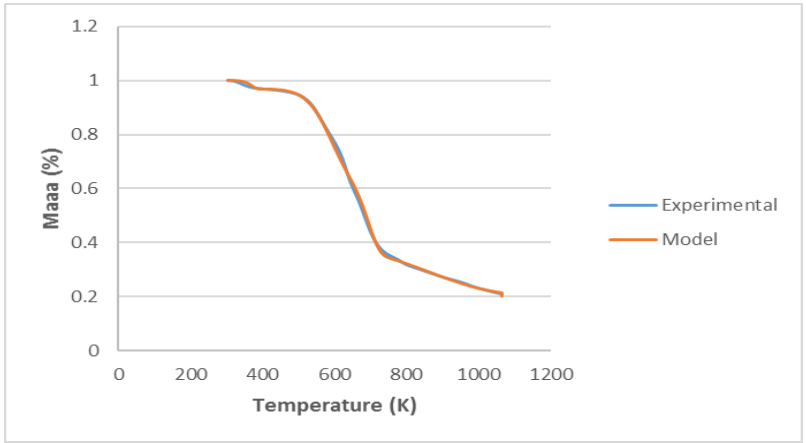

Figure 58 Six pseudo component model

20 °C /min heating rate

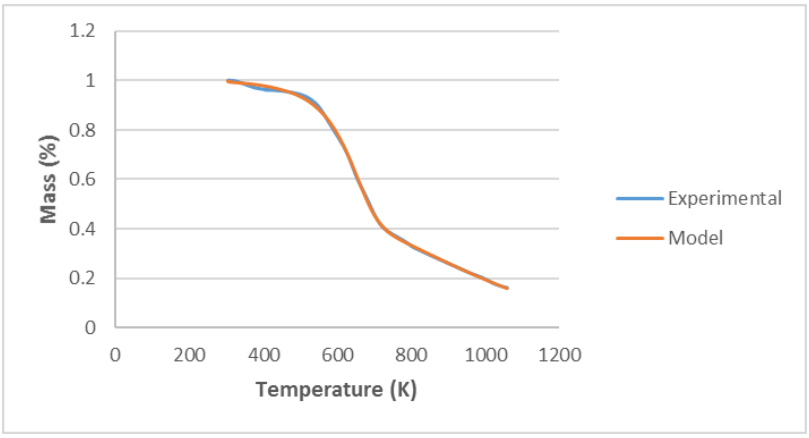

Figure 59 Four-pseudo component model

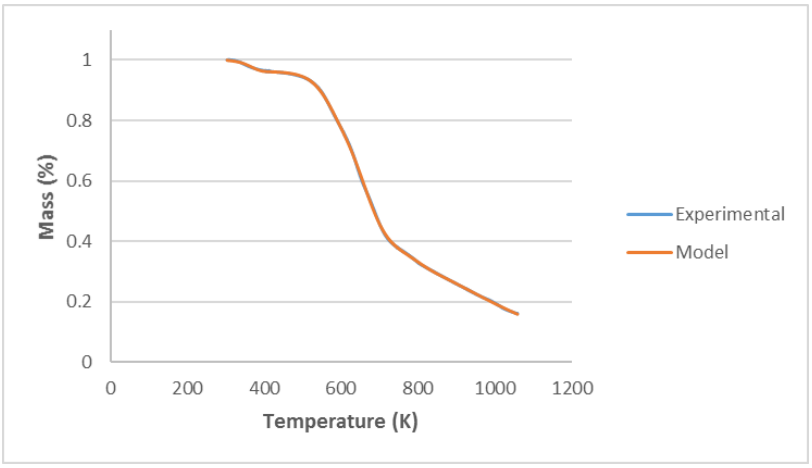

Figure 60 Five-pseudo component model

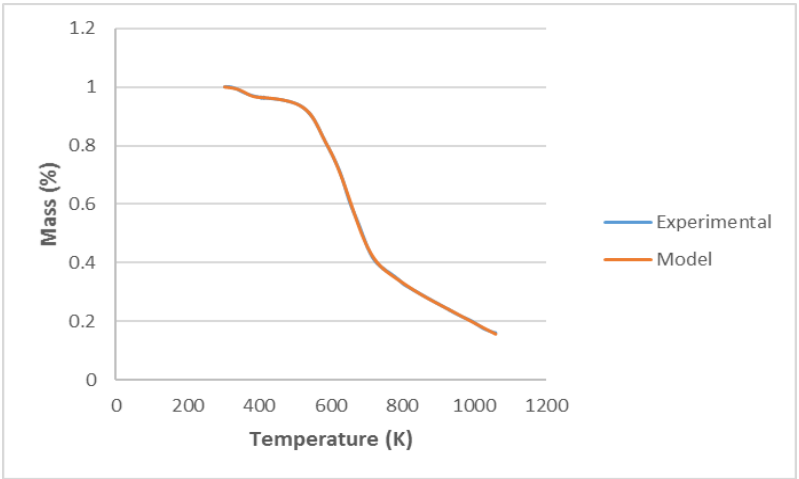

Figure 61 Six-pseudo component model

50 °C /min heating rate

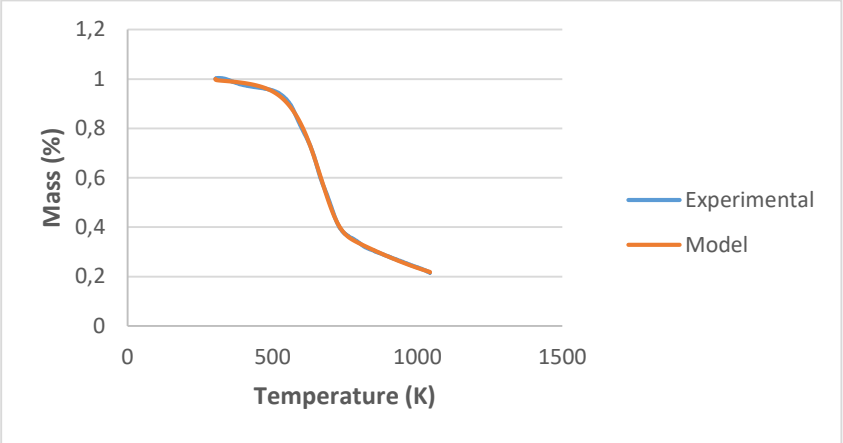

Figure 62 Four-pseudo component model

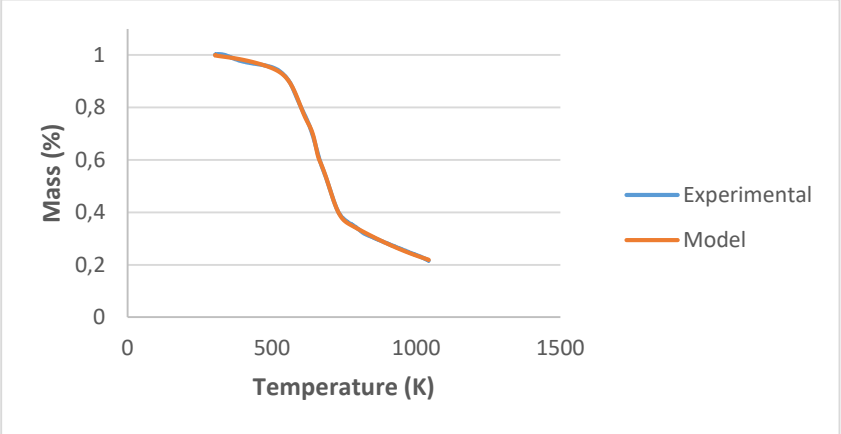

Figure 63 Five-pseudo component model

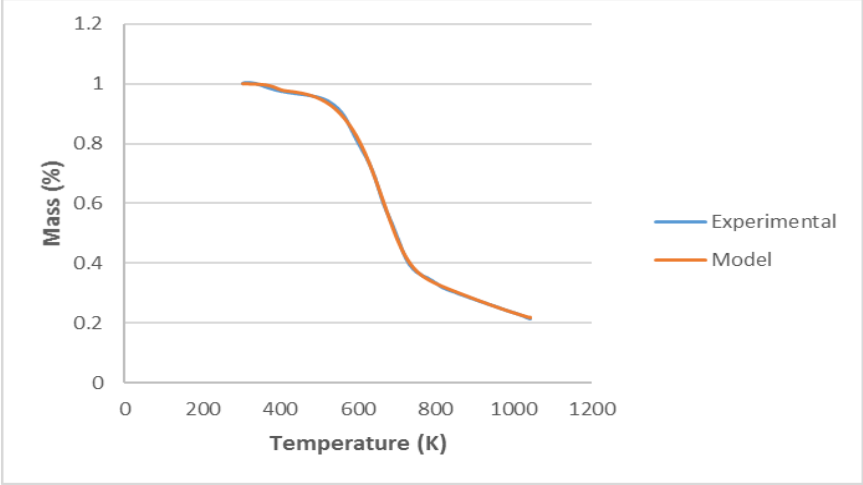

Figure 64 Six-pseudo component model

100 °C /min heating rate

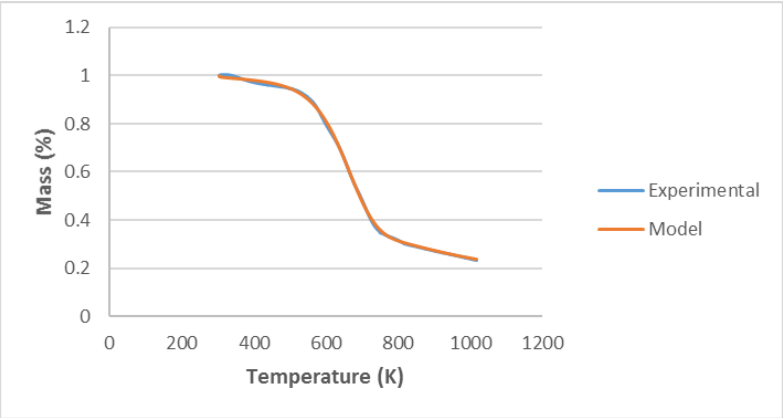

Figure 65 Four-pseudo component model

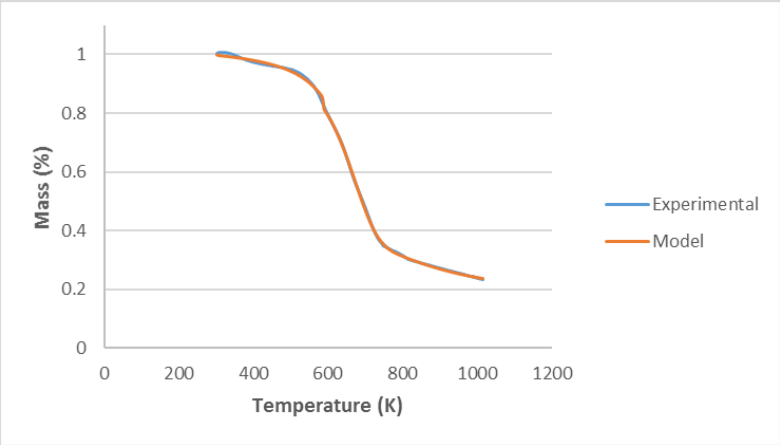

Figure 66 Five-pseudo component model

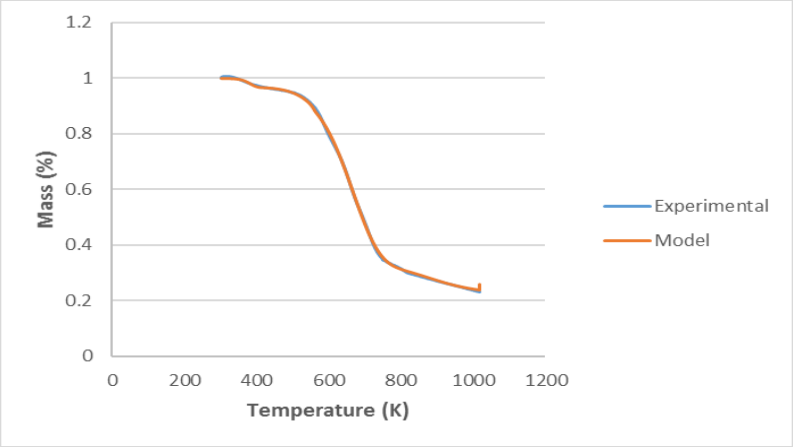

Figure 67 Six-pseudo component model

150 °C /min heating rate

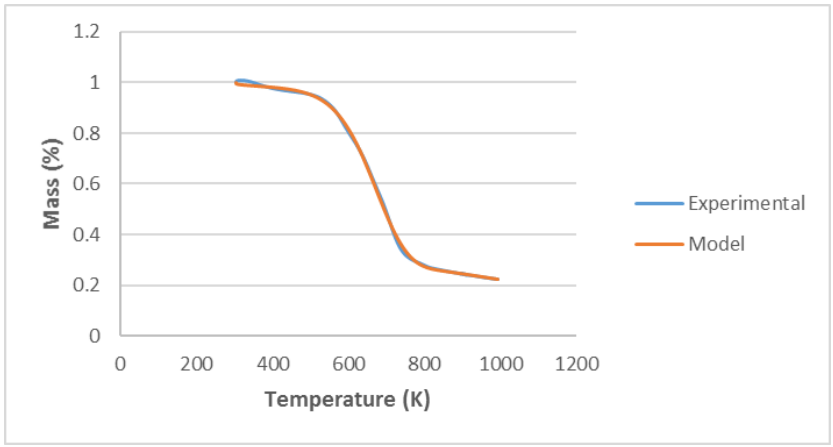

Figure 68 Four-pseudo component model

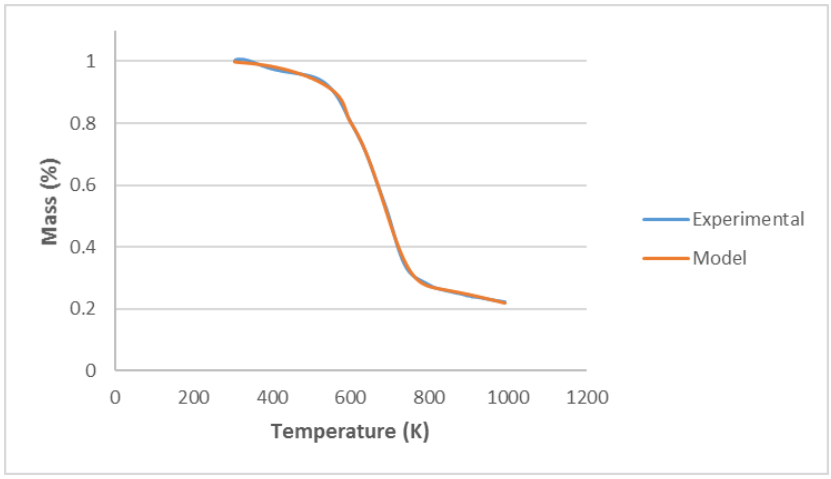

Figure 69 Five-pseudo component model

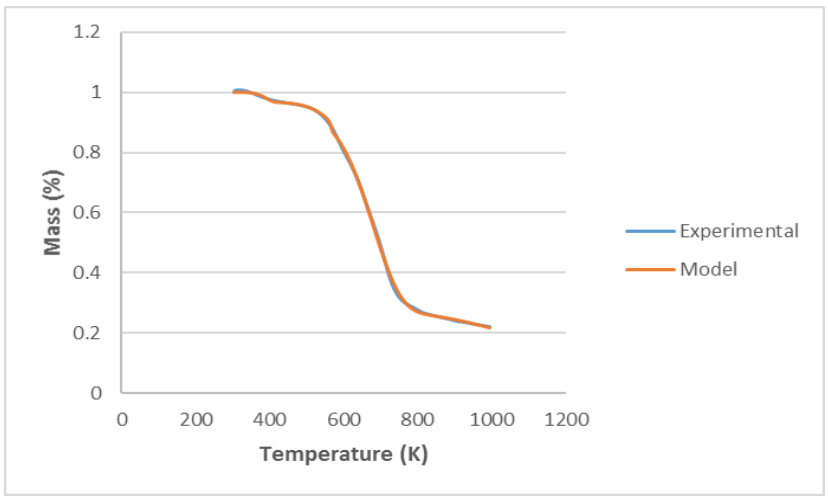

Figure 70 Six-pseudo component model

200 °C /min heating rate

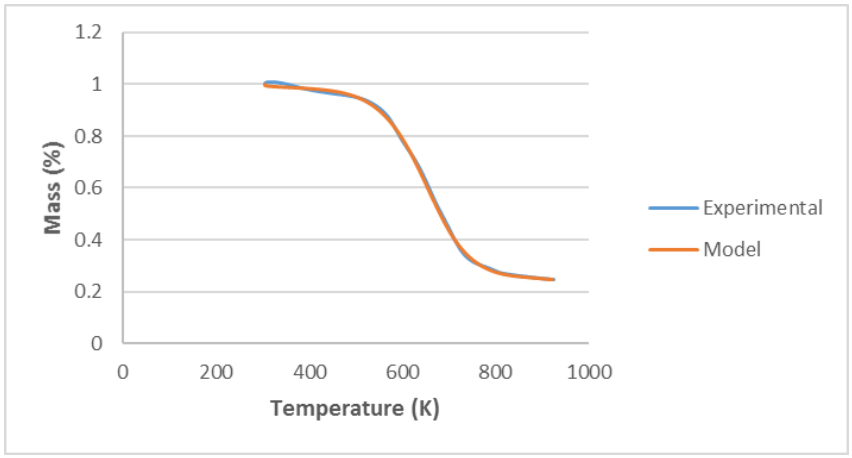

Figure 71 Four-pseudo component model

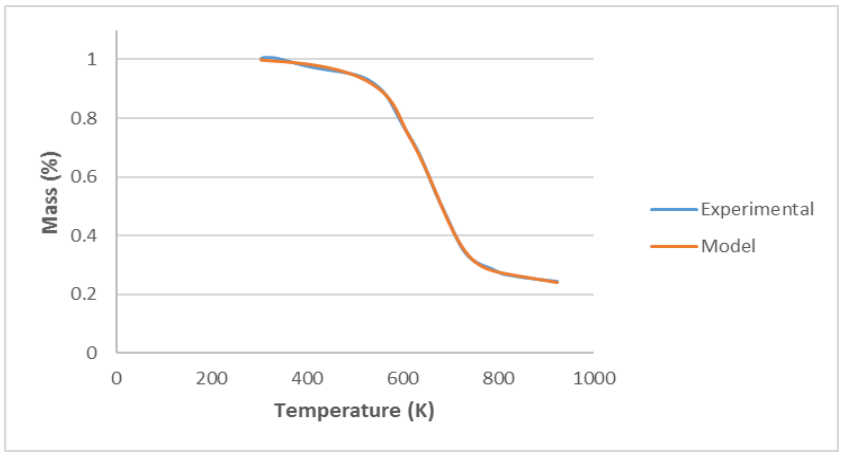

Figure 72 Five-pseudo component model

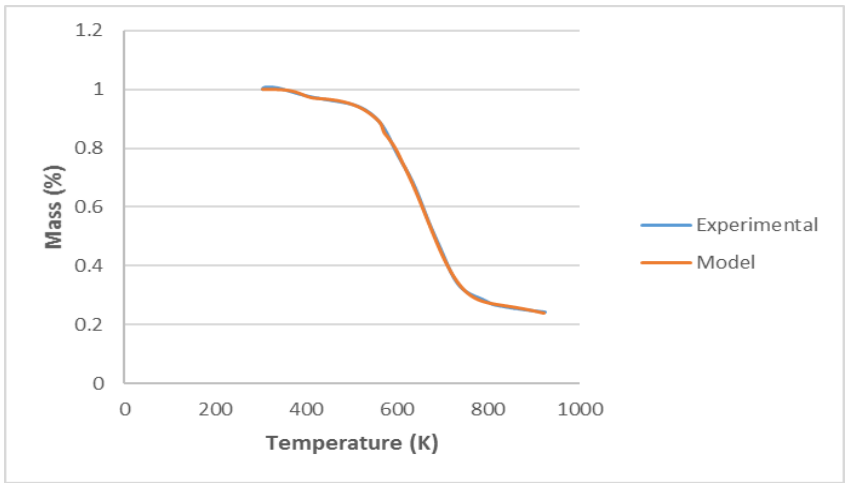

Figure 73 Six-pseudo component model

Appendix II *Q. cerris* cork (40-60 mesh) kinetic modelling

10 °C /min heating rate

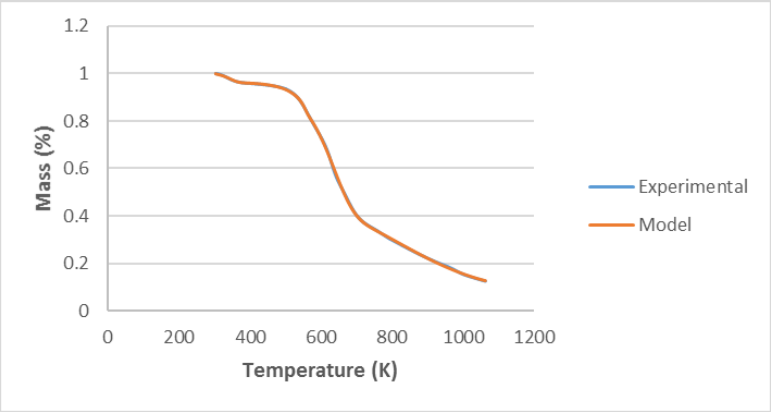

Figure 74 Four-pseudo component model

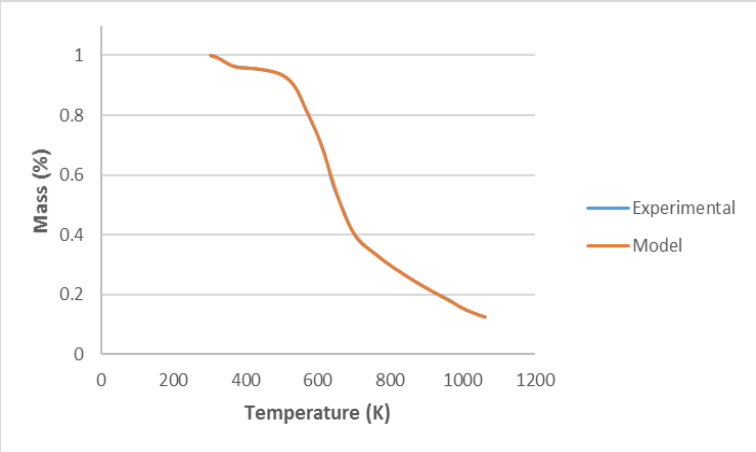

Figure 75 Five-pseudo component model

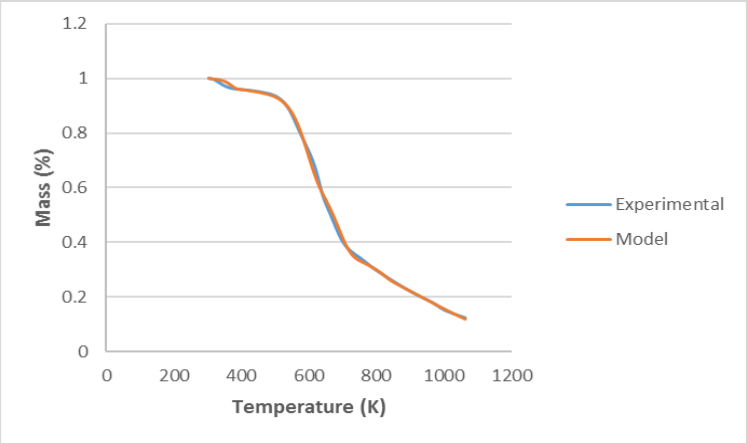

Figure 76 Six-pseudo component model

20 °C /min heating rate

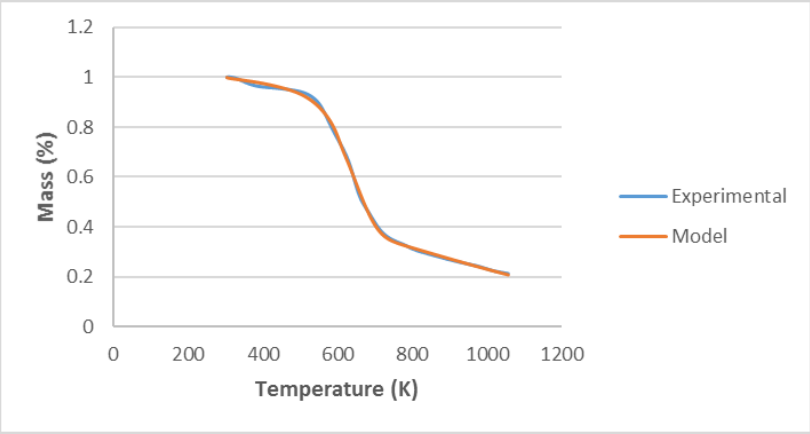

Figure 77 Four-pseudo component model

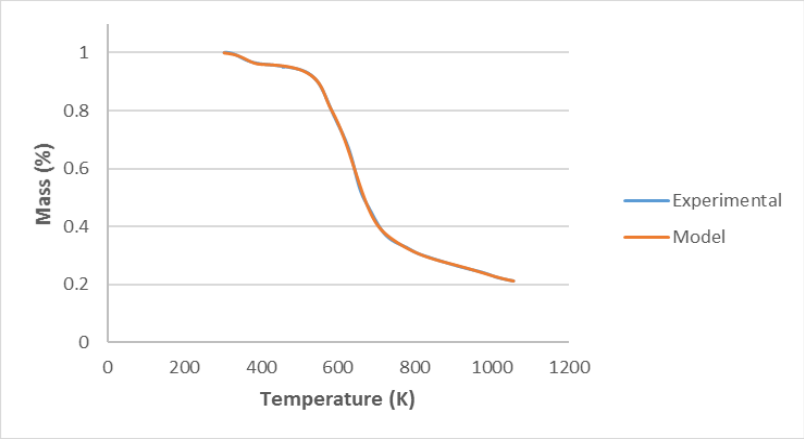

Figure 78 Five-pseudo component model

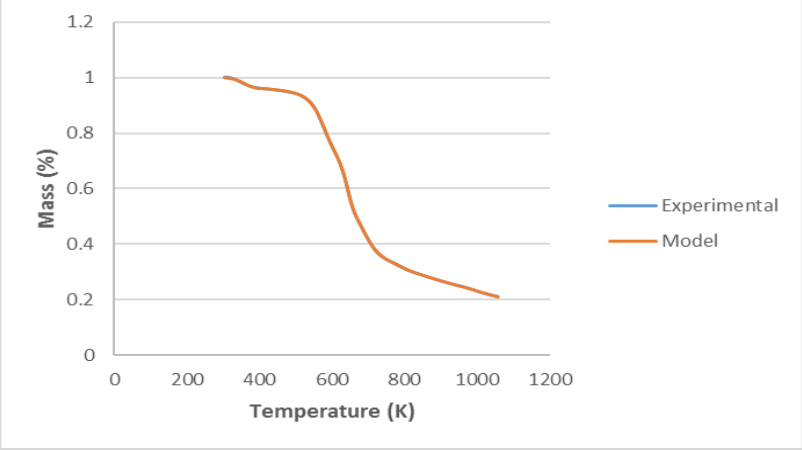

Figure 79 Six-pseudo component model

50 °C /min heating rate

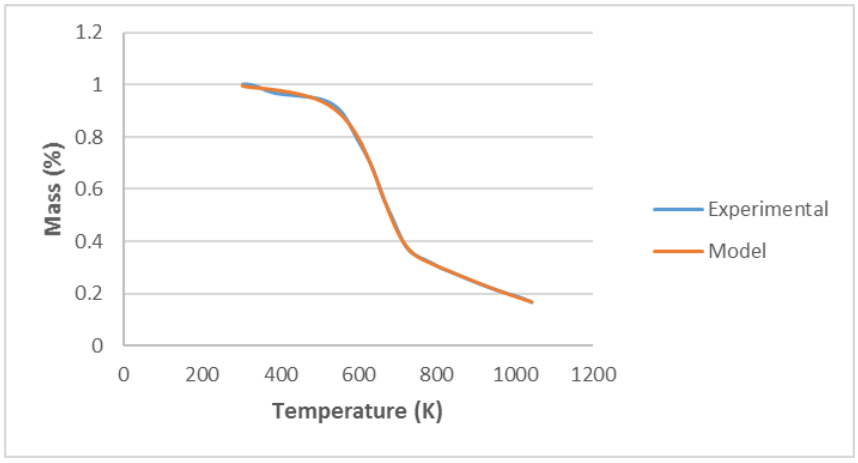

Figure 80 Four-pseudo component model

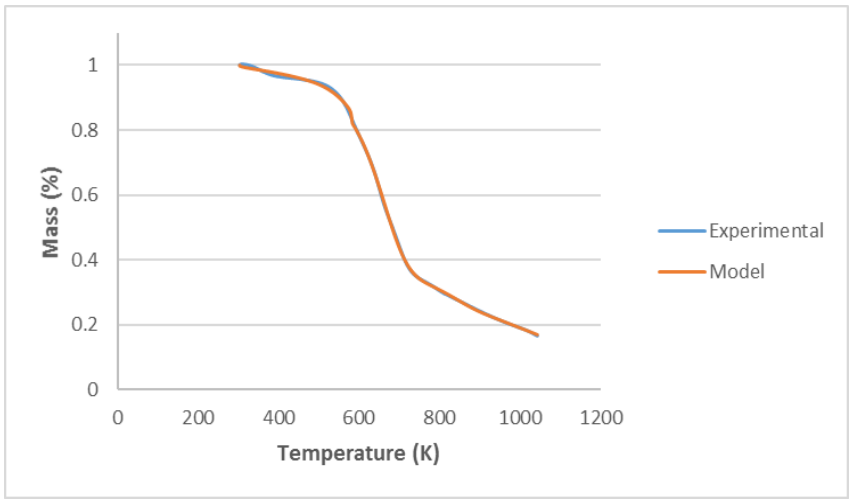

Figure 81 Five-pseudo component model

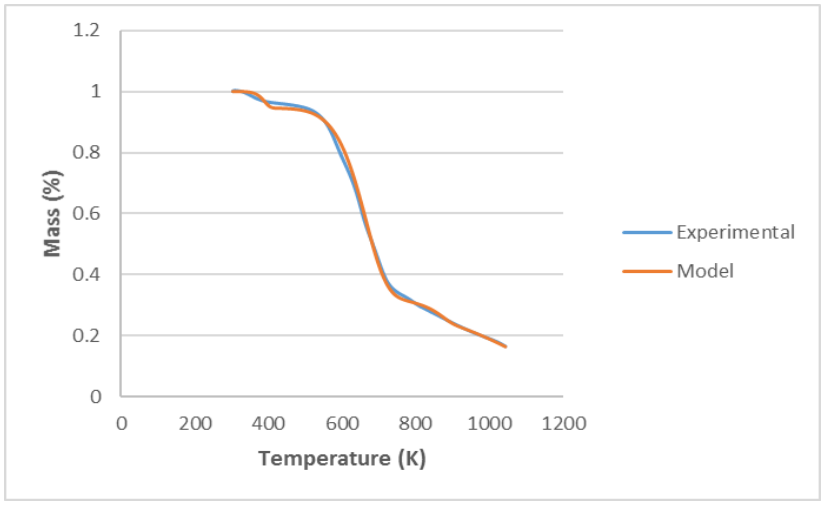

Figure 82 Six-pseudo component model

100 °C /min heating rate

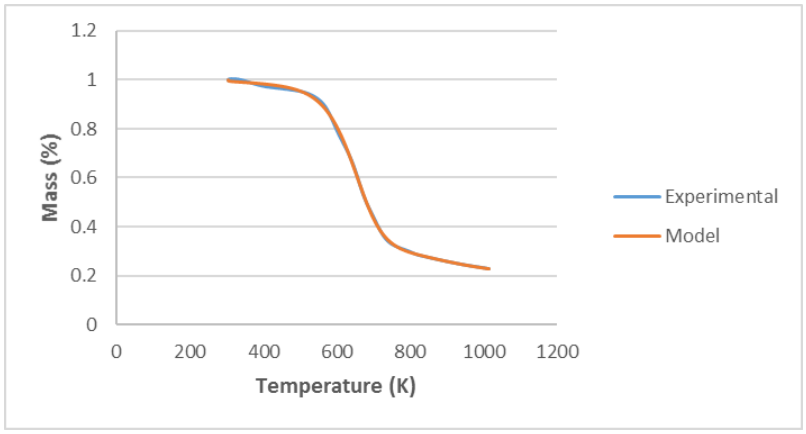

Figure 83 Four-pseudo component model

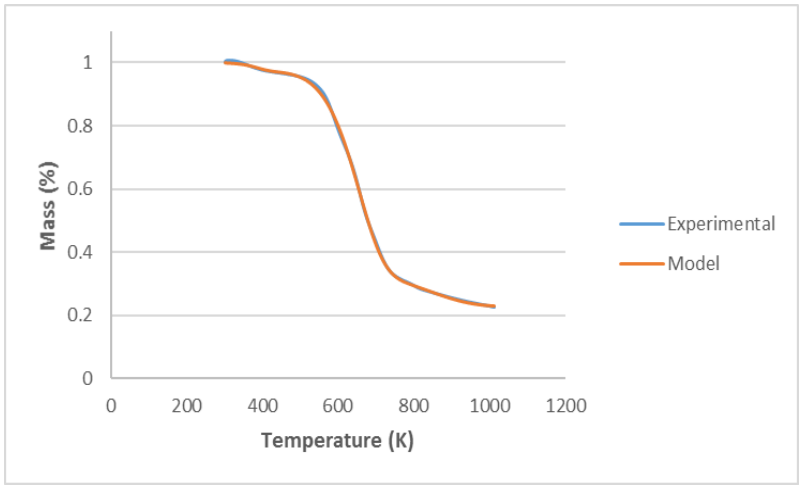

Figure 84 Five-pseudo component model

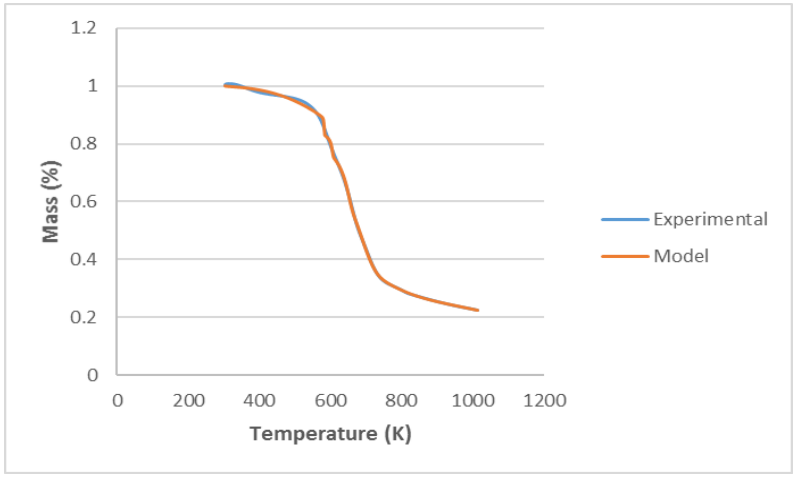

Figure 85 Six-pseudo component model

150 °C /min heating rate

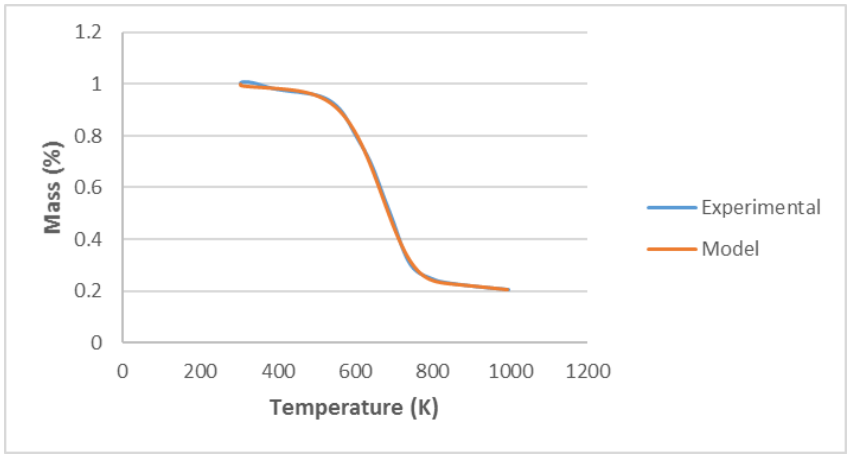

Figure 86 Four-pseudo component model

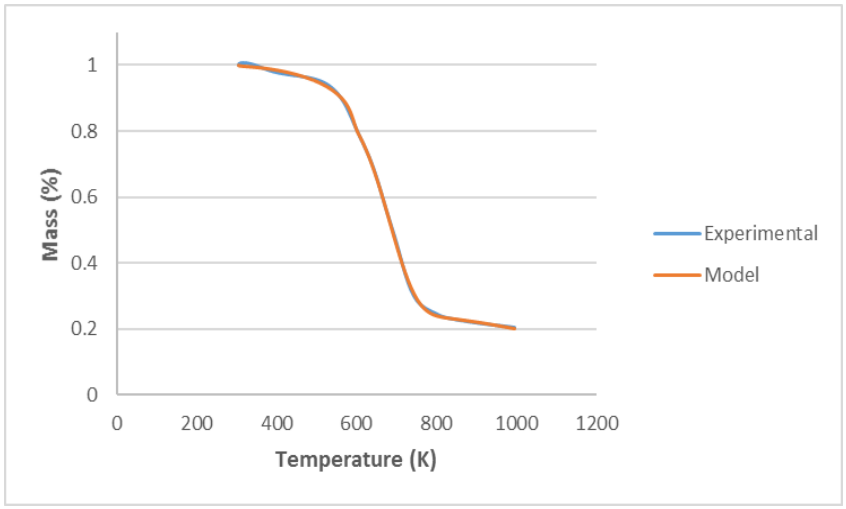

Figure 87 Five-pseudo component model

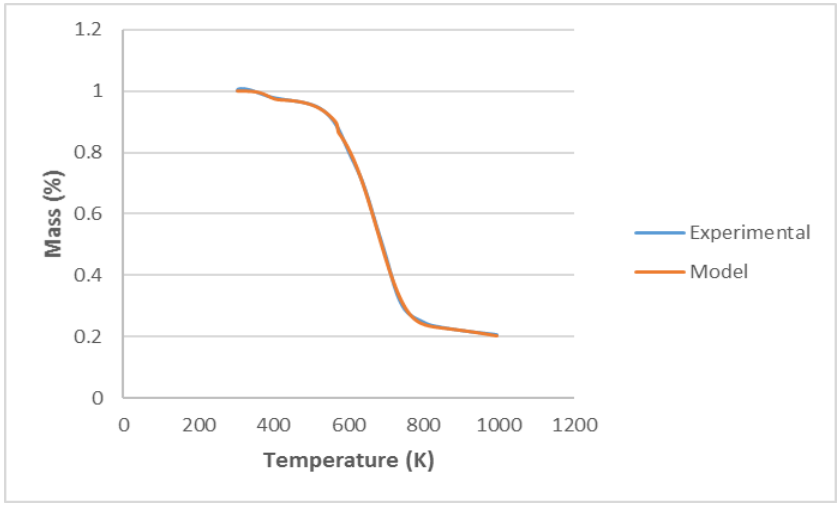

Figure 88 Six-pseudo component model

200 °C /min heating rate

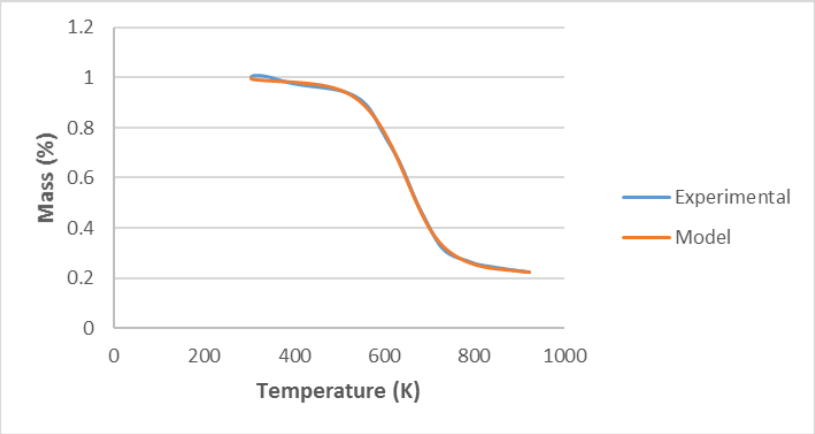

Figure 89 Four-pseudo component model

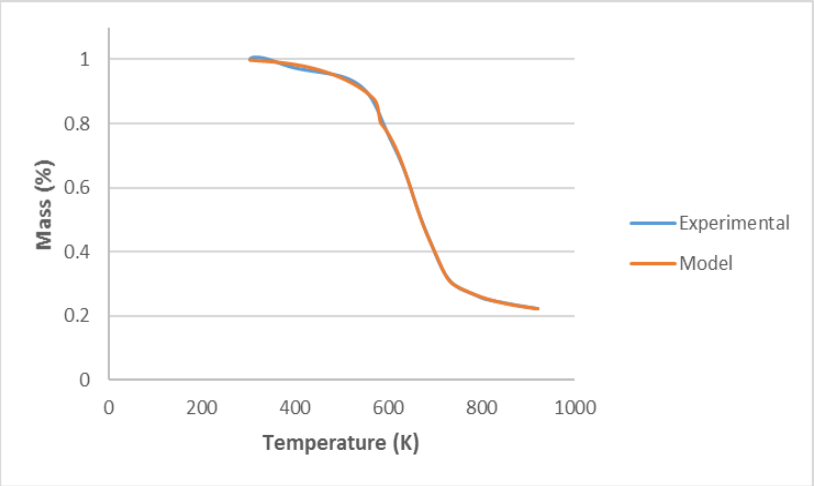

Figure 90 Five-pseudo component model

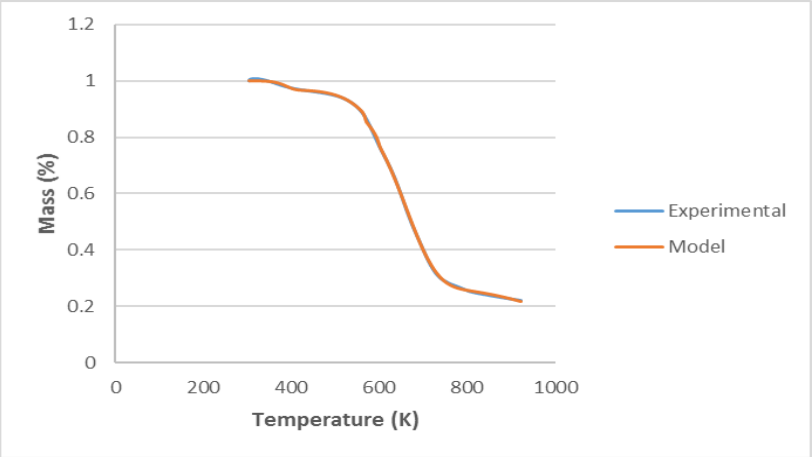

Figure 91 Six-pseudo component model

Appendix III *Q. cerris* cork (60-80 mesh) kinetic modelling

10 °C /min heating rate

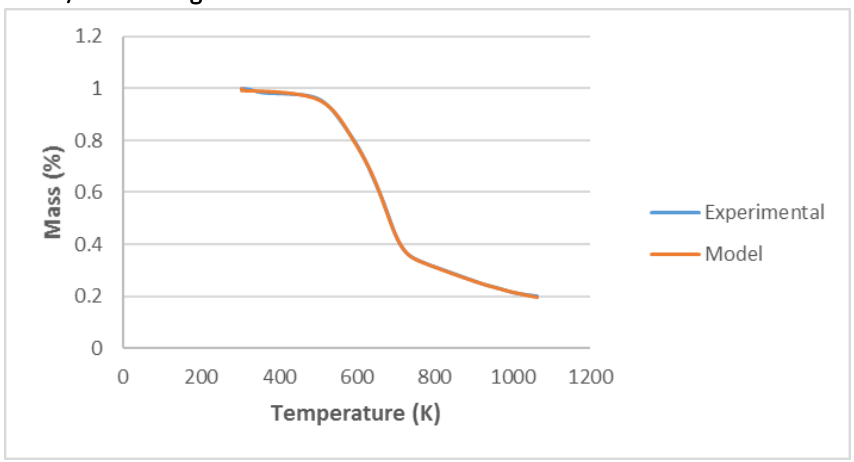

Figure 92 Four-pseudo component model

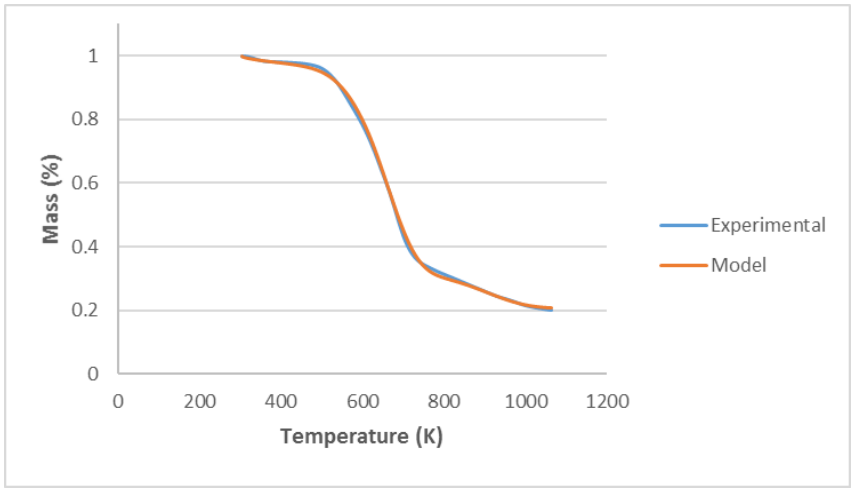

Figure 93 Five-pseudo component model

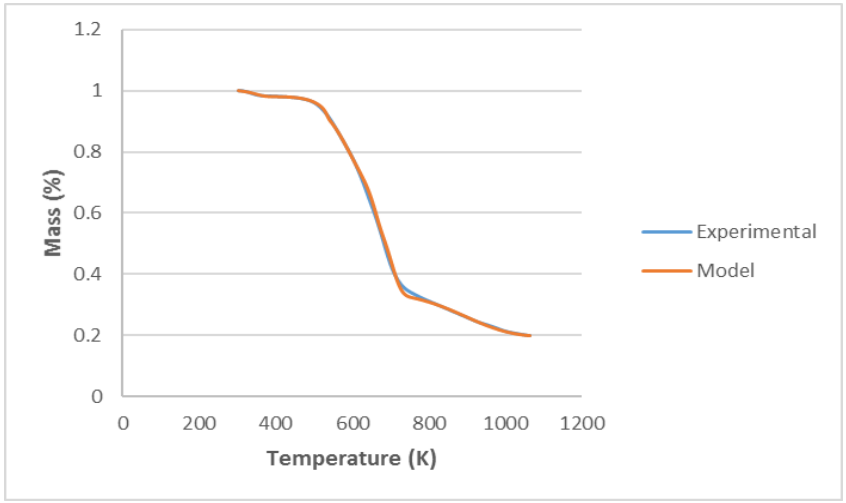

Figure 94 Six-pseudo component model

20 °C /min heating rate

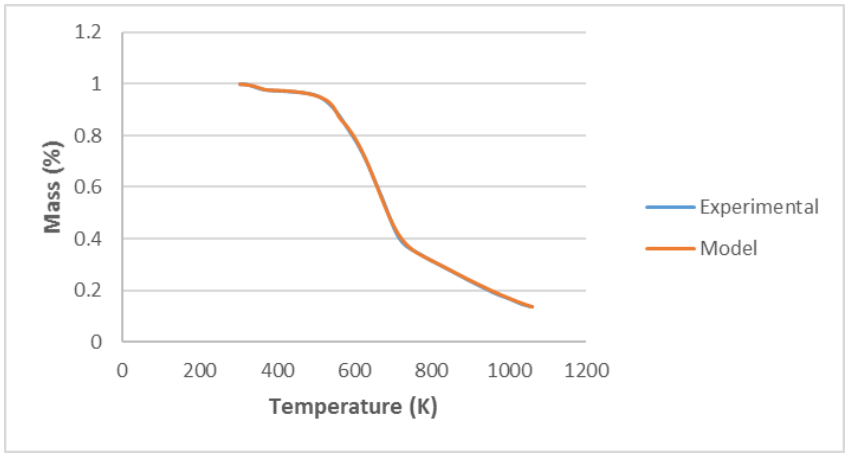

Figure 95 Four-pseudo component model

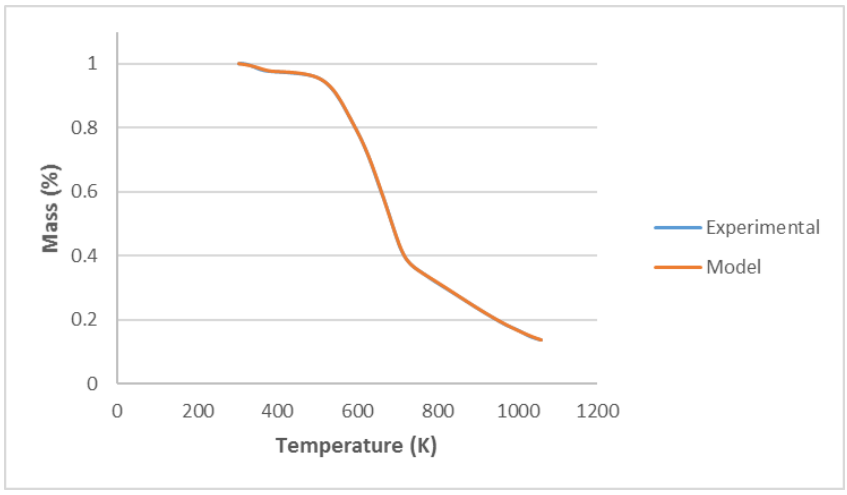

Figure 96 Five-pseudo component model

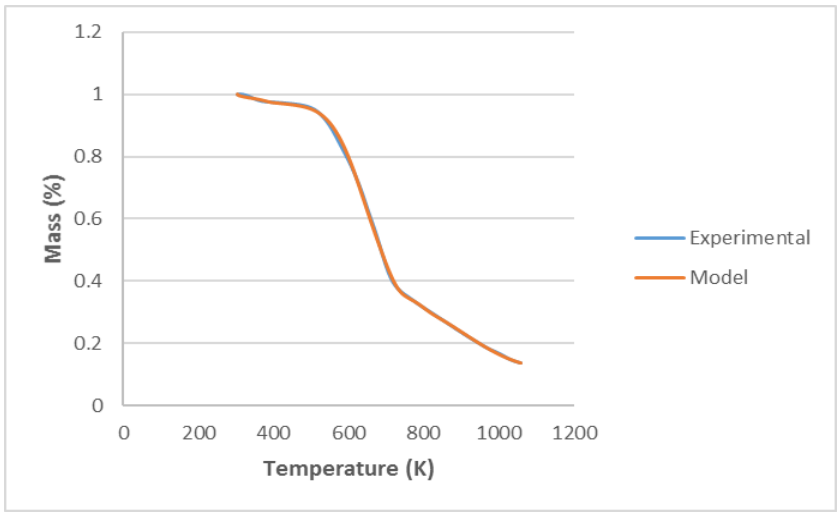

Figure 97 Six-pseudo component model

50 °C /min heating rate

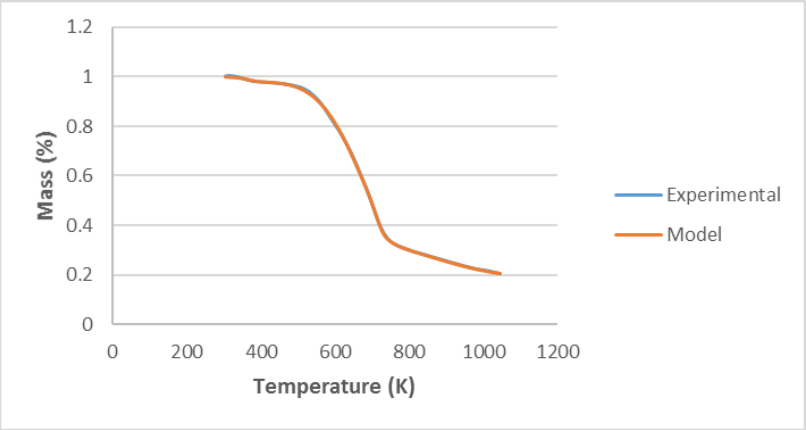

Figure 98 Four-pseudo component model

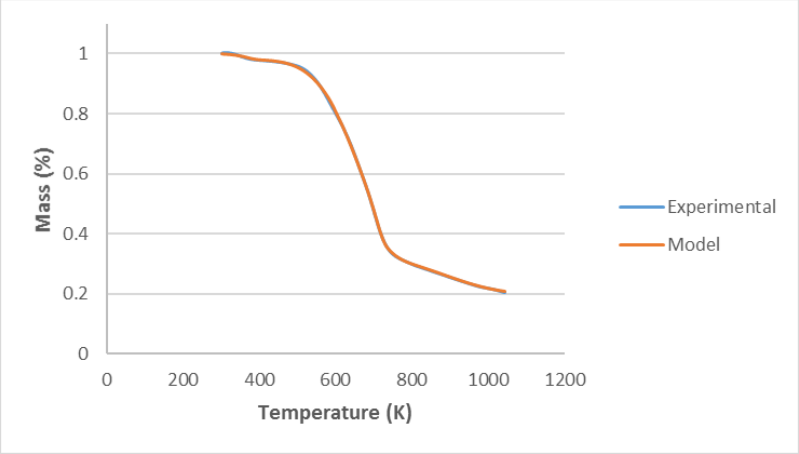

Figure 99 Five-pseudo component model

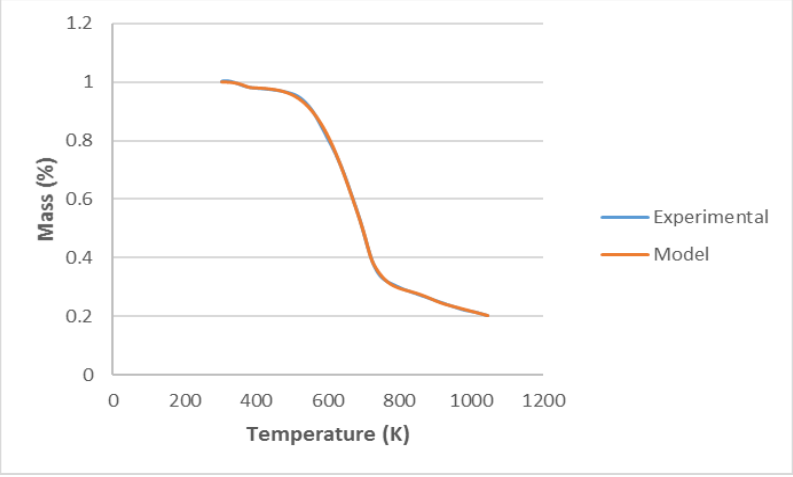

Figure 100 Six-pseudo component model

100 °C /min heating rate

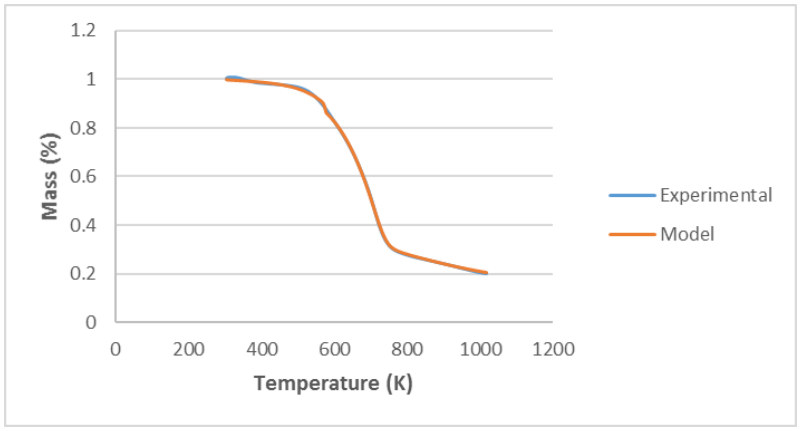

Figure 101 Four-pseudo component model

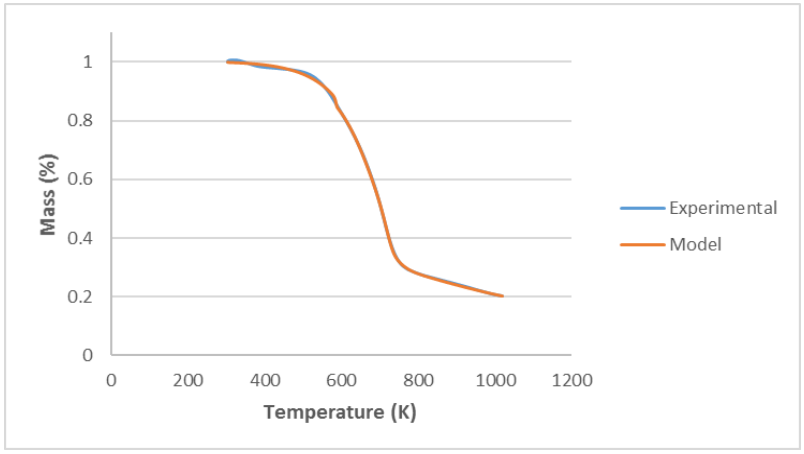

Figure 102 Five-pseudo component model

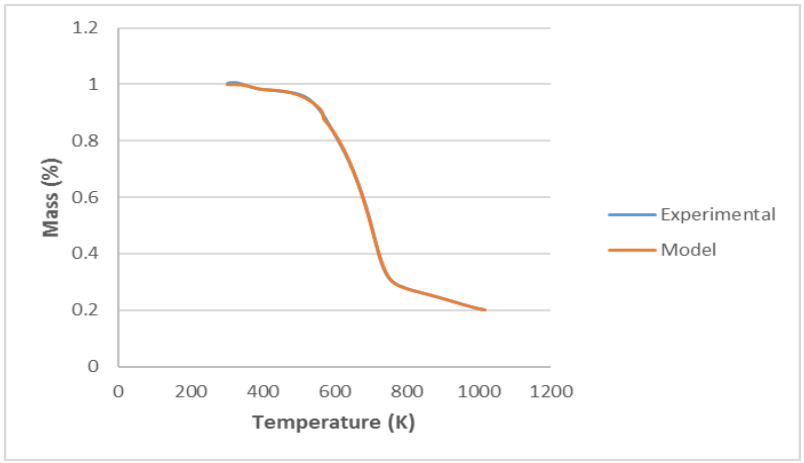

Figure 103 Six-pseudo component model

150 °C /min heating rate

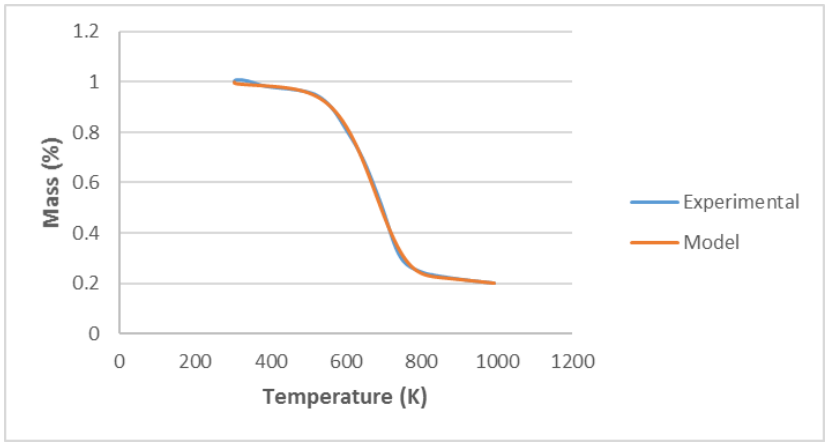

Figure 104 Four-pseudo component model

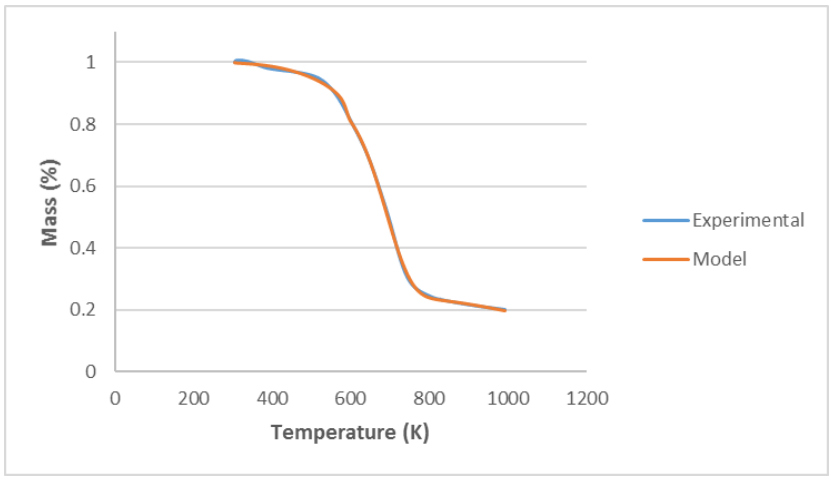

Figure 105 Five-pseudo component model

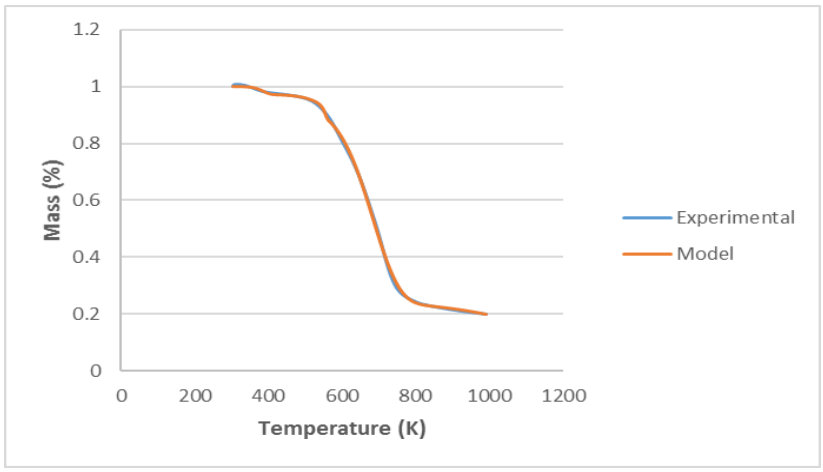

Figure 106 Six-pseudo component model

200 °C /min heating rate

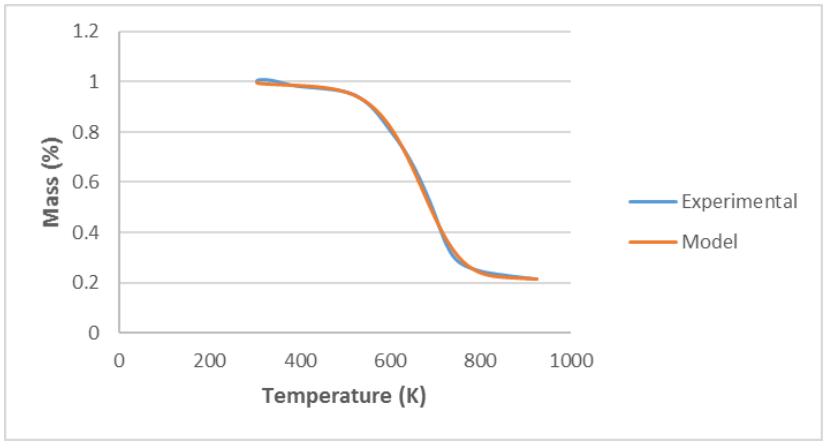

Figure 107 Four-pseudo component model

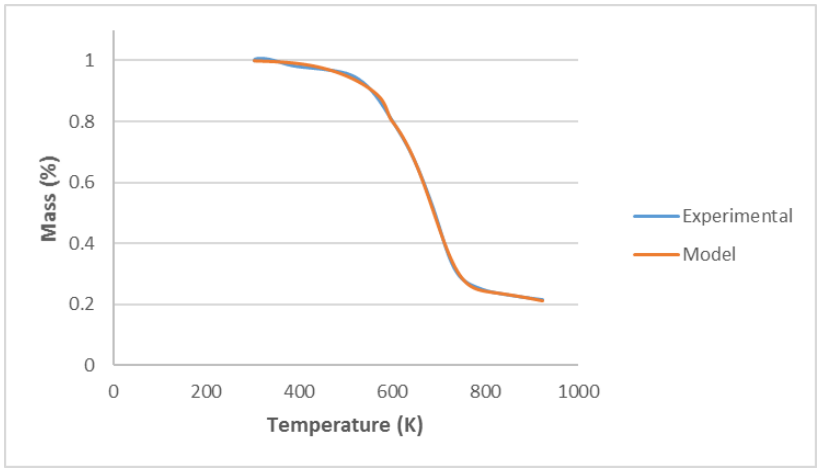

Figure 108 Five-pseudo component model

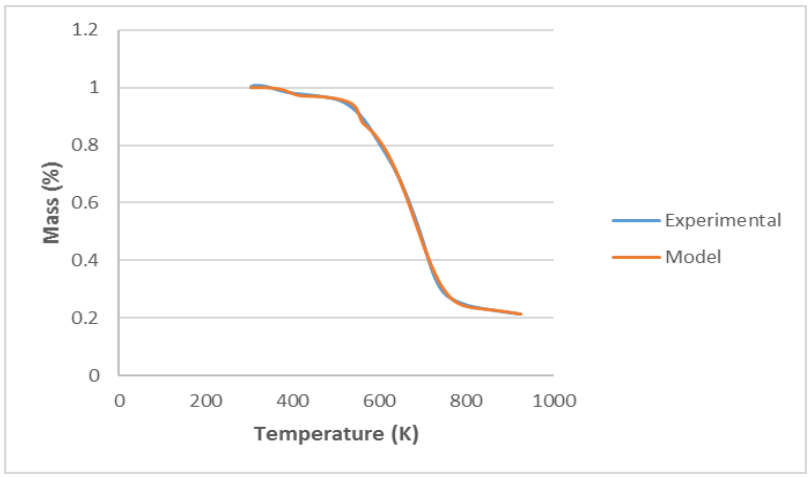

Figure 109 Six-pseudo component model

Appendix IV *Q. cerris* phloem (40-60 mesh) kinetic modelling

10 °C /min heating rate

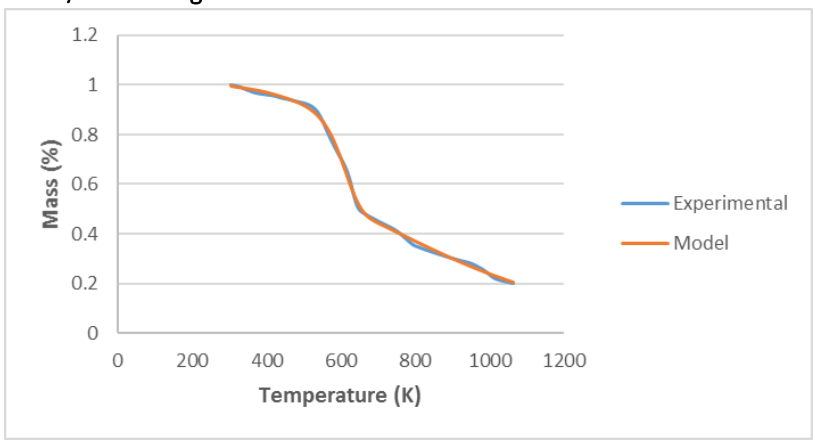

Figure 110 Four-pseudo component model

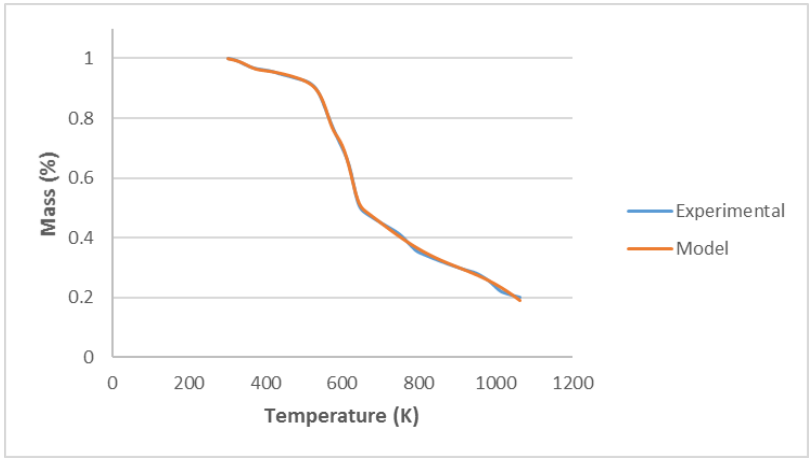

Figure 111 Five-pseudo component model

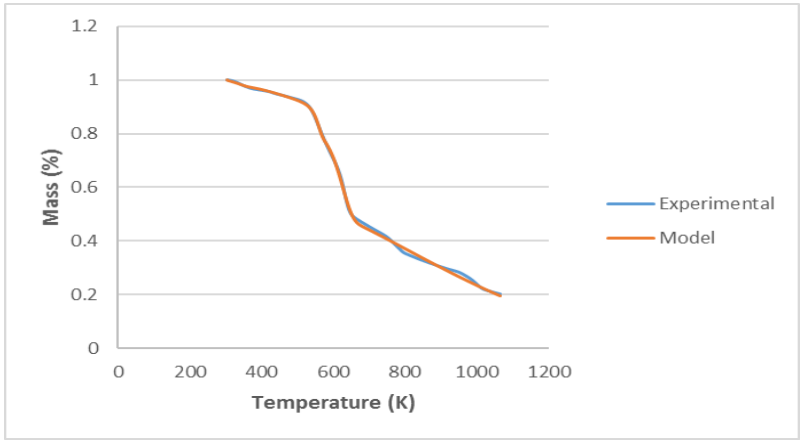

Figure 112 Six-pseudo component model

20 °C /min heating rate

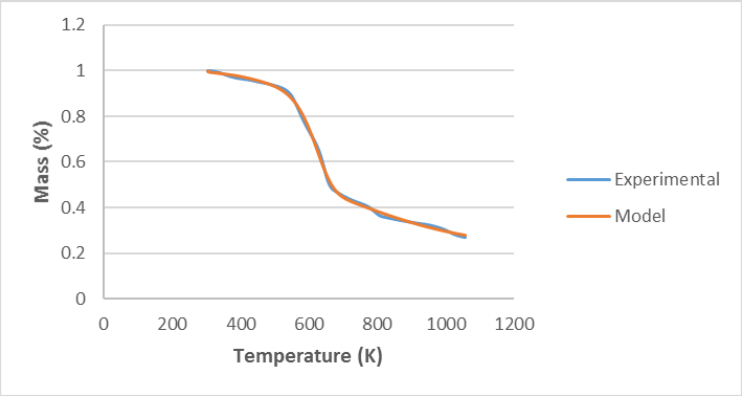

Figure 113 Four-pseudo component model

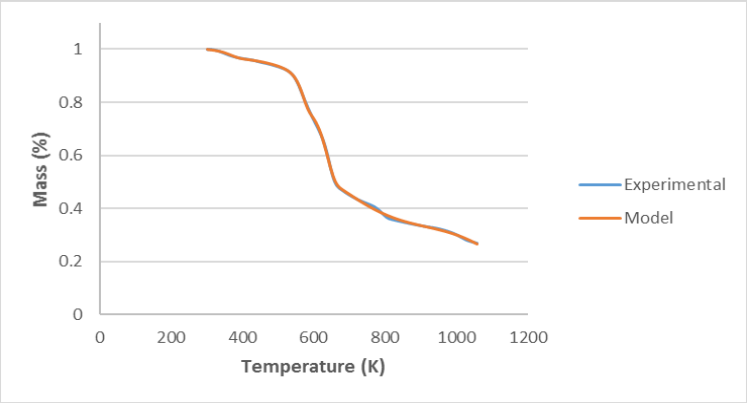

Figure 114 Five-pseudo component model

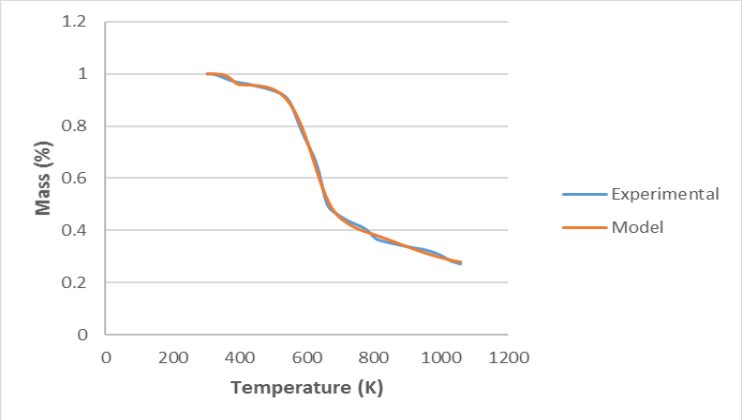

Figure 115 Six-pseudo component model

50 °C /min heating rate

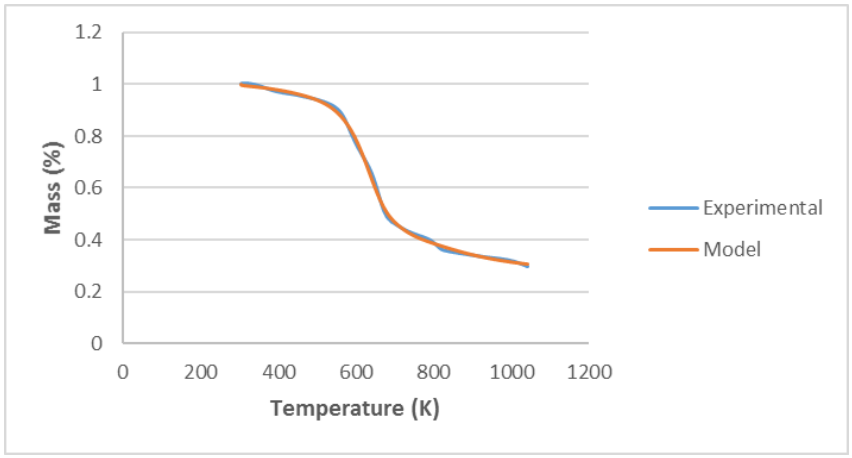

Figure 116 Four-pseudo component model

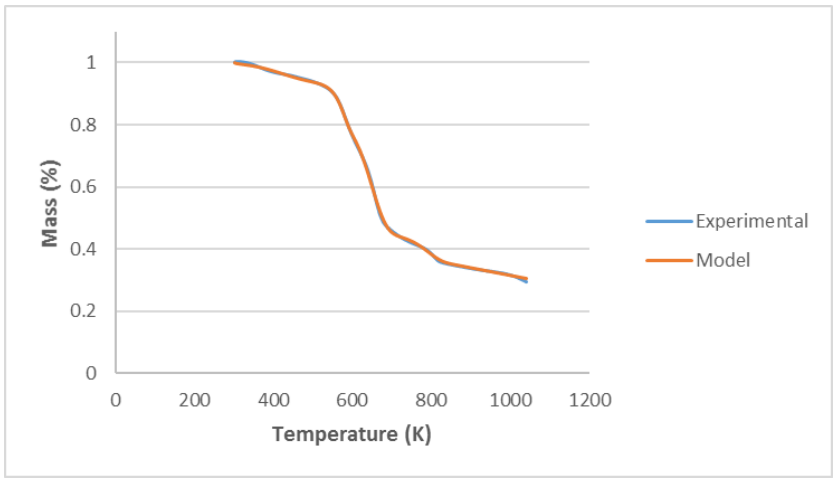

Figure 117 Five-pseudo component model

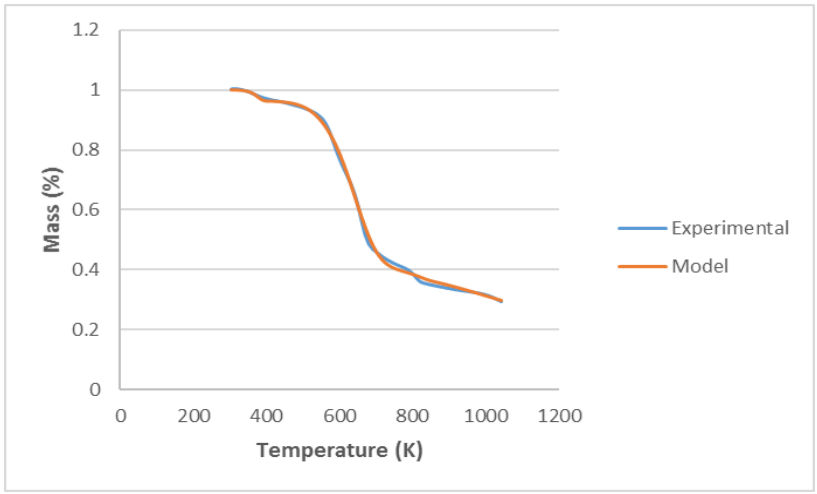

Figure 118 Six-pseudo component model

100 °C /min heating rate

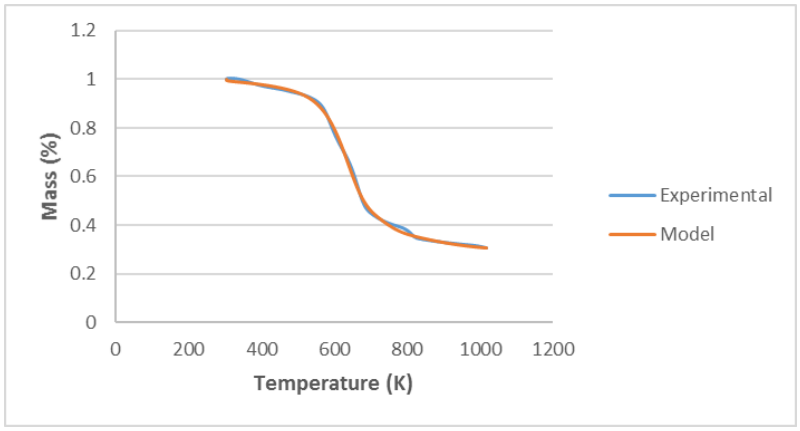

Figure 119 Four-pseudo component model

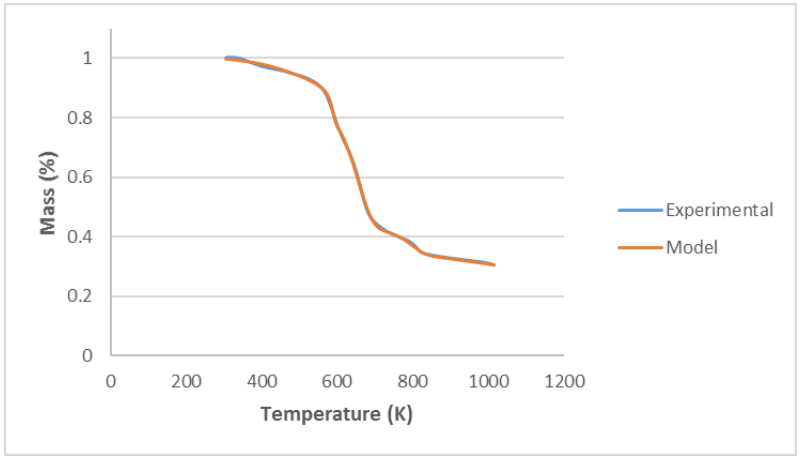

Figure 120 Five-pseudo component model

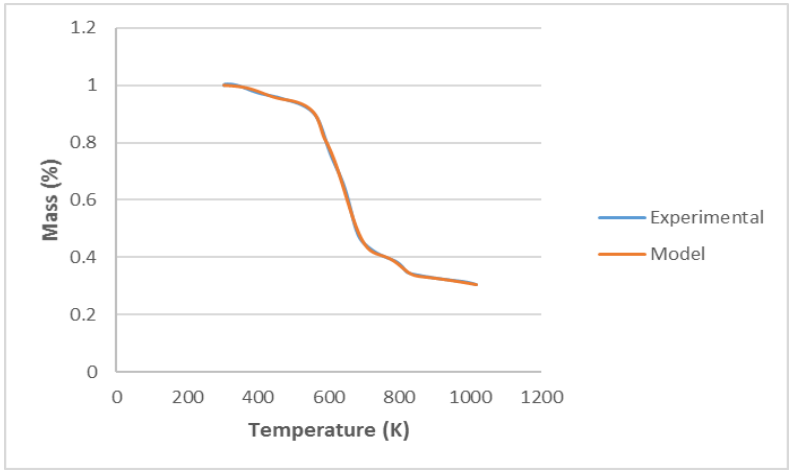

Figure 121 Six-pseudo component model

150 °C /min heating rate

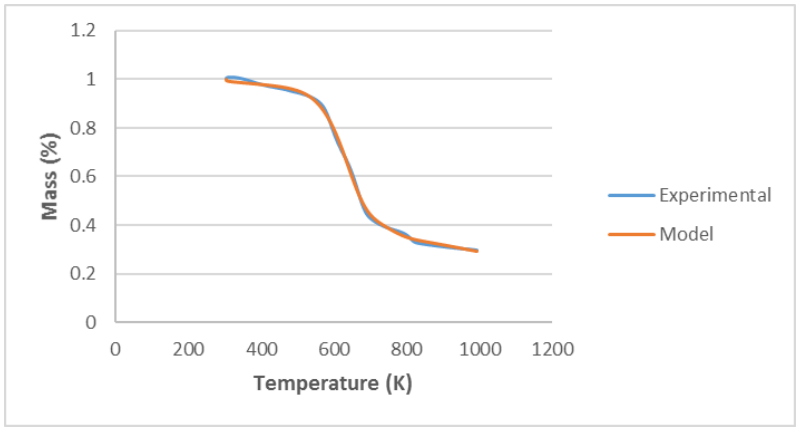

Figure 122 Four-pseudo component model

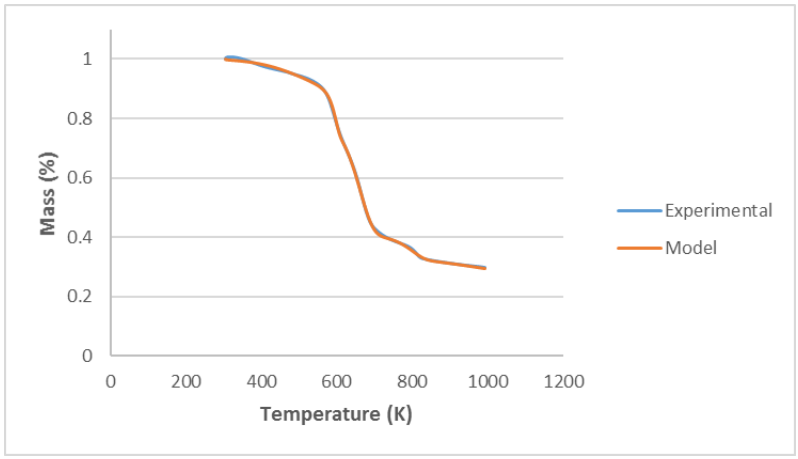

Figure 123 Five-pseudo component model

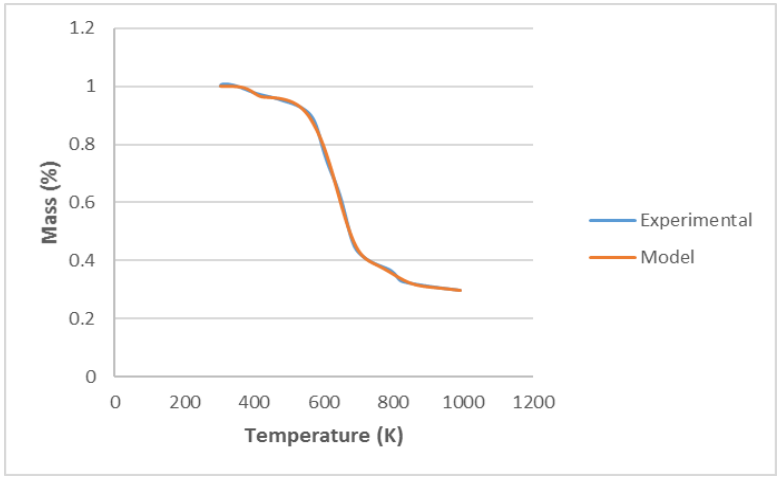

Figure 124 Six-pseudo component model

200 °C /min heating rate

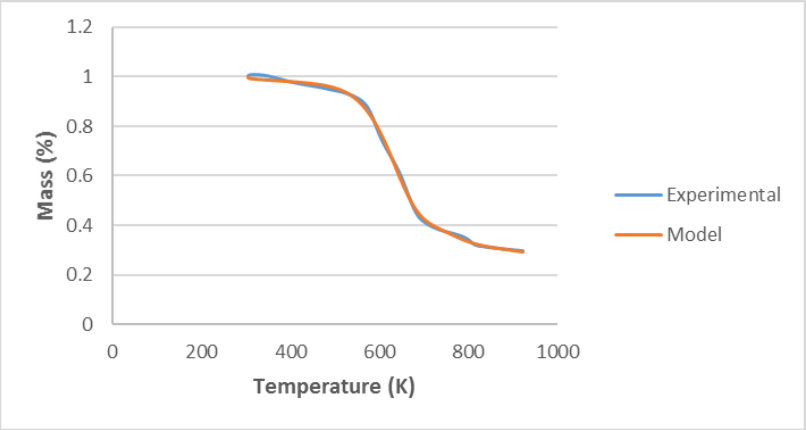

Figure 125 Four-pseudo component model

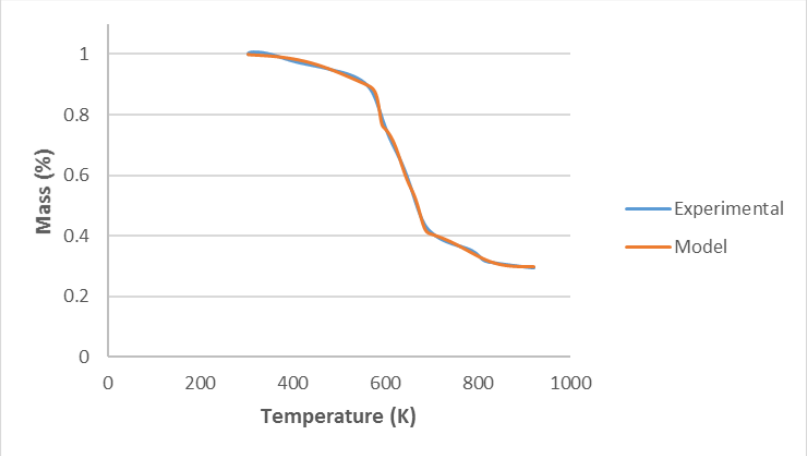

Figure 126 Five-pseudo component model

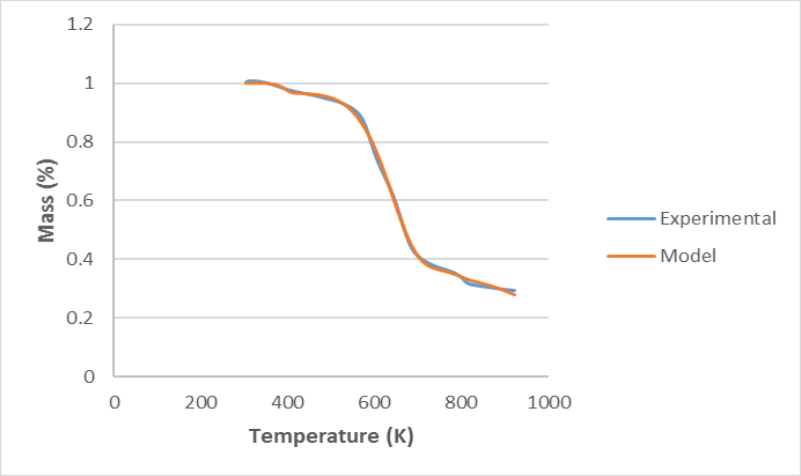

Figure 127 Six-pseudo component model

Appendix V *B. recurvata* cork (40-60 mesh) kinetic modelling

10 °C /min heating rate

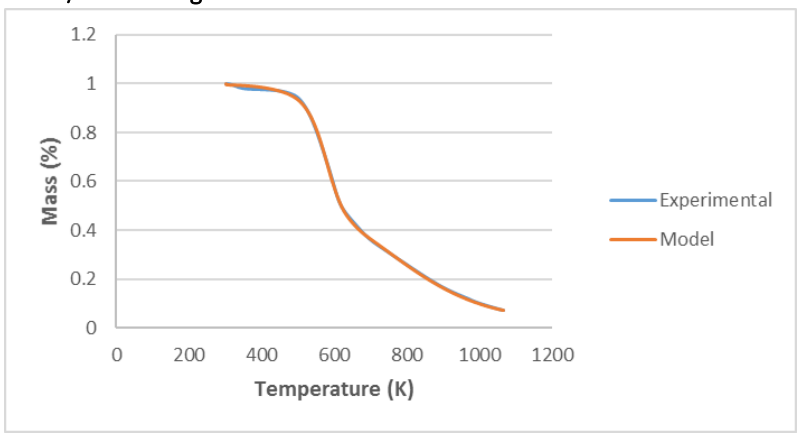

Figure 128 Four-pseudo component model

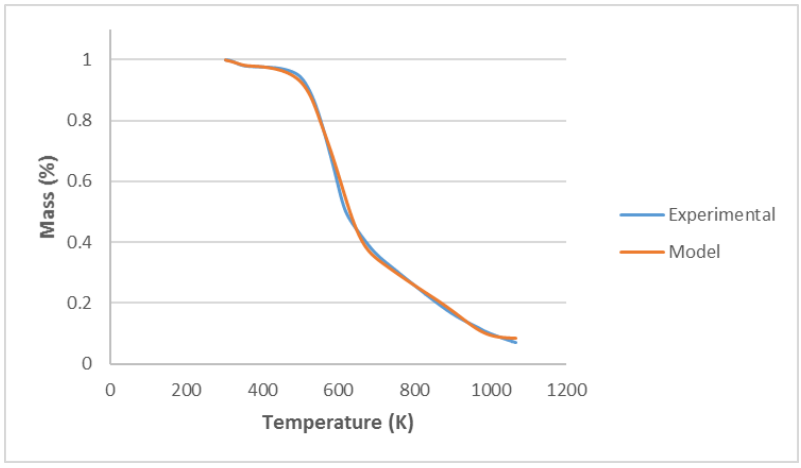

Figure 129 Five-pseudo component model

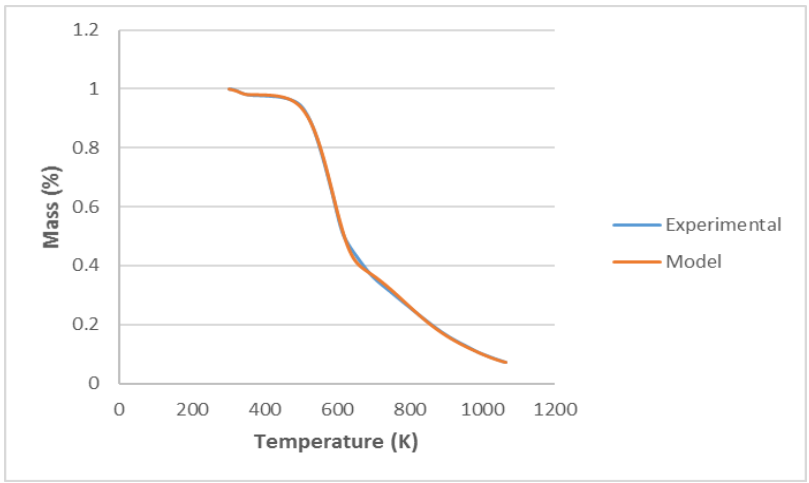

Figure 130 Six-pseudo component model

20 °C /min heating rate

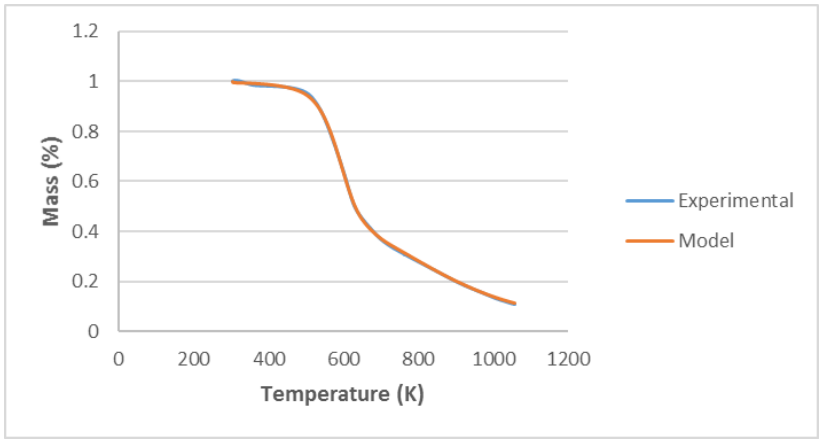

Figure 131 Four-pseudo component model

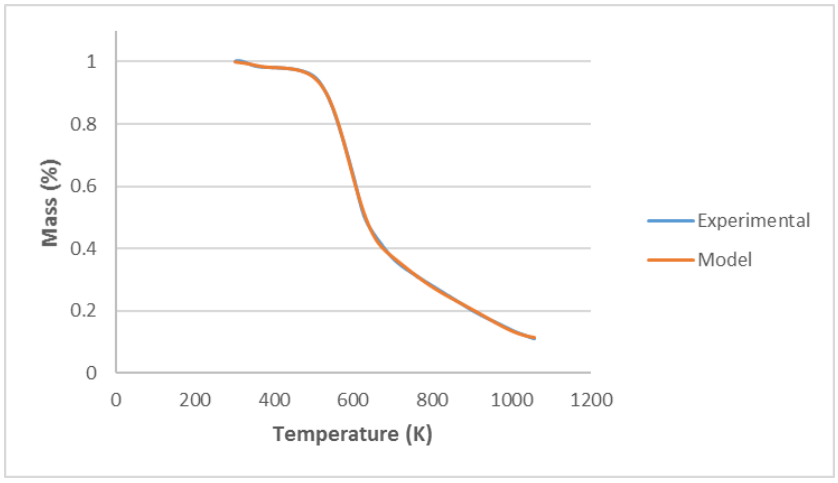

Figure 132 Five-pseudo component model

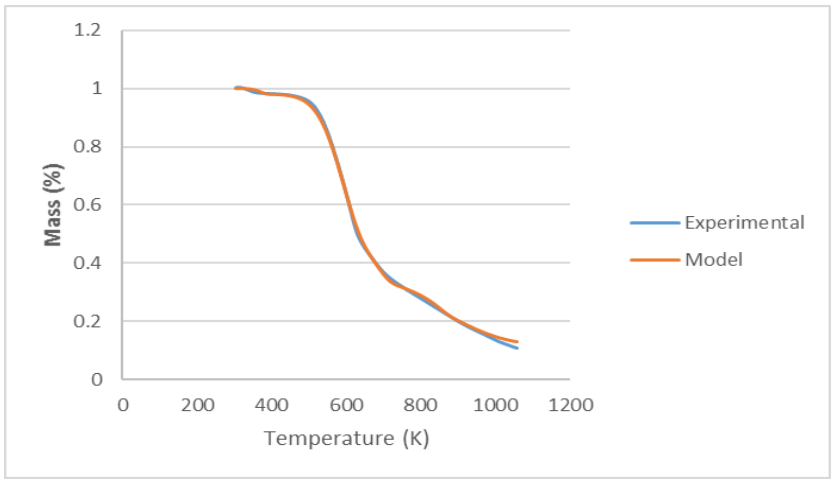

Figure 133 Six-pseudo component model

50 °C /min heating rate

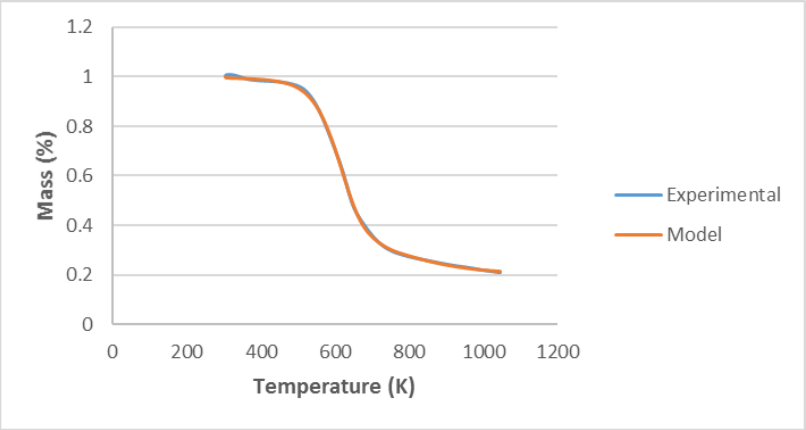

Figure 134 Four-pseudo component model

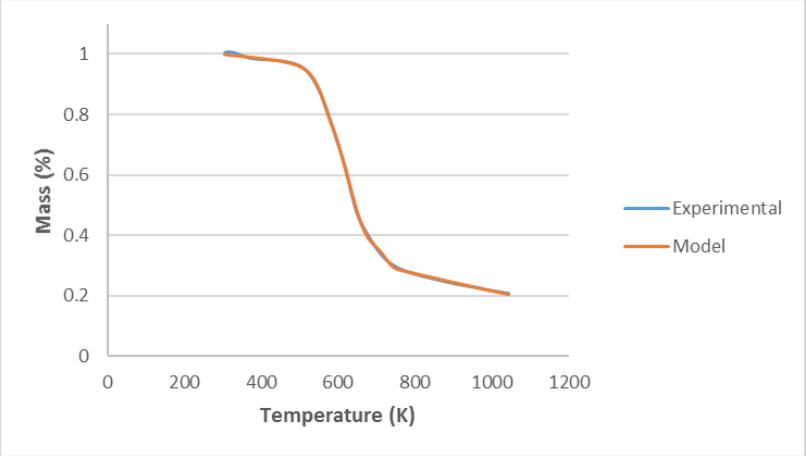

Figure 135 Five-pseudo component model

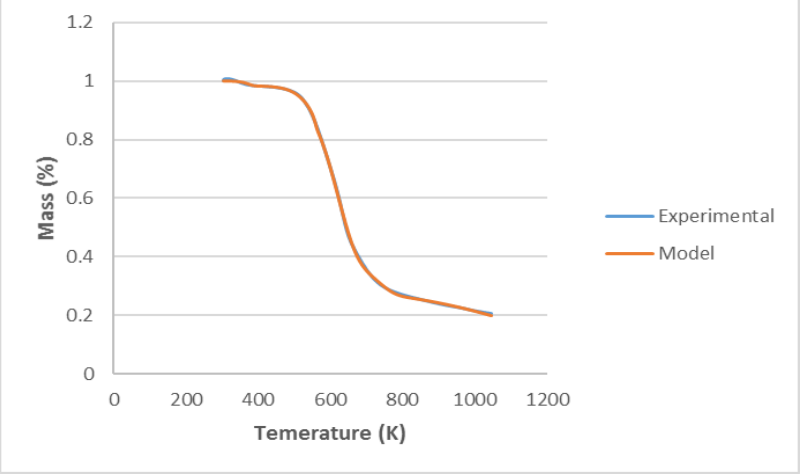

Figure 136 Six-pseudo component model

100 °C /min heating rate

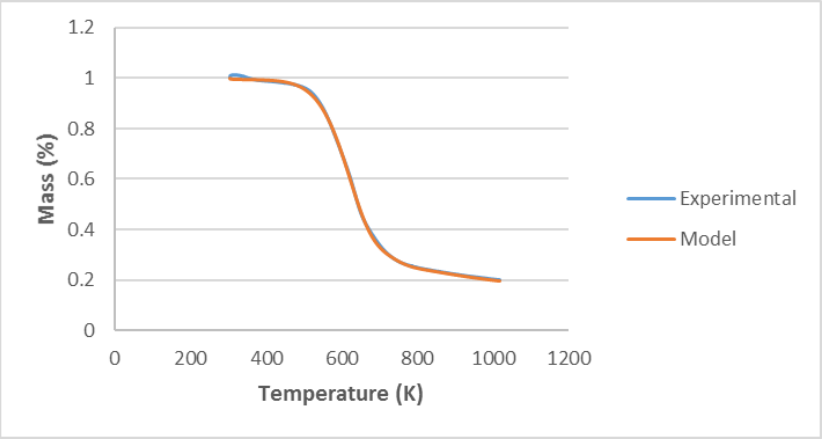

Figure 137 Four-pseudo component model

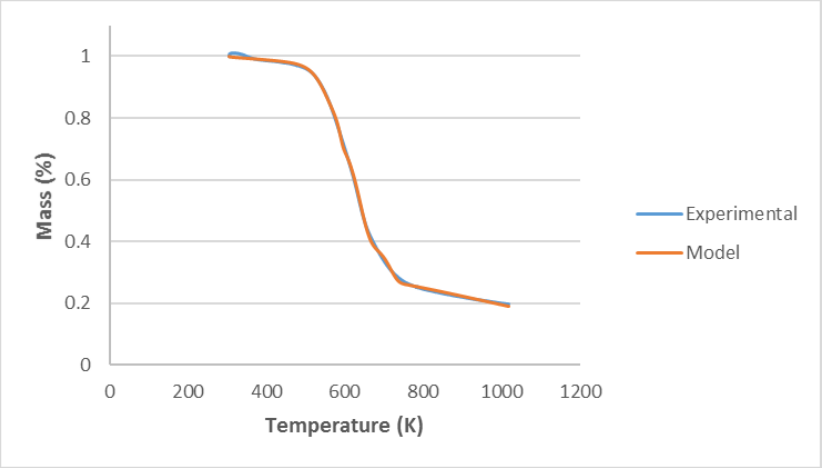

Figure 138 Five-pseudo component model

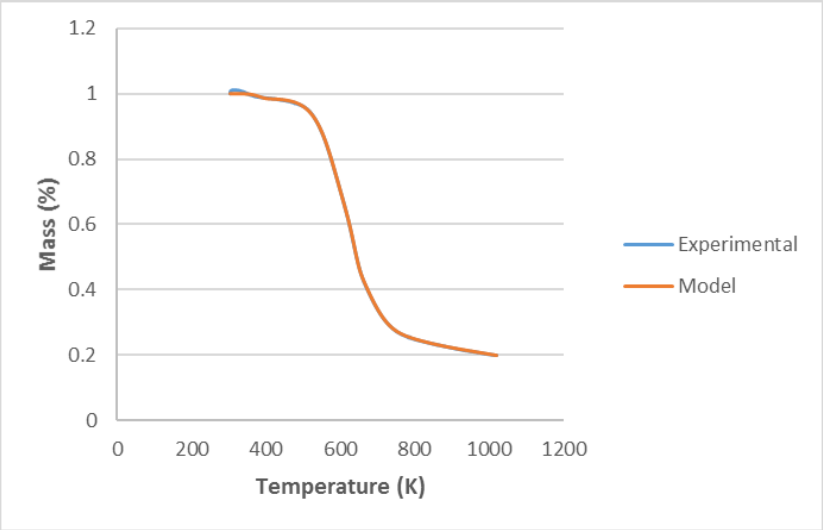

Figure 139 Six-pseudo component model

150 °C /min heating rate

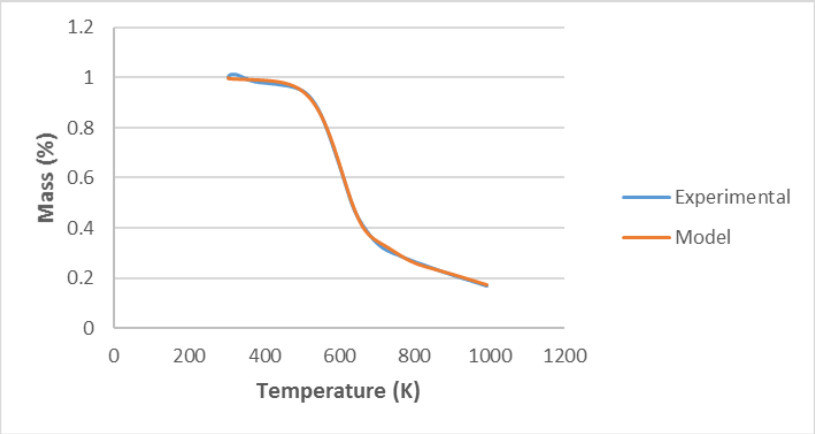

Figure 140 Four-pseudo component model

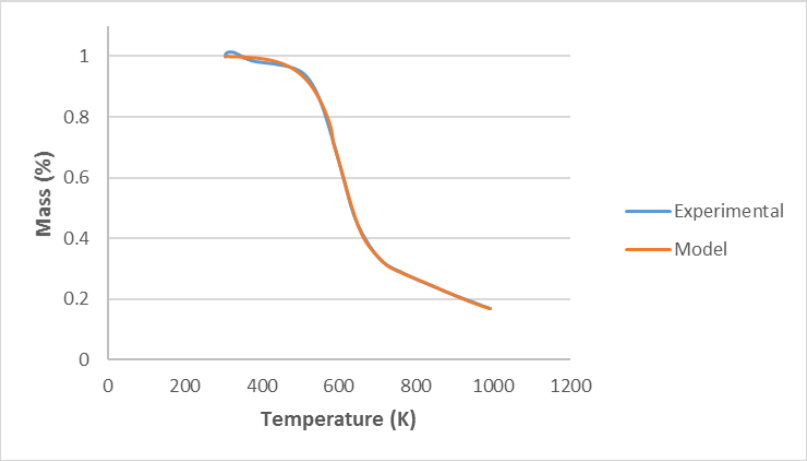

Figure 141 Five-pseudo component model

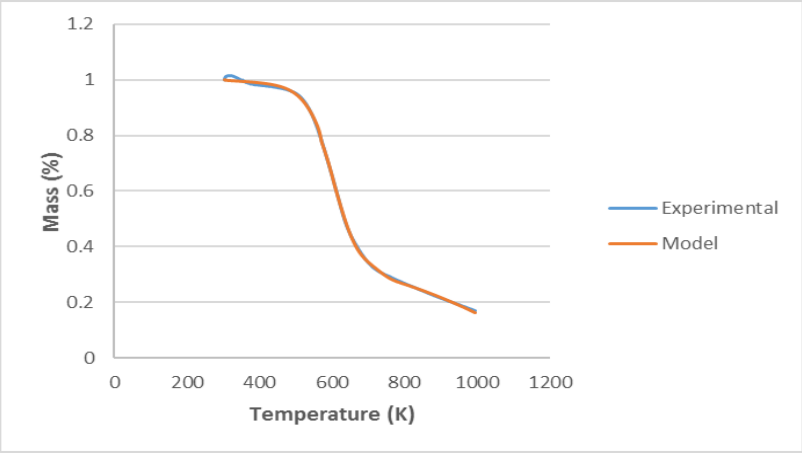

Figure 142 Six-pseudo component model

200 °C /min heating rate

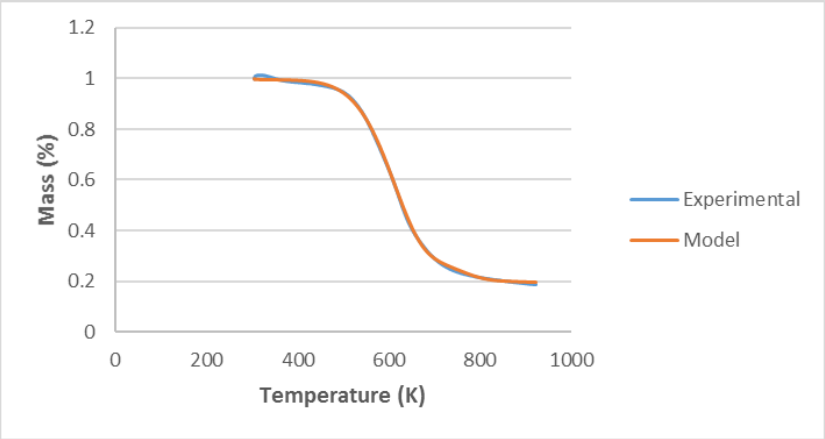

Figure 143 Four-pseudo component model

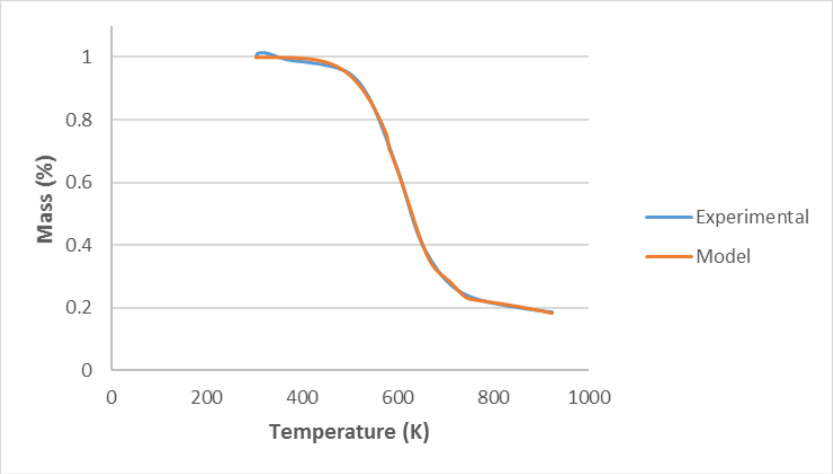

Figure 144 Five-pseudo component model

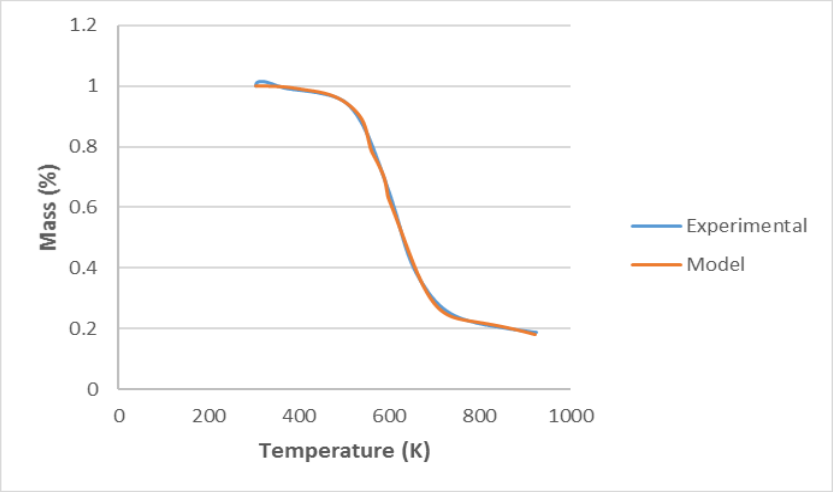

Figure 145 Six-pseudo component model

Appendix VI *B. pendula* cork (40-60 mesh) kinetic modelling

10 °C /min heating rate

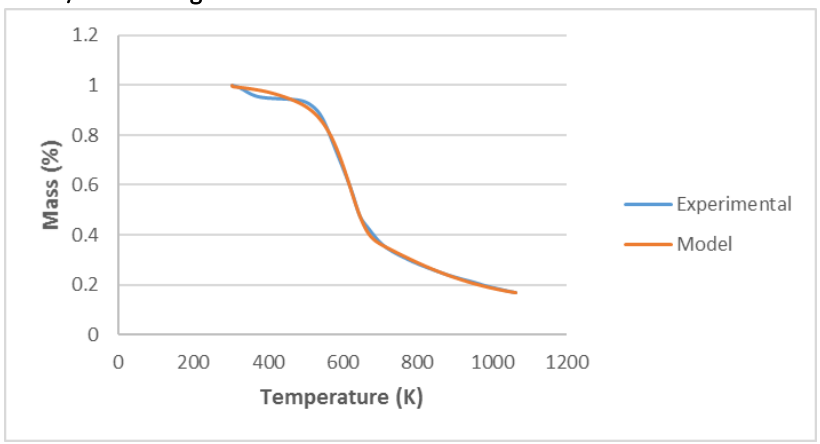

Figure 146 Four-pseudo component model

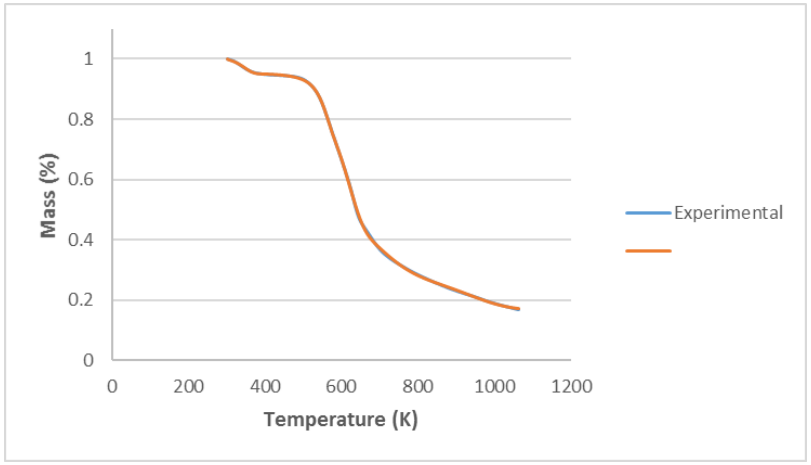

Figure 147 Five-pseudo component model

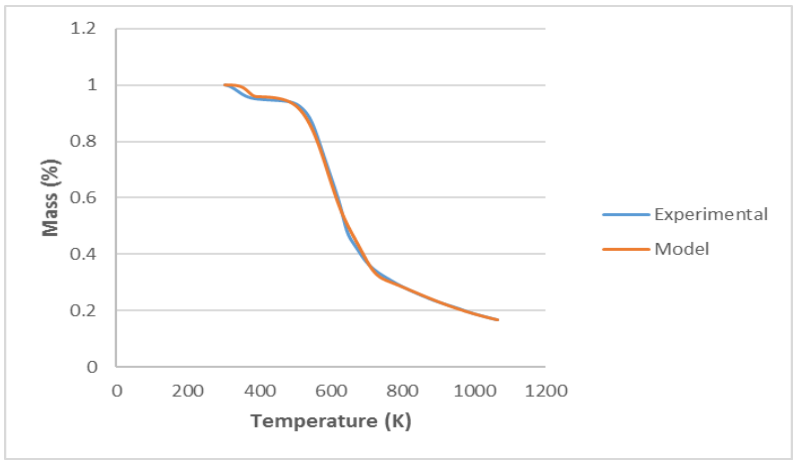

Figure 148 Six-pseudo component model

20 °C /min heating rate

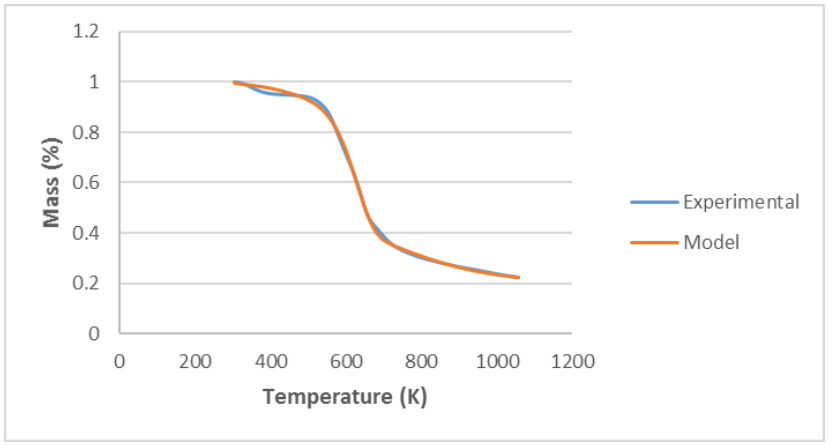

Figure 149 Four-pseudo component model

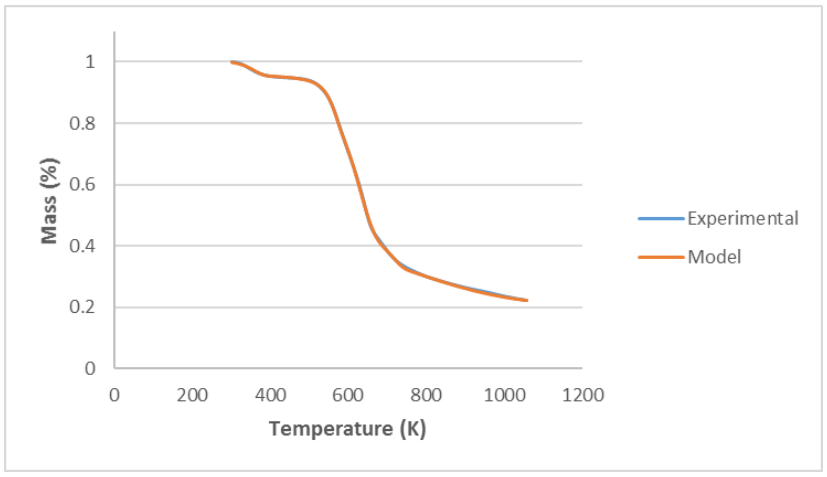

Figure 150 Five-pseudo component model

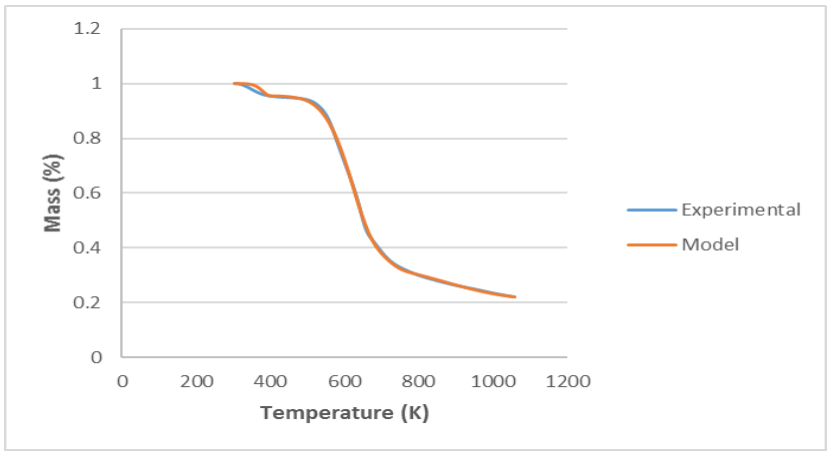

Figure 151 Six-pseudo component model

50 °C /min heating rate

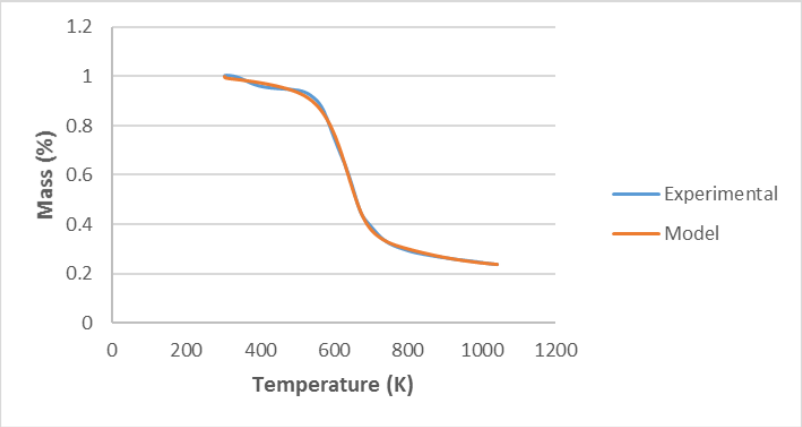

Figure 152 Four-pseudo component model

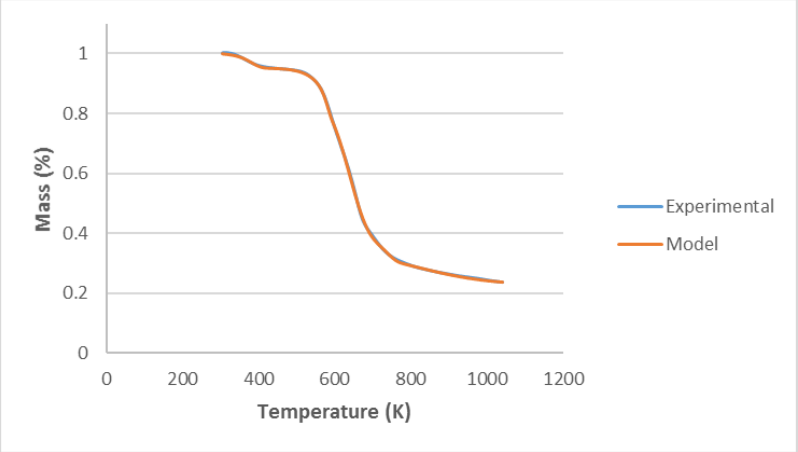

Figure 153 Five-pseudo component model

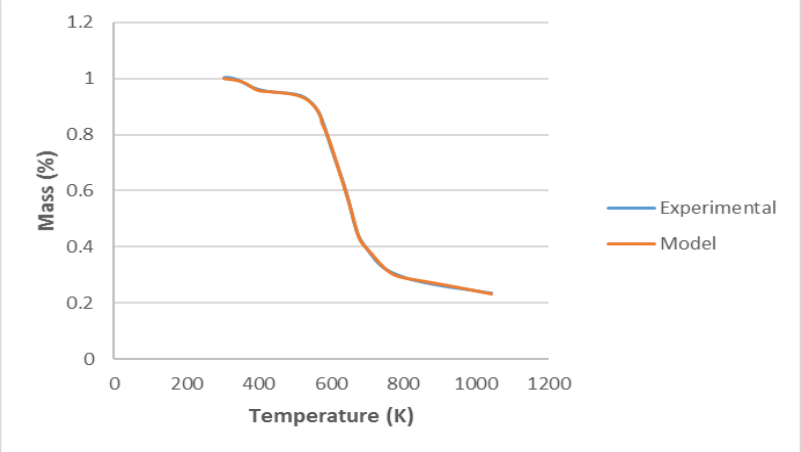

Figure 154 Six-pseudo component model

100 °C /min heating rate

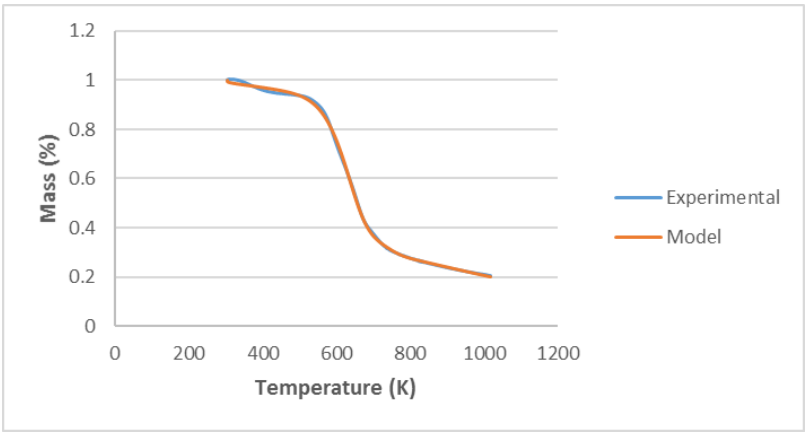

Figure 155 Four-pseudo component model

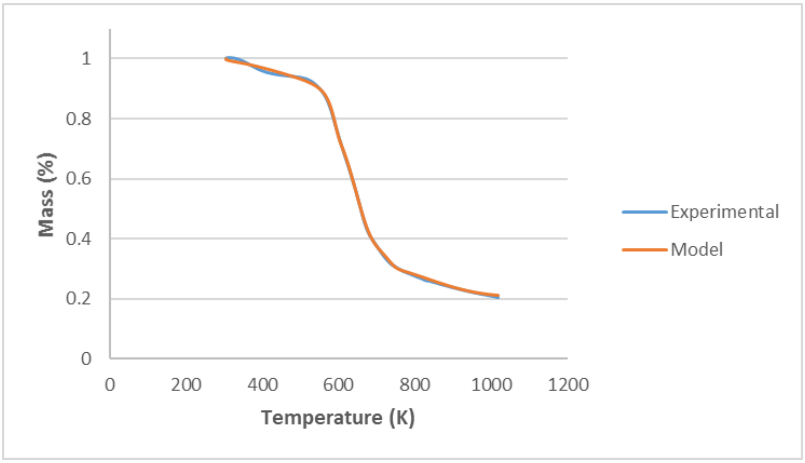

Figure 156 Five-pseudo component model

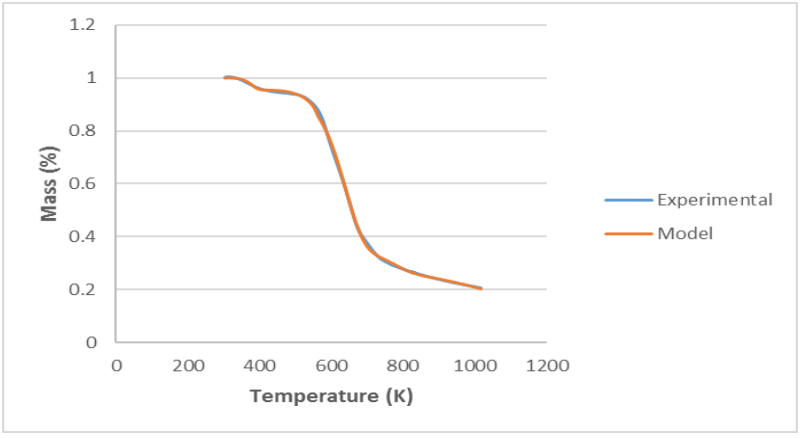

Figure 157 Six-pseudo component model

150 °C /min heating rate

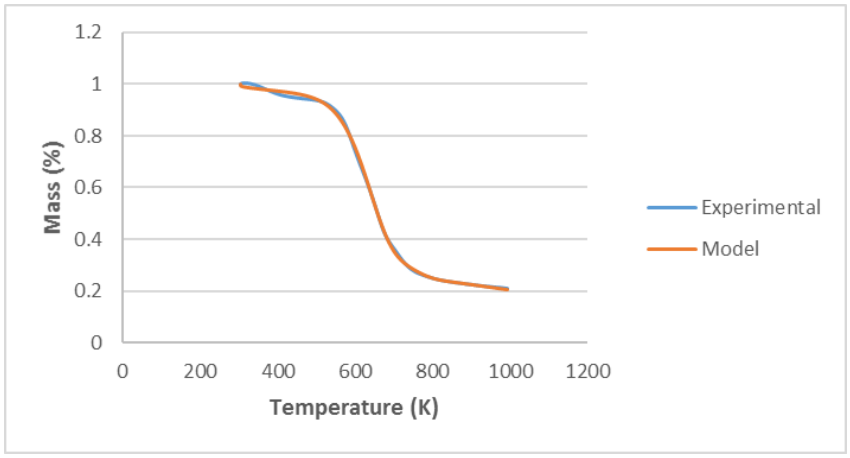

Figure 158 Four-pseudo component model

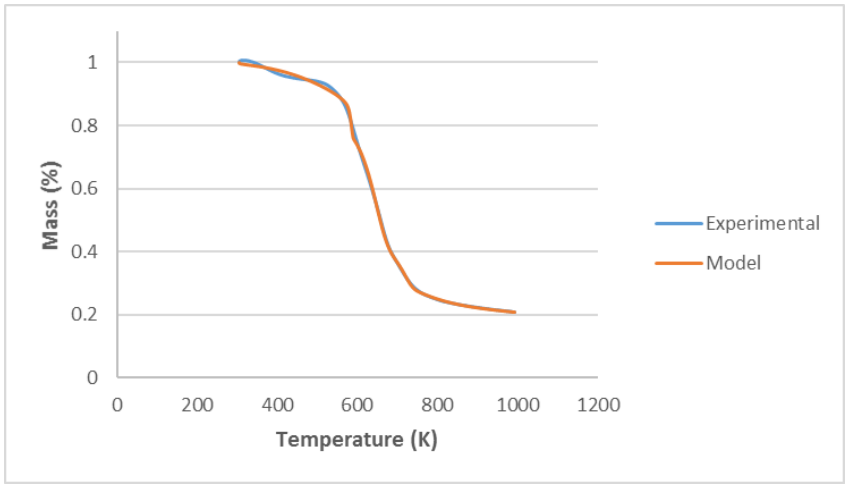

Figure 159 Five-pseudo component model

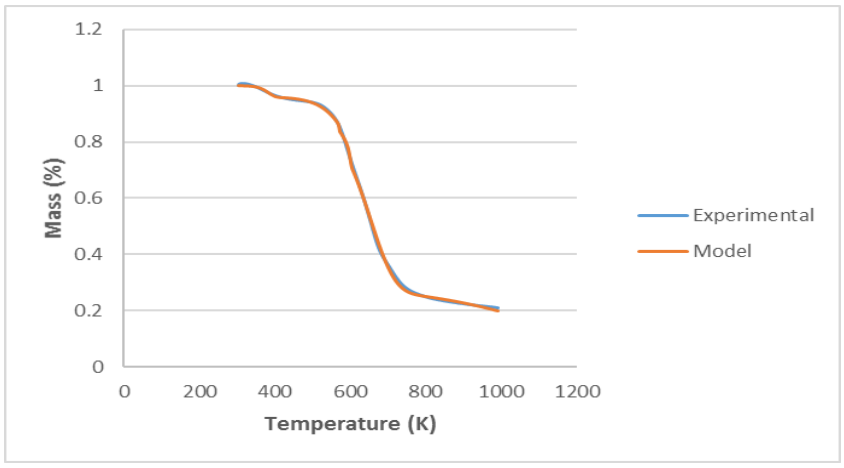

Figure 160 Six-pseudo component model

200 °C /min heating rate

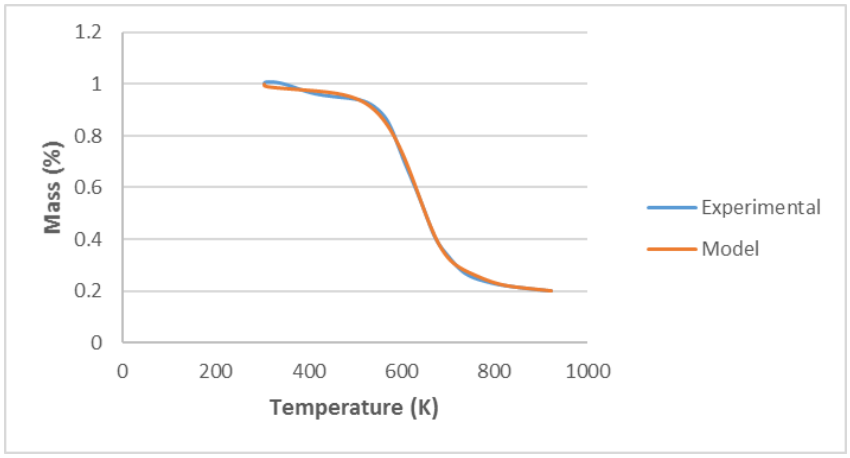

Figure 161 Four-pseudo component model

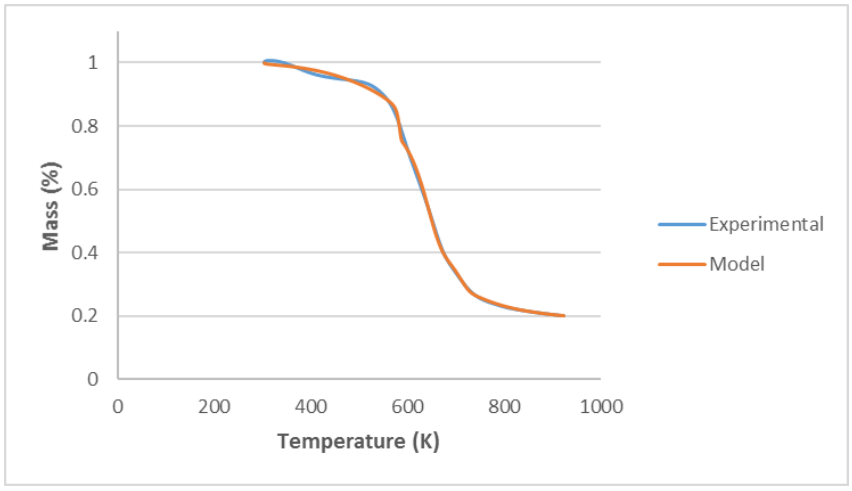

Figure 162 Five-pseudo component model

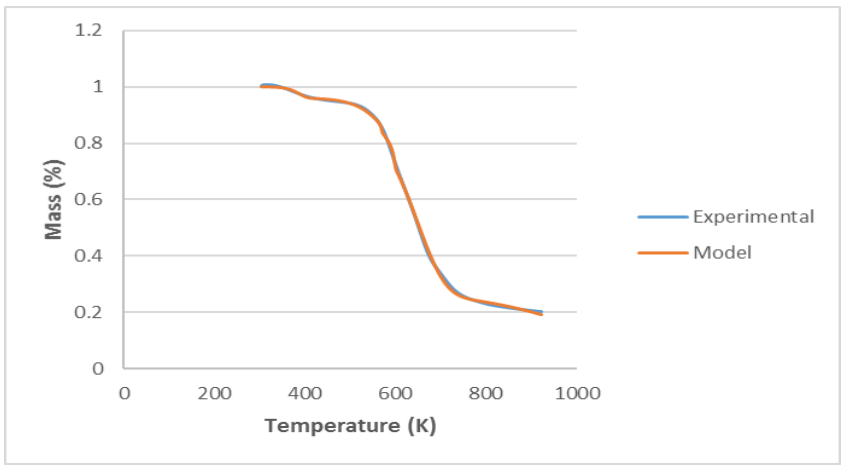

Figure 163 Six-pseudo component model

Appendix VII Global modelling kinetic parameters

Table 15 Q. cerris cork (20-40 mesh) kinetic model

	Ps1	Ps2	Ps3	Ps4	Ps5	Ps6	Charcoal
k0	2.46E+01	2.28E-03	1.90E+00	1.58E-03	3.04E-06	2.84E-06	
Ea	9.07E+03	7.30E+04	4.35E+04	8.77E+03	7.97E+04	3.86E+04	
xi	0.05	0.21	0.17	0.00	0.22	0.12	0.23

Table 16 Q. cerris cork (40-60 mesh) kinetic model

	Ps1	Ps2	Ps3	Ps4	Ps5	Ps6	Charcoal
k0	1.34E+01	1.21E+00	9.69E-03	7.26E-05	1.18E-05	1.36E-06	
Ea	7.31E+03	3.48E+04	5.54E+04	1.94E+04	7.56E+04	5.35E+04	
xi	0.05	0.19	0.24	0.18	0.16	0.08	0.09

Table 17 Q. cerris cork (60-80 mesh) kinetic model

	Ps1	Ps2	Ps3	Ps4	Ps5	Ps6	Charcoal
k0	2.57E+01	7.30E-03	3.56E+00	9.97E-09	8.70E-06	4.86E-08	
Ea	8.13E+03	6.89E+04	4.00E+04	5.57E+04	8.16E+04	8.32E+04	
xi	0.04	0.19	0.16	0.07	0.24	0.09	0.20

Table 18 Q. cerris phloem (40-60 mesh) kinetic model

	Ps1	Ps2	Ps3	Ps4	Ps5	Ps6	Charcoal
k0	1.50E+01	7.89E-07	4.05E-01	1.15E-05	1.01E-07	1.09E-05	
Ea	8.73E+03	6.42E+04	3.75E+04	3.03E+04	1.36E+05	2.48E+04	
xi	0.09	0.09	0.34	0.00	0.16	0.15	0.18

Table 19 B. recurvata cork (40-60 mesh) kinetic model

	Ps1	Ps2	Ps3	Ps4	Ps5	Ps6	Charcoal
k0	1.23E+02	9.70E+00	2.41E-02	2.20E-05	1.04E-06	3.45E-03	
Ea	2.70E+04	6.87E+04	7.50E+04	2.83E+04	9.19E+04	9.40E+03	
xi	0.10	0.22	0.28	0.15	0.16	0.00	0.11

Table 20 B. pendula cork (40-60 mesh) kinetic model

	Ps1	Ps2	Ps3	Ps4	Ps5	Ps6	Charcoal
k0	4.69E+01	1.76E-11	5.23E+00	3.22E-03	1.69E-07	2.23E-07	
Ea	8.91E+03	1.55E+05	5.89E+04	1.20E+05	1.57E+05	5.83E+04	
xi	0.07	0.11	0.20	0.17	0.17	0.06	0.23

Appendix VIII Overall model fit qualities

Table 21 Fit qualities (%) in different models (10 °C/min heating rate)

Biomass types	Four Pseudo component Model	Five Pseudo component Model	Six Pseudo component Model
Q. cerris cork 20-40 mesh	99.45	99.81	99.25
Q. cerris cork 40-60 mesh	99.73	99.79	99.10
Q. cerris cork 60-80 mesh	99.71	99.19	99.33
Q. cerris phloem 40-60 mesh	99.06	99.55	99.23
Ponytail palm cork 40-60 mesh	99.55	98.80	99.44
Birch cork 40-60 mesh	98.90	99.78	98.91

Table 22 Fit qualities (%) in different models (20 °C/min heating rate)

Biomass types	Four Pseudo component Model	Five Pseudo component Model	Six Pseudo component Model
Q. cerris cork 20-40 mesh	99.37	99.80	99.81
Q. cerris cork 40-60 mesh	99.23	99.72	99.88
Q. cerris cork 60-80 mesh	99.73	99.89	99.50
Q. cerris phloem 40-60 mesh	99.16	99.65	99.13
Ponytail palm cork 40-60 mesh	99.61	99.69	99.28
Birch cork 40-60 mesh	99.04	99.80	99.40

Table 23 Fit qualities (%) in different models (50 °C/min heating rate)

Biomass types	Four Pseudo component Model	Five Pseudo component Model	Six Pseudo component Model
Q. cerris cork 20-40 mesh	99.45	99.63	99.55
Q. cerris cork 40-60 mesh	99.38	99.53	98.79
Q. cerris cork 60-80 mesh	99.74	99.74	99.71
Q. cerris phloem 40-60 mesh	99.21	99.64	99.13
Ponytail palm cork 40-60 mesh	99.50	99.61	99.65
Birch cork 40-60 mesh	99.17	99.75	99.72

Table 24 Fit qualities (%) in different models (100 °C/min heating rate)

Biomass types	Four Pseudo component Model	Five Pseudo component Model	Six Pseudo component Model
Q. cerris cork 20-40 mesh	100.00	99.48	99.61
Q. cerris cork 40-60 mesh	99.37	99.54	99.45
Q. cerris cork 60-80 mesh	99.58	99.56	99.70
Q. cerris phloem 40-60 mesh	99.17	99.57	99.59
Ponytail palm cork 40-60 mesh	99.43	99.39	99.66
Birch cork 40-60 mesh	99.18	99.46	99.45

Table 25 Fit qualities (%) in different models (150 °C/min heating rate)

Biomass types	Four Pseudo component Model	Five Pseudo component Model	Six Pseudo component Model
Q. cerris cork 20-40 mesh	99.19	99.44	99.52
Q. cerris cork 40-60 mesh	99.28	99.50	99.59
Q. cerris cork 60-80 mesh	99.18	99.45	99.47
Q. cerris phloem 40-60 mesh	99.06	99.53	99.43
Ponytail palm cork 40-60 mesh	99.19	99.28	99.31
Birch cork 40-60 mesh	99.09	99.25	99.41

Table 26 Fit qualities (%) in different models (200 °C/min heating rate)

Biomass types	Four Pseudo component Model	Five Pseudo component Model	Six Pseudo component Model
Q. cerris cork 20-40 mesh	99.20	99.43	99.60
Q. cerris cork 40-60 mesh	99.17	99.39	99.62
Q. cerris cork 60-80 mesh	99.01	99.42	99.40
Q. cerris phloem 40-60 mesh	99.01	99.32	99.29
Ponytail palm cork 40-60 mesh	99.22	99.25	99.20
Birch cork 40-60 mesh	98.98	99.19	99.46